

PL-TR-94-2250

# **MEASUREMENTS OF THE HIGH ALTITUDE INFRARED CHARACTERISTICS OF THE ATMOSPHERE**

**Frank J. Murcray  
D.G. Murcray  
A. Goldman  
R.D. Blatherwick**

**University of Denver  
Department of Physics  
2112 East Wesley Avenue  
Denver, CO 80208-0202**

**DTIC QUALITY INSPECTED**

**December 1994**

**19960212 108**

**Final Report  
1 June 1989-30 September 1994**

**Approved for public release; distribution unlimited**

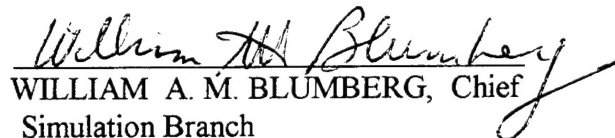


**PHILLIPS LABORATORY  
Directorate of Geophysics  
AIR FORCE MATERIEL COMMAND  
HANSCOM AIR FORCE BASE, MA 01731-3010**

"This technical report has been reviewed and is approved for publication."



LAILA S. JEONG  
Contract Manager  
Simulation Branch



WILLIAM A. M. BLUMBERG, Chief  
Simulation Branch  
Optical Environment Division



ROGER A. VAN TASSEL, Director  
Optical Environment Division

This report has been reviewed by the ESC Public Affairs Office (PA) and is releasable to the National Technical Information Service (NTIS).

Qualified requestors may obtain additional copies from the Defense Technical Information Center (DTIC). All Others should apply to the National Technical Information Service (NTIS).

If your address has changed, if you wish to be removed from the mailing list, or if the addressee is no longer employed by your organization, please notify PL/IM, 29 Randolph Road, Hanscom AFB, MA 01731-3010. This will assist us in maintaining a current mailing list.

Do not return copies of this report unless contractual obligations or notices on a specific document require that it be returned.

## REPORT DOCUMENTATION PAGE

Form Approved  
OMB No. 0704-0188

Public reporting burden for this collection of information is estimated to average 1 hour per response, including the time for reviewing instructions, searching existing data sources, gathering and maintaining the data needed, and completing and reviewing the collection of information. Send comments regarding this burden estimate or any other aspect of this collection of information, including suggestions for reducing this burden, to Washington Headquarters Services, Directorate for Information Operations and Reports, 1215 Jefferson Davis Highway, Suite 1204, Arlington, VA 22202-4302, and to the Office of Management and Budget, Paperwork Reduction Project (0704-0188), Washington, DC 20503.

1. AGENCY USE ONLY (Leave blank)		2. REPORT DATE December 1994		3. REPORT TYPE AND DATES COVERED 1 June 1989 - 30 September 1994	
4. TITLE AND SUBTITLE Measurements of the High Altitude Infrared Characteristics of the Atmosphere				5. FUNDING NUMBERS PE 61102F PR 2310 TA G1 WUCB Contract F19628-89-K-0033	
6. AUTHOR(S) Frank J. Murcray, D.G. Murcray, A. Goldman and R.D. Blatherwick					
7. PERFORMING ORGANIZATION NAME(S) AND ADDRESS(ES) University of Denver Department of Physics - Research 2112 East Wesley Avenue Denver, CO 80208-0202				8. PERFORMING ORGANIZATION REPORT NUMBER	
9. SPONSORING/MONITORING AGENCY NAME(S) AND ADDRESS(ES) Phillips Laboratory 29 Randolph Road Hanscom AFB, MA 01731-3010 Contract Manager: Laila Jeong/GPOS				10. SPONSORING/MONITORING AGENCY REPORT NUMBER  PL-TR-94-2250	
11. SUPPLEMENTARY NOTES					
12a. DISTRIBUTION/AVAILABILITY STATEMENT Approved for public release: distribution unlimited				12b. DISTRIBUTION CODE	
13. ABSTRACT (Maximum 200 words) <p>The object of this contract was to obtain data concerning the optical properties of the atmosphere at high altitudes. Experimental data were obtained by performing balloon flights with either atmospheric emission or solar absorption interferometer spectrometers. The atmospheric emission spectrometers take data at various zenith angles including scans close to the limb. The solar spectral flights also emphasized obtaining data during sunrise or sunset. The long optical paths associated with limb viewing enhance many of the atmospheric absorption features.</p> <p>Interpretation of the data obtained with these systems depends on our knowledge of the molecular spectra of the compounds present in the atmosphere. In many cases laboratory data were not available for compounds of atmospheric interest and we obtained laboratory data for some of these compounds.</p>					
14. SUBJECT TERMS  Balloon instruments, Atmospheric measurements, Infrared				15. NUMBER OF PAGES 80	
				16. PRICE CODE	
17. SECURITY CLASSIFICATION OF REPORT Unclassified	18. SECURITY CLASSIFICATION OF THIS PAGE Unclassified	19. SECURITY CLASSIFICATION OF ABSTRACT Unclassified	20. LIMITATION OF ABSTRACT SAR		

# TABLE OF CONTENTS

	<u>Page</u>
1. INTRODUCTION . . . . .	1
2. BALLOON FLIGHT PROGRAM . . . . .	2
3. LABORATORY STUDIES . . . . .	3
4. THEORETICAL STUDIES . . . . .	4
5. PUBLICATIONS RESULTING FROM WORK ON THIS CONTRACT . . . . .	5
6. PERSONNEL . . . . .	6
Appendix 1: Recent Infrared Emission Measurements of Predawn N <sub>2</sub> O <sub>5</sub> Over New Mexico . . . . .	7
Appendix 2: High Resolution Studies of Heavy NO <sub>y</sub> Molecules in Atmospheric Spectra . . . . .	11
Appendix 3: Stratospheric N <sub>2</sub> O <sub>5</sub> , CH <sub>4</sub> , and N <sub>2</sub> O Profiles from IR Solar Occultation Spectra . . . . .	22
Appendix 4: The $\nu_2$ and $2\nu_2 - \nu_2$ Bands of <sup>14</sup> N <sup>16</sup> O <sub>2</sub> : Electron Spin-Rotation and Hyperfine Contact Resonances in the (010) Vibrational State . . . . .	32
Appendix 5: Stratospheric HNO <sub>3</sub> Measurements from 0.002-cm <sup>-1</sup> Resolution Solar Occultation Spectra and Improved Spectroscopic Line Parameters in the 5.8- $\mu$ m Region . . . . .	40
Appendix 6: High-Resolution Studies of Atmospheric IR Emission Spectra . . . . .	47
Appendix 7: The Fundamental Quadrupole Band of <sup>14</sup> N <sub>2</sub> : Line Positions from High-Resolution Stratospheric Solar Absorption Spectra . . . . .	53
Appendix 8: Analysis of Atmospheric Trace Constituents from High Resolution Infrared Balloon-Borne and Ground-Based Solar Absorption Spectra . . . . .	59
Appendix 9: Improved Line Parameters for Ozone Bands in the 10- $\mu$ m Spectral Region . . . . .	68
Appendix 10: Infrared Emission Measurements of Morning Stratospheric N <sub>2</sub> O <sub>5</sub> . . . . .	73



## 1. INTRODUCTION

The objective of this contract is to obtain data on the optical properties of the earth's atmosphere at high altitudes. Particular emphasis is placed on obtaining data in the mid infrared region of the spectrum at high spectral resolution. Our group at the University of Denver has a number of instruments designed to be operated from balloon platforms that can be used to obtain such data. Data concerning the optical properties can be obtained by either measuring the intensity and spectral distribution of the radiation emitted by the atmosphere at high altitude, or by using the sun as an infrared source to study the atmospheric transmission by observing the spectral distribution of the solar radiation at balloon altitudes. The sensitivity of both techniques to the atmospheric optical properties can be enhanced by viewing the sun or the atmosphere close to the limb. Particular emphasis of this program has been placed on obtaining atmospheric spectral emission data from high altitude. A cryogenically cooled interferometer spectrometer constructed for the Air Force for balloon use was used for this purpose. This system, which has the acronym SCRIBE, has been flown numerous times on a previous Air Force Program.

These flights were performed by the Air Force balloon detachment and launched from Holloman Air Force Base. Reduction of the number of groups using this capability increased the per flight costs and reduced the number of flights which could be performed on this contract. This reduction in flight opportunities was partially offset by an agreement with NASA to fly the system as part of the Upper Atmosphere Research Satellite (UARS) correlative measurements program. This required the flights be performed using the National Scientific Balloon Facility. The Air Force support included a TM ground station capable of receiving a 700K bit/sec signal. The NSBF system did not have this capability and the SCRIBE TM system had to be modified so it could be accommodated by the NSBF system. The other changes required for NSBF operation were minor.

In addition to the atmospheric measurements, the program also included taking high resolution laboratory data for compounds of upper atmospheric interest.

## 2. BALLOON FLIGHT PROGRAM

The SCRIBE system was flown on May 23, 1989. Since this flight was performed just prior to the start of this contract, reduction of the data obtained during the flight has been performed as part of the effort on this contract. The results will be discussed below. Everything worked well on this flight and the spectra obtained illustrated the capability of the system. In view of the reduced flight schedule due to the increased cost of flying the system it was decided to use the time to incorporate a second detector into the system. This allows us to obtain data from 4 $\mu$ m to 8 $\mu$ m in addition to the nominal 8-15 $\mu$ m region scanned by the primary detector. The SCRIBE interferometer is operated in a large vacuum dewar so it can be cooled to 77K by liquid nitrogen. Incorporation of the second detector required extensive modification to the vacuum dewar and data handling system. A flight with the modified system was scheduled for late spring 1991. The flight was flown on May 23, 1991.

As noted in the Introduction, the additional flight with the system was flown with balloon support provided by NASA. The modifications required to perform the flight using National Scientific Ballooning Facility support were completed and the flight scheduled for February 1992 from Barstow, California. When the instrument was cooled prior to shipment to Barstow a major vacuum leak occurred. The leak was associated with the cryogen fill lines and only occurred when the instrument was cold. Detection and repair of the leak precluded taking advantage of the Barstow flight opportunity and the flight was delayed until fall 1992 from Ft. Sumner, NM.

The final flight with the SCRIBE instrument was performed from Ft. Sumner, NM on October 17, 1992. The flight was launched after considerable delay due to weather. We also had some problems with leaks in the cryogen fill lines. Our initial problems with these lines occurred at the fittings. The recent problems were due to pin-hole leaks developing in the lines. Evidently the extended use causes some weakening of the material. It is evident that before additional flights can be performed with the system the entire cryogenic system needs to be replaced. Since resources were not available for accomplishing this, we decided to use our balloon-borne cold grating spectrometer system for the last flight on the program. This system

has very good sensitivity but lower spectral resolution than SCRIBE. The system was checked out, and the gondola used with the system was refurbished in preparation for the flight. The flight with the system was scheduled for the fall of 1994 in support of a UARS overpass. Preparations for this flight were delayed several days due to high surface winds. The flight was launched October 9th and everything went very well with excellent data throughout the flight. Recovery was accomplished without incident.

### 3. LABORATORY STUDIES

As noted in the Introduction, a second technique for obtaining data on the properties of the upper atmosphere is by flying infrared solar spectrometer systems. Analysis of the spectra obtained yield information on composition and physical state of the atmosphere. During the period covered by this contract several balloon flights were performed using our ultrahigh spectral resolution solar spectrometer system. These flights were made using NASA support, however the data obtained are of interest to the Air Force. Phillips Laboratory has a long history of developing methods of predicting transmission over various atmospheric paths. This program has developed a number of computer programs for performing such calculations including Lowtran, Modtran and Fascode. The heart of the calculations with any of these codes is the molecular line parameters data base. This data base, which started modestly over 20 years ago, has been increasing in complexity as more spectral regions and chemical compounds are included in the data base.

In addition to adding new compounds, the data base is continually updated to include newer data, and to correct mistakes that occurred in the earlier versions. This data base, which has had various names over the years, is currently referred to as the HiTran Data Base and the various versions are referred to by the year of issue, i.e., 86 HiTran Data Base. The latest version has data for over 500,000 absorption lines. The solar spectra obtained from high altitude during sunset or sunrise contain a large number of absorption features which cannot be observed over shorter atmospheric paths. The spectra therefore contain many absorption features due to compounds present at low concentrations or weak lines due to the more abundant compounds.

Identification of these features is aided by comparison with the predictions made using the HiTran data base. The comparisons quite often lead to changes in the data base. In order to identify some features that do not agree with predictions it has often proved necessary to obtain laboratory data at higher resolution and over different temperature and pressure conditions than the laboratory data currently available. During the period covered by this report we have obtained such data for the following compounds:  $\text{COCl}_2$ ,  $\text{NO}_2$ ,  $\text{NO}$ ,  $\text{COF}_2$ ,  $\text{HNO}_3$ ,  $\text{OCS}$ , and  $\text{CH}_3\text{Cl}$ .

The data are incorporated into the HiTran data and are also available on computer discs. The identification of the features in the spectra are incorporated into a series of Atlases which are available from our group.

#### 4. THEORETICAL STUDIES

The identification of weak lines in the solar spectra coupled with the laboratory studies often enables significant improvements to be made in the theoretical analysis of many compounds. These studies play an important role in improving the HiTran data base. The results of these studies are included in the various versions of the HiTran data base.

5. PUBLICATIONS RESULTING FROM WORK ON THIS CONTRACT

- Blatherwick, R.D., F.H. Murcray, F.J. Murcray and D.G. Murcray, "Recent Infrared Measurements of Predawn  $\text{N}_2\text{O}_5$  Over New Mexico," Optical Remote Sensing-1990 Technical Digest, 4, 491-494, 1990.
- Goldman, A., C.P. Rinsland, F.J. Murcray, R.D. Blatherwick and D.G. Murcray, "High Resolution Studies of Heavy  $\text{NO}$  Molecules in Atmospheric Spectra," J. Quant. Spectrosc. Radiat. Transfer, 52, 367-377, 1994.
- Camy-Peyret, C., J.M. Flaud, A. Perrin, C.P. Rinsland, A. Goldman and F.J. Murcray, "Stratospheric  $\text{N}_2\text{O}_5$ ,  $\text{CH}_4$  and  $\text{N}_2\text{O}$  Profiles from IR Solar Occultation Spectra," J. Atmos. Chemistry, 16, 31-40, 1993.
- Perrin, A., J.-M. Flaud, C. Camy-Peyret, A. Goldman, F.J. Murcray, R.D. Blatherwick and C.P. Rinsland, "The  $\nu_2$  and  $2\nu_2 - \nu_2$  of  $^{14}\text{N}^{16}\text{O}$ : Electron Spin - Rotation and Hyperfine Contact Resonances in the (010) Vibrational State," J. Mol. Spectrosc., 160, 456-463, 1993.
- Goldman, A., F.J. Murcray, R.D. Blatherwick, J.J. Kusters, D.G. Murcray, C.P. Rinsland, J.-M. Flaud and C. Camy-Peyret, "Stratospheric  $\text{HNO}_3$  Measurements from  $0.002\text{-cm}^{-1}$  Resolution Solar Occultation Spectra and Improved Spectroscopic Line Parameters in the  $5.8\text{-}\mu\text{m}$  Region," J. Geophys. Res., 97, 2561-2567, 1992.
- Murcray, F.J., F.H. Murcray, A. Goldman, R.D. Blatherwick and D.G. Murcray, "High-Resolution Studies of Atmospheric IR Emission Spectra," SPIE-Remote Sensing of Atmospheric Chemistry, 1941, 282-287, 1991.
- Rinsland, C.P., R. Zander, A. Goldman, F.J. Murcray, D.G. Murcray, M.R. Gunson and C.B. Farmer, "The Fundamental Quadrupole Band  $^{14}\text{N}_2$ : Line positions from High-Resolution Stratospheric Solar Absorption Spectra," J. Mol. Spectrosc., 148, 274-269, 1991.
- Goldman, A., F.J. Murcray, C.P. Rinsland, R.D. Blatherwick, F.H. Murcray and D.G. Murcray, "Analysis of Atmospheric Trace Constituents from High Resolution Infrared Balloon-Borne Sensing of Atmospheric Chemistry, 1491, 194-202, 1991.
- Flaud, J.-M., C. Camy-Peyret, C.P. Rinsland, V.M. Devi, M.A.H. Smith and A. Goldman, "Improved Line Parameters for Ozone Bands in the  $10\text{-}\mu\text{m}$  Spectral Region," Appl. Opt., 29, 3667-3671, 1990.
- Blatherwick, R.D., D.G. Murcray, F.H. Murcray, F.J. Murcray, A. Goldman, G.A. Vanasse, S.T. Massie and R.J. Cicerone, "Infrared Emission Measurements of Morning Stratospheric  $\text{N}_2\text{O}_5$ , J. Geophys. Res., 94, 18337-18340, 1989.

6. PERSONNEL

In addition to the authors, the following personnel have made significant contributions to this program:

John Van Allen, John Kusters, John Williams and Troy Dow.

## APPENDIX 1

### RECENT INFRARED EMISSION MEASUREMENTS OF PREDAWN $\text{N}_2\text{O}_5$ OVER NEW MEXICO

R.D. Blatherwick, F.H. Murcray, F.J. Murcray, D.G. Murcray  
Department of Physics, University of Denver, Denver, CO 80208

G.A. Vanasse and M. Hoke  
Air Force Geophysics Laboratory, Hanscom Field, Bedford MA 01731

#### Introduction

Data obtained with the AFGL SCRIBE system (Stratospheric CRYogenic Interferometer Balloon Experiment) during a balloon flight in July, 1984 were recently used to perform the first post-dawn morning measurement of  $\text{N}_2\text{O}_5$  [1].

The SCRIBE instrument was most recently flown on 23 May, 1989, and data analysis is currently in progress. Preliminary analysis of the spectra for predawn  $\text{N}_2\text{O}_5$  has been completed and the results are presented here.

#### Observations

The data were obtained during a balloon flight by the University of Denver from Alamogordo, NM. Instrumentation consisted of the SCRIBE  $\text{LN}_2$  cooled interferometer system, as described by Murcray et al. [2], which has a maximum path difference of  $\sim 9$  cm (resulting in an apodized FWHM resolution of  $\sim 0.12$   $\text{cm}^{-1}$ ). On this flight, the view angle was selected by rotation of a cooled input mirror positioned at the entrance to the interferometer, and radiometric calibration was performed by occasionally rotating the input mirror to view an on-board black body. Data presented here were recorded at zenith angles of  $86.6^\circ$ ,  $90.0^\circ$ , and  $92.7^\circ$ , from a float altitude of 29.8 km. Each scan shown here is actually the sum of 10 or 11 individual scans, representing about 5 minutes total observation time.

#### Analysis and Results

The data were analyzed by comparison with synthetic spectra generated using a line-by-line computer program developed at the University of Denver. The program, which takes refractive effects into account through a ray-tracing routine, calculates transmittance or emission over a user-selected number of atmospheric layers at a net interval of  $0.001$   $\text{cm}^{-1}$ . The 1986 edition of the HITRAN database [3] is used as input to the program. Line parameters for  $\text{N}_2\text{O}_5$  do not exist, but the absorption coefficients needed to compute the  $\text{N}_2\text{O}_5$  contribution to the atmospheric emission are generated by the program using the absorption cross-sections for  $\text{N}_2\text{O}_5$  which are included in the HITRAN database. Finally, the computed radiances are convolved with a line shape function for comparison to the experimental data. Residual background radiances in the observed data at  $86.6^\circ$  and  $90.0^\circ$  were adequately accounted for by assuming a 0.5% gray background in the synthetic spectra, but in the  $92.7^\circ$  scan, an additional  $0.025$  microwatts/ $\text{cm}^2\text{-sr-cm}^{-1}$  background was subtracted from the data to achieve agreement with the computed spectrum. The pressure-temperature profile used in these simulations was taken from a drop-sonde released from the payload shortly after reaching float altitude. Mixing ratio profiles for the  $\text{H}_2\text{O}$ ,  $\text{O}_3$ , and  $\text{N}_2\text{O}$  were taken from Smith [4],  $\text{CO}_2$  was taken as constant at 330 ppm v/v, and the  $\text{CH}_4$  profile was based on the 1985 WMO report [5].

Figures 1a-1c show comparisons between the calculated (solid line) and observed (dotted line) emission for view angles of  $86.6^\circ$ ,  $90.0^\circ$ , and  $92.7^\circ$ , (relative to vertical) respectively. The sharp emission lines in this

region arise from  $\text{CH}_4$ ,  $\text{N}_2\text{O}$ ,  $\text{H}_2\text{O}$ , and to a considerably lesser extent,  $\text{CO}_2$  and  $\text{O}_3$ , while the broad, smooth emission feature from 1230 to 1265  $\text{cm}^{-1}$  is attributable to  $\text{N}_2\text{O}_5$ . The  $\text{N}_2\text{O}_5$  mixing ratio profile used in generating the synthetic spectra in these figures was computed by scaling the one dimensional model calculations for predawn  $\text{N}_2\text{O}_5$  presented in reference [1] or (below 25 km) values extrapolated therefrom. For the 86.6° and 90.0° scans, the scaling factor was 1.0. Of course, one would expect from geometrical considerations that the same  $\text{N}_2\text{O}_5$  profile would fit both of these scans, although the 90.0° scan is more heavily weighted toward the balloon altitude. For these angles, a six-layer calculation was performed, and the  $\text{N}_2\text{O}_5$  mixing ratio was multiplied by the same scaling factor in all layers. For the 92.7° scan, with a tangent height of 22.6 km, three additional layers were added, and the mixing ratio profile below 29.8 km was scaled in three steps to provide continuity while achieving a good fit to the observed data. Hence, the layer from 22.6 to 24.0 km was scaled by 0.5, the layer from 24.0 to 26.0 km was scaled by 0.7, the region from 26.0 to 29.8 km was scaled by 0.9, and the mixing ratio above the balloon was kept fixed at the previously determined values.

Figure 2 shows the final  $\text{N}_2\text{O}_5$  profile used in generating all of the synthetic spectra. As indicated, the profile above 29.8 km was determined from fitting the 86.6° and 90.0° scans, while the values below 29.8 km were determined by fitting the 92.7° scan in such a way as to produce a smooth continuation of the profile above 29.8 km.

Data analysis on this flight is continuing, and additional results, if available, will be presented.

#### Acknowledgments

Research at the University of Denver was supported in part by the Air Force Office of Scientific Research (AFOSR) as part of AFGL task 2310G1, by NASA under grant NAG2-351, and by NSF under grant ATM-87-11572. Acknowledgment is made to the National Center for Atmospheric Research, which is supported by the National Science Foundation, for computer time used in this research.

#### References

1. Blatherwick, R.D., D.G. Murcray, F.H. Murcray, F.J. Murcray, A. Goldman, G.A. Vanasse, S.T. Massie, and R.J. Cicerone, Infrared emission measurements of morning stratospheric  $\text{N}_2\text{O}_5$ , *J. Geophys. Res.*, in press, 1989.
2. Murcray, F.H., F.J. Murcray, D.G. Murcray, J. Pritchard, G. Vanasse, and H. Sakai, Liquid nitrogen-cooled fourier transform spectrometer system for measuring atmospheric emission at high altitudes, *J. Atm. Ocean. Tech.*, 1, 351-357, 1984.
3. Rothman, L.S., R.R. Gamache, A. Goldman, L.R. Brown, R.A. Toth, H.M. Pickett, R. Poynter, J.-M. Flaud, C. Camy-Peyret, A. Barbe, N. Husson, C.P. Rinsland, and M.A.H. Smith, The HITRAN database: 1986 edition, *Appl. Opt.*, 26, 4058-4097, 1987.
4. Smith, M.A.H., Compilation of atmospheric gas concentration profiles from 0 to 50 km, NASA Tech. Memo., No. 83289, 1982.
5. World Meteorological Organization/NASA, Atmospheric Ozone 1985: Assessment of our understanding of the processes controlling its present distribution and change, World Meteorological Organization, Geneva, 1986.



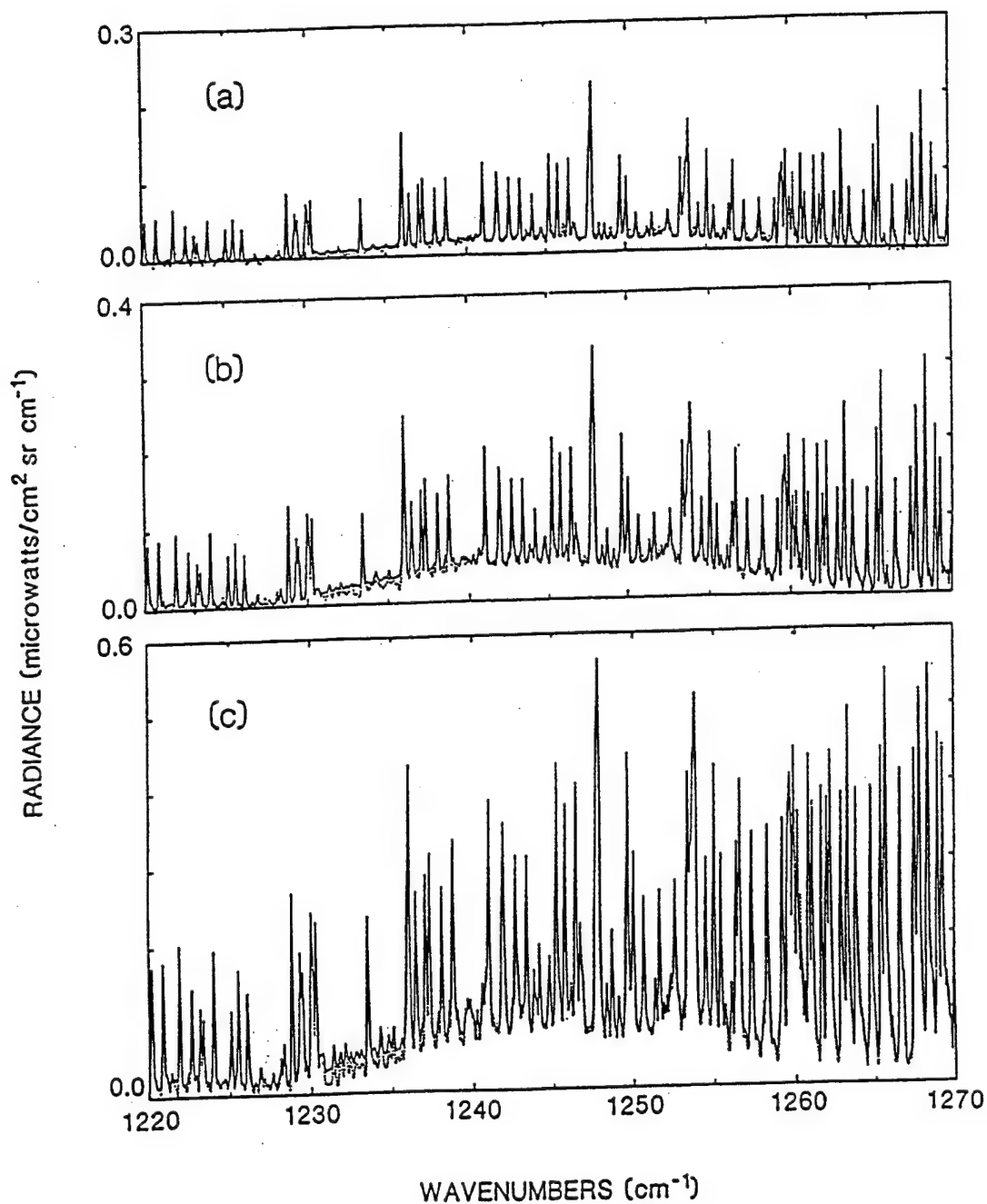


Figure 1a-1c. Comparison of observed (dotted curves) and calculated (solid curves) atmospheric emission spectra. Observed spectra were obtained on 23 May, 1989 by the University of Denver with the AFGL SCRIBE system. Data were recorded from a float altitude of 29.8 km at zenith angles of 86.6° (top), 90.0° (middle), and 92.7° (bottom).

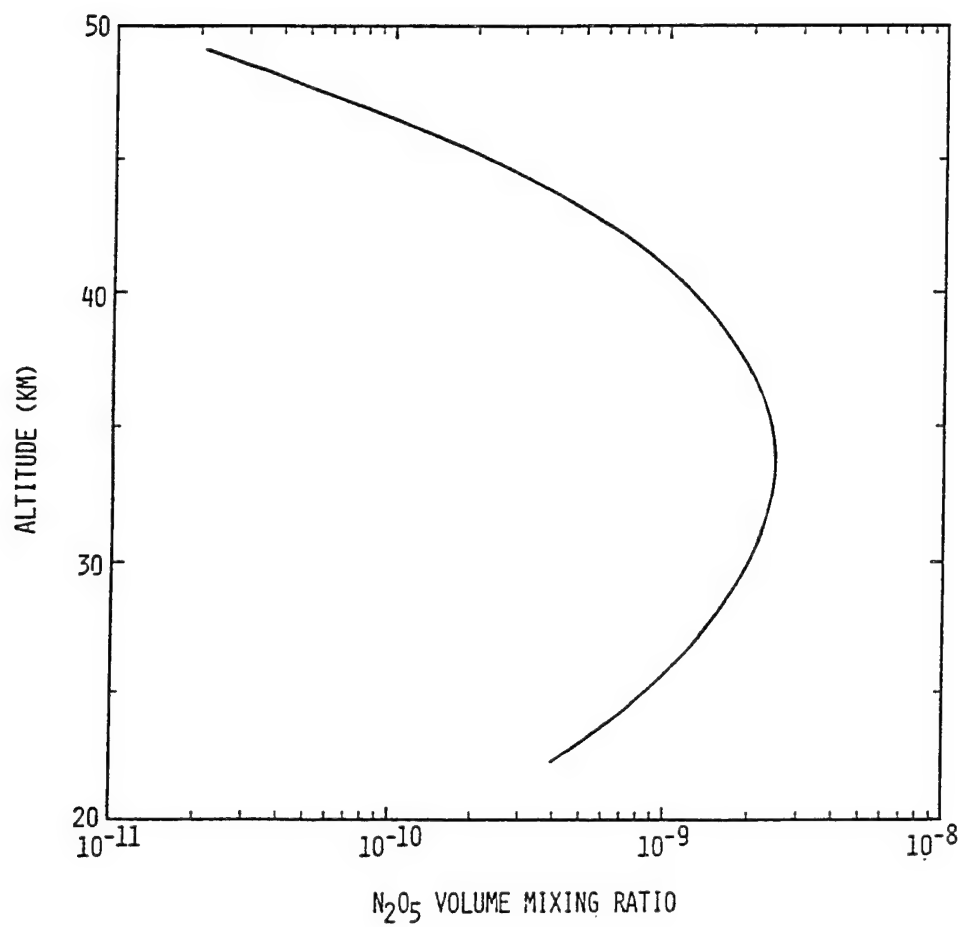


Figure 2.  $\text{N}_2\text{O}_5$  volume mixing ratio profile used in generating the synthetic spectra of Figure 1.



The U.S. Government is authorized to reproduce and sell this report.  
Permission for further reproduction by others must be obtained from  
the copyright owner.

## HIGH RESOLUTION STUDIES OF HEAVY NO<sub>x</sub> MOLECULES IN ATMOSPHERIC SPECTRA

A. GOLDMAN,<sup>†</sup> C. P. RINSLAND,<sup>‡</sup> F. J. MURCRAY,<sup>†</sup> R. D. BLATHERWICK,<sup>†</sup>  
and D. G. MURCRAY<sup>†</sup>

<sup>†</sup>Department of Physics, University of Denver, Denver, CO 80208, and <sup>‡</sup>Atmospheric Sciences Division,  
NASA Langley Research Center, Hampton, VA 23681-0001, U.S.A.

**Abstract**—New line parameters for two heavy odd nitrogen molecules HNO<sub>3</sub> in the  $\nu_3/2\nu_9$  region, and ClONO<sub>2</sub> in the  $\nu_4$  region are incorporated in the analysis of high resolution i.r. atmospheric spectra. The line parameters are tested and renormalized vs laboratory spectra, and then applied to retrievals from balloon-borne and ground-based solar absorption spectra.

### INTRODUCTION

High resolution (0.002–0.003 cm<sup>-1</sup>) Michelson type interferometer systems are used at the University of Denver to obtain i.r. solar absorption spectra of the stratosphere during balloon flights, as well as ground-based solar spectra. The stratospheric spectra in the region 700–2200 cm<sup>-1</sup> cover spectral signatures of O<sub>3</sub> (including isotopic species), NO<sub>2</sub>, HNO<sub>3</sub>, O<sub>2</sub>, N<sub>2</sub>, COF<sub>2</sub>, ClONO<sub>2</sub>, SF<sub>6</sub>, and others. For a typical study of new spectral features observable in such spectra see the discussion of the 6 June 1988 flight data by Goldman et al.<sup>1</sup> Ground-based spectra in the 3–12  $\mu$ m region are obtained regularly from Mauna Loa (Hawaii) and Denver (CO), in support of the Network for Detection of Stratospheric Change (NDSC) and the Upper Atmospheric Research satellite (UARS).

In support of the atmospheric observations, numerous laboratory spectra have been obtained with the same interferometer systems. The laboratory spectra cover mostly the region 700–3000 cm<sup>-1</sup> and have also been extended down to 500 or up to 5000 cm<sup>-1</sup>. The molecules covered include CCl<sub>4</sub>, CCl<sub>2</sub>F<sub>2</sub>, CCl<sub>3</sub>F, CF<sub>4</sub>, CHClF<sub>2</sub>, CH<sub>3</sub>Cl, CHCl<sub>3</sub>, CH<sub>2</sub>O, C<sub>2</sub>H<sub>6</sub>, ClONO<sub>2</sub>, COF<sub>2</sub>, COCl<sub>2</sub>, COClF, HCOOH, HNO<sub>4</sub>, H<sub>2</sub>O<sub>2</sub>, NO<sub>2</sub>, HNO<sub>3</sub>, N<sub>2</sub>O<sub>5</sub>, and others. Analysis of stratospheric spectral features, combined with analysis of laboratory molecular absorption spectra, improves the spectral line parameters and leads to more complete line identifications and more accurate retrieval quantification of atmospheric gases.

In the present paper, updates of line parameters and their application to the University of Denver spectra will be presented for the 11  $\mu$  region of HNO<sub>3</sub> and the 780 cm<sup>-1</sup> region of ClONO<sub>2</sub>.

### RESULTS AND DISCUSSION

Recent updates of line parameters for the HNO<sub>3</sub>  $\nu_3/2\nu_9$  bands, beyond the HITRAN 92 data base,<sup>2</sup> have allowed improved quantitative analysis of atmospheric spectra in the 11  $\mu$  region. The first update was initiated by A. G. Maki (unpublished) and included Fermi resonance effects on the energy levels but unperturbed intensities. This provided improved modeling of the  $\nu_3$  manifolds in the 860–875 cm<sup>-1</sup> region of the atmospheric spectra, as reported by Goldman et al.<sup>1,2</sup> This set has been used successfully for most retrievals to date from high resolution airborne and ground-based solar spectra. Subsequent update was based on Maki and Wells,<sup>3</sup> who extended the analysis with Fermi resonance, by adding unperturbed intensities to the published energies and line positions. This update covered both bands, with improved agreement in the  $\nu_3$  manifolds and

$Q$ -branch, but the  $2\nu_2$   $Q$ -branch was still poorly modeled. The more recent update, based on the work of Perrin et al.,<sup>4</sup> extended the treatment with both Fermi and Coriolis interactions, including perturbed intensities. With this update the modeling of both the  $\nu_2$  and the  $2\nu_2$   $Q$ -branches is significantly improved, and the  $Q$ -branches are now consistent with most  $P$  and  $R$  manifolds. Line intensity plots for the two latest updates were shown in Fig. 1.

In order to apply these data to atmospheric spectra in a fashion consistent with previous retrievals from these bands and from the other major  $\text{HNO}_3$  bands, the total band intensities were normalized to the measured intensities of Giver et al.,<sup>5</sup> divided by a hot bands factor of 1.30, which amounts to multiplying the Perrin et al. lines<sup>4</sup> (shown in Fig. 1) by 1.43. The hot bands are not analyzed yet, but are not significant in the spectral intervals used for stratospheric retrievals; they are thus not considered in the line list for this study.

Figure 2 shows a typical fitting in the  $\nu_2$  manifolds with the latest lines to data from the University of Denver balloon flight of 6 June 1988. The improvements in the  $Q$ -branches modeling is demonstrated in Fig. 3, also with data from the 6 June 1988 flight. Comparisons with ground-based spectra to be presented elsewhere, also show significant improvements in the spectral fitting. Comparisons with retrievals with the previous two line parameters updates show consistency of better than 4% over the  $860\text{--}870\text{ cm}^{-1}$  manifolds.

The first update of the initial cross-sections for  $\text{ClONO}_2$  (HITRAN 1986) was provided by the work of Ballard et al.,<sup>6</sup> which generated cross-sections in the  $700\text{--}1800\text{ cm}^{-1}$  at  $213\text{--}296\text{ K}$ . These cross-sections were included in the HITRAN 92 data base.<sup>7</sup>

Recent analysis of the  $\nu_4\text{ClONO}_2$  region (the most useful for atmospheric retrievals) by Bell et al.,<sup>8</sup> provided spectroscopic constants for the three main bands in this region,  $\nu_4$   $^{35}\text{ClONO}_2$ ,  $\nu_4$   $^{37}\text{ClONO}_2$ , and  $\nu_4 + \nu_2 - \nu_2$   $^{35}\text{ClONO}_2$ . Based on this analysis, line parameters were generated in the  $\nu_4$  region, with the relative intensities of the three bands normalized to  $0.002\text{ cm}^{-1}$  resolution laboratory spectra taken at the University of Denver, and absolute intensities normalized to the values of Ballard et al.,<sup>6</sup> with the continuum removed (providing consistency of better than 3% with previous retrievals). The new line parameters were then applied to retrievals in the  $780.2\text{ cm}^{-1}$  region from D.U. balloon-borne and ground-based spectra taken at  $0.002\text{--}0.006\text{ cm}^{-1}$  resolution. The new line parameters showed improved agreement with observed data, even though the fine structure is not fully modeled yet. Intensity plots of the normalized line parameters are shown in Fig. 4. Modeling of the  $780.2\text{ cm}^{-1}$  region from University of Denver laboratory data is shown in Fig. 5. Fitting to stratospheric spectra obtained by University of Denver during the 6 June 1988 flight is shown in Fig. 6.

The new line parameters of  $\text{HNO}_3$  and  $\text{ClONO}_2$  were thus applied in retrievals of altitude mixing ratio profiles from sunset spectra obtained during two D.U. balloon flights made on 6 June 1988 (from Palestine, Texas, with float altitude of  $36.7\text{ km}$ ) and 24 July 1992 (Palestine, Texas, float altitude of  $34\text{ km}$ ). Sunset scans were obtained during the 6 June 1988 flight down to  $15.60\text{ km}$  tangent altitude, but only down to  $24.30\text{ km}$  tangent altitude during the 24 July 1992 flight; the Pinatubo aerosol caused loss of the source signal below this altitude. Both flights covered the same spectral interval of  $700\text{--}1350\text{ cm}^{-1}$  with resolution of  $\sim 0.0025\text{ cm}^{-1}$ . The resolution and the signal to noise ratio were slightly better during the 6 June 1988 flight. Spectral fitting results were tested by two non-linear spectral least squares programs, one based on the work of Niple et al.,<sup>9</sup> and one on Rinsland et al.,<sup>10</sup> combined with the onion-peeling method for the mixing ratio profile. The agreement between the two methods is better than 2% in any step of the onion-peeling, assuming the same atmospheric and spectroscopic parameters.

The retrieved mixing ratios are shown in Figs. 7, 8, which also include comparisons with previous results— $\text{HNO}_3$  from D.U.,<sup>11</sup> ATMOS,<sup>12</sup> LIMS,<sup>13</sup> WMO (1986),<sup>14</sup> and BLISS,<sup>15</sup> and  $\text{ClONO}_2$  from ATMOS.<sup>16</sup> The results from the two flights are included in the comparisons of CLAES-UARS retrievals and other correlative measurements and 2-D global model calculations, as reported by Mergenthaler et al.<sup>17</sup> These comparisons show that both  $\text{HNO}_3$  and  $\text{ClONO}_2$  profiles exhibits significant variabilities, not fully modeled yet, even for mid latitudes. In particular, shifts in the altitudes of the peak of the  $\text{ClONO}_2$  profiles such as seen in Fig. 8, also appear in the CLAES results.<sup>17</sup> The improved line parameters will provide a more accurate and consistent quantification of these species from i.r. atmospheric spectra.

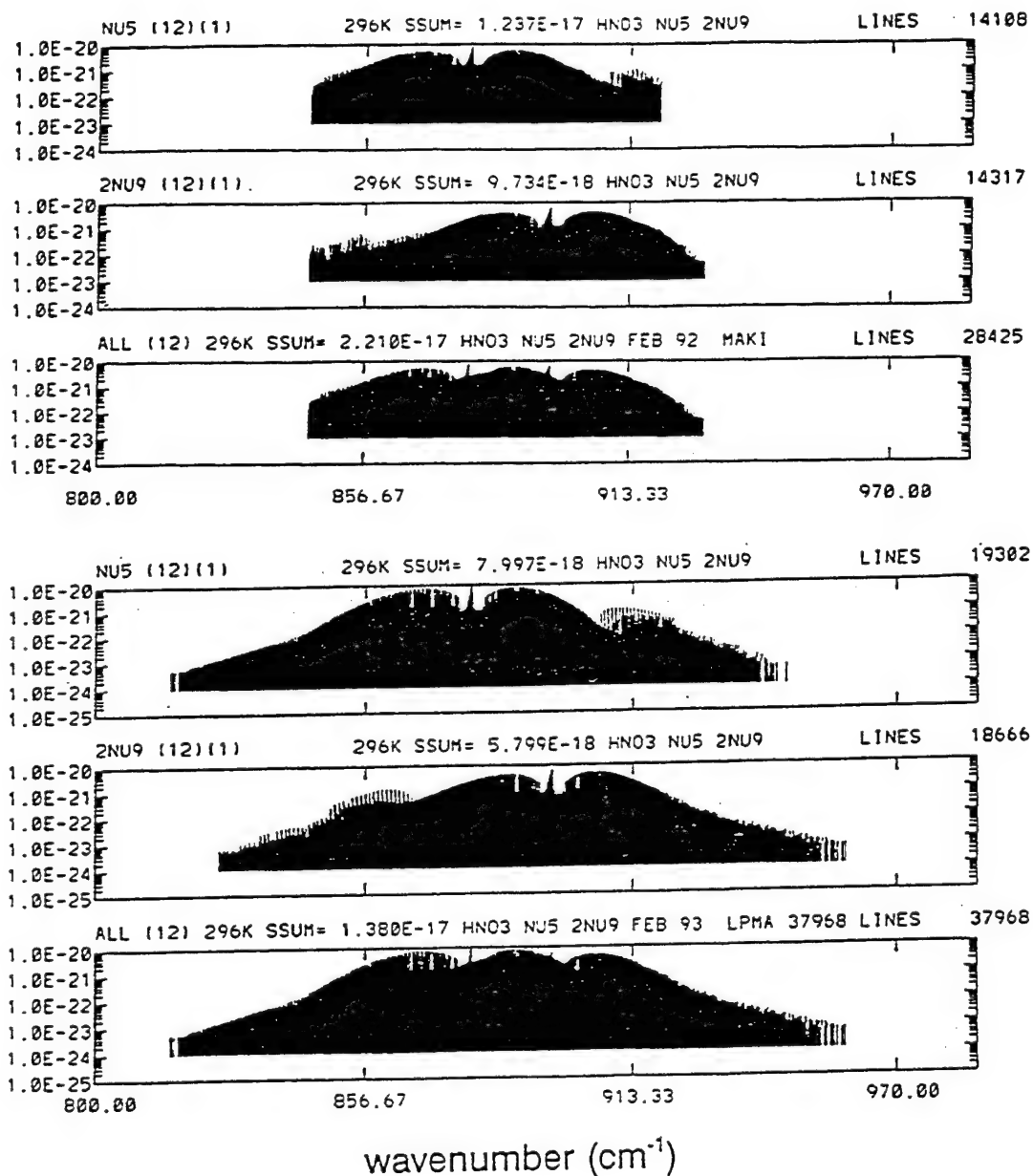


Fig. 1. Line intensity plots for the new sets of  $\text{HNO}_3$  line parameters incorporated in the recent analysis of atmospheric spectra for the  $\text{HNO}_3$   $\nu_3/\nu_2$  bands. The line parameters are based on Maki and Wells<sup>3</sup> and on Perrin et al.<sup>4</sup> The later set is for wider spectral interval and lower intensity cutoff.

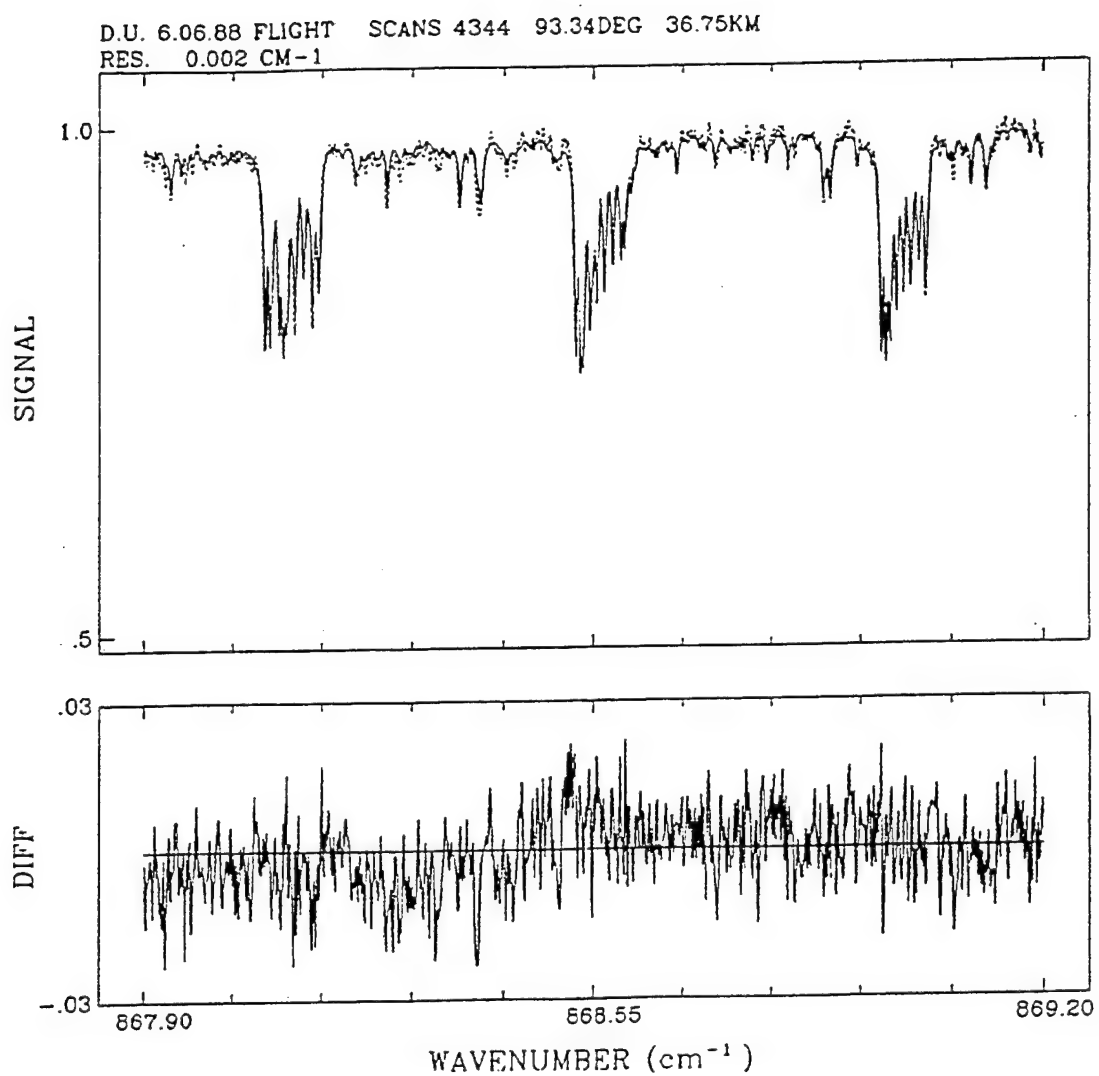


Fig. 2. Sample retrieval of HNO<sub>3</sub> from *P*-branch manifolds in the  $\nu_3$  region by spectral least-squares fitting to balloon-borne solar spectra obtained during D.U. balloon flight of 6 June 1988.

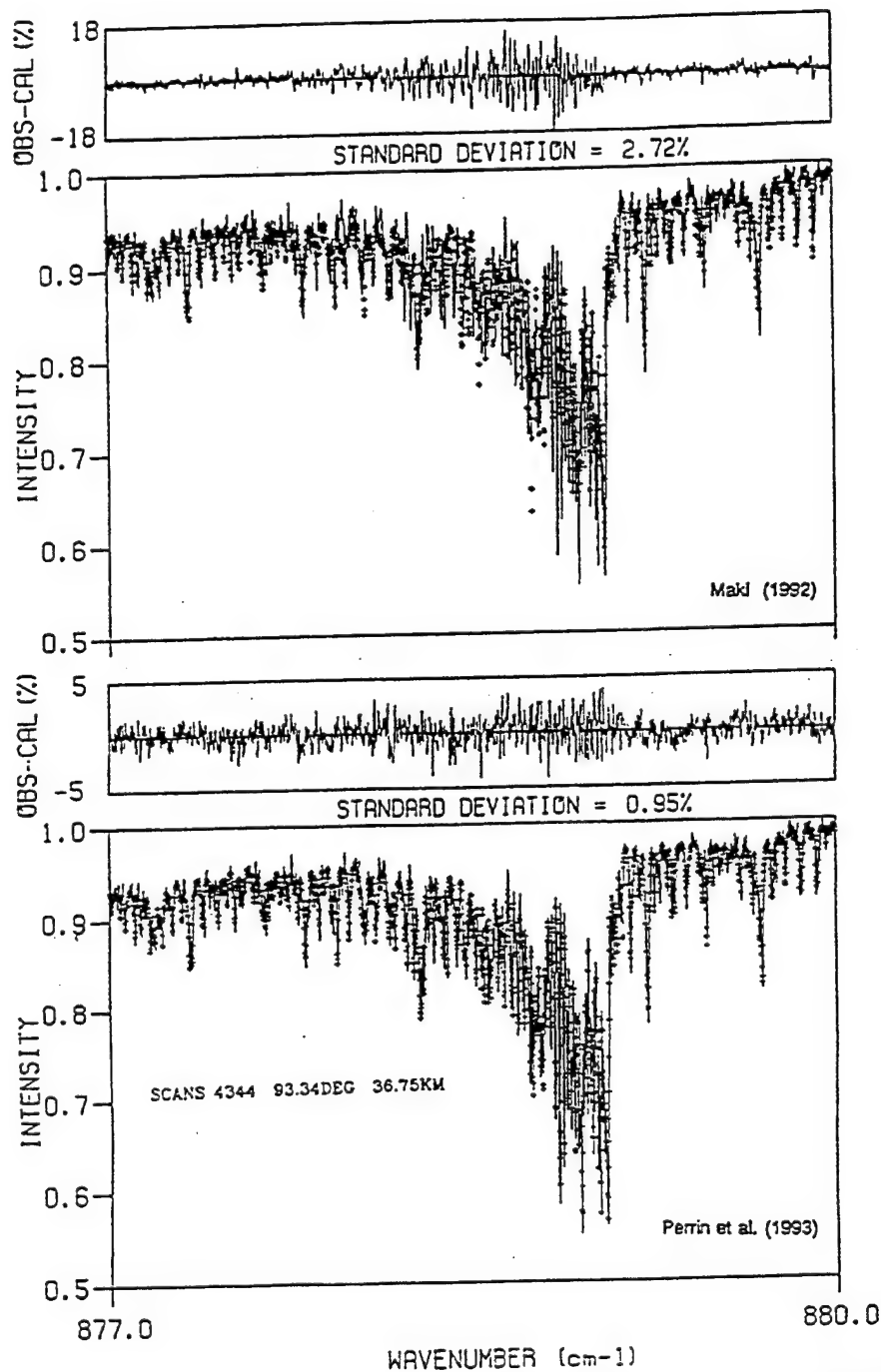


Fig. 3. Comparisons of spectral least-squares fitting to balloon-borne solar spectra obtained during D.U. balloon flight of 6 June 1988, with the recent sets of  $\text{HNO}_2$  line parameters in the  $\nu_3$  Q-branch region.

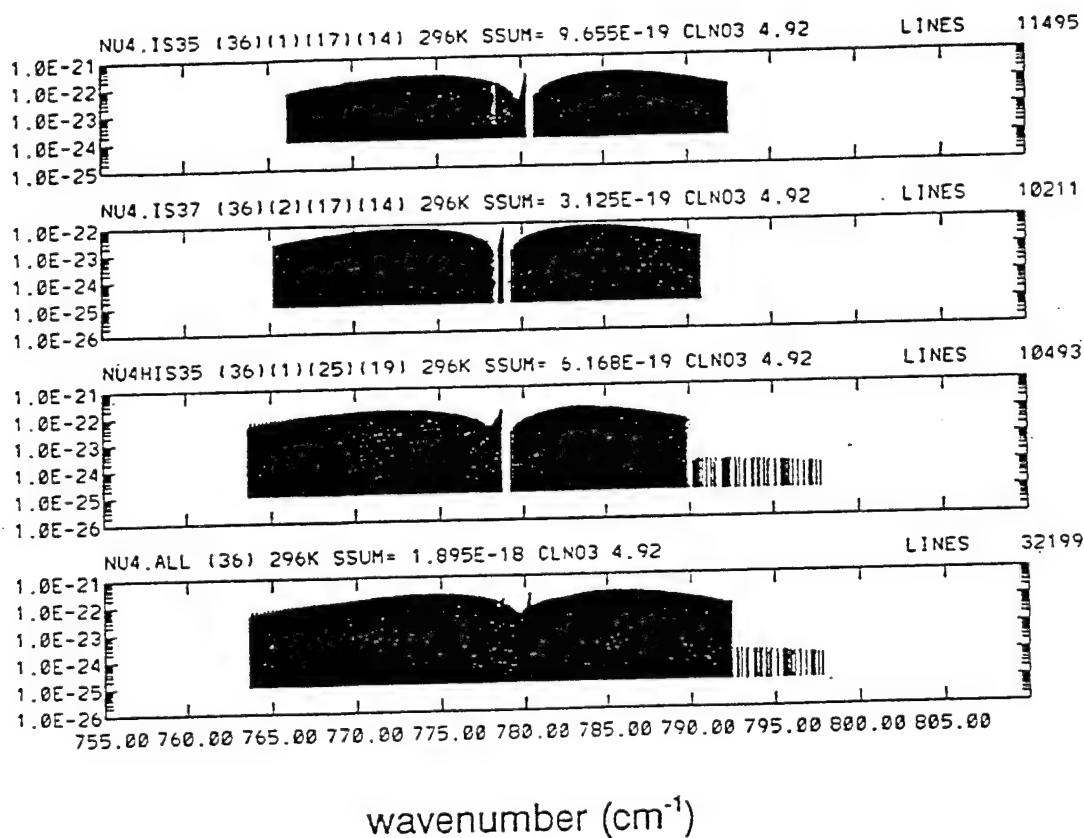


Fig. 4. Line intensity plots of the new  $\text{ClONO}_2$  line parameters incorporated in recent analysis of atmospheric spectra for the  $\nu_4$  bands of  $^{35}\text{ClONO}_2$ ,  $^{37}\text{ClONO}_2$ , and  $\nu_4 + \nu_9 - \nu_9$  of  $^{35}\text{ClONO}_2$ . The line positions are based on the spectroscopic constants of Bell et al.<sup>8</sup>, with intensity cutoff for each band of  $5 \times 10^{-3}$  and  $K_{\text{max}} = J_{\text{max}} = 74$ . The relative band intensities are normalized to a University of Denver laboratory spectrum, and absolute intensities normalized to Ballard et al.<sup>6</sup> values, with the continuum removed.



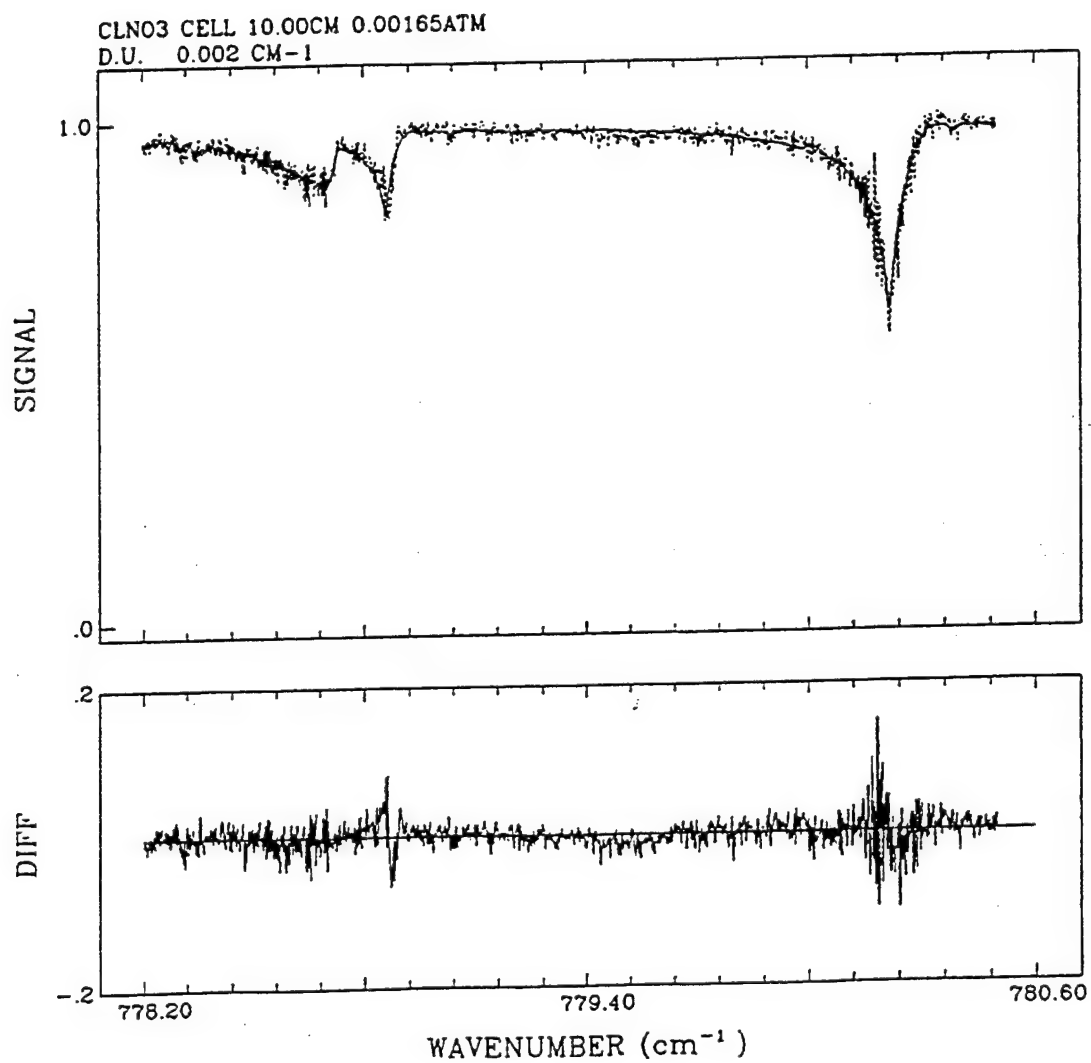


Fig. 5. Spectral least-squares fitting to the ClONO<sub>2</sub> laboratory spectrum with the new line parameters in the  $\nu_4$  <sup>35</sup>ClONO<sub>2</sub> region. Fine structure is not fully accounted for yet.

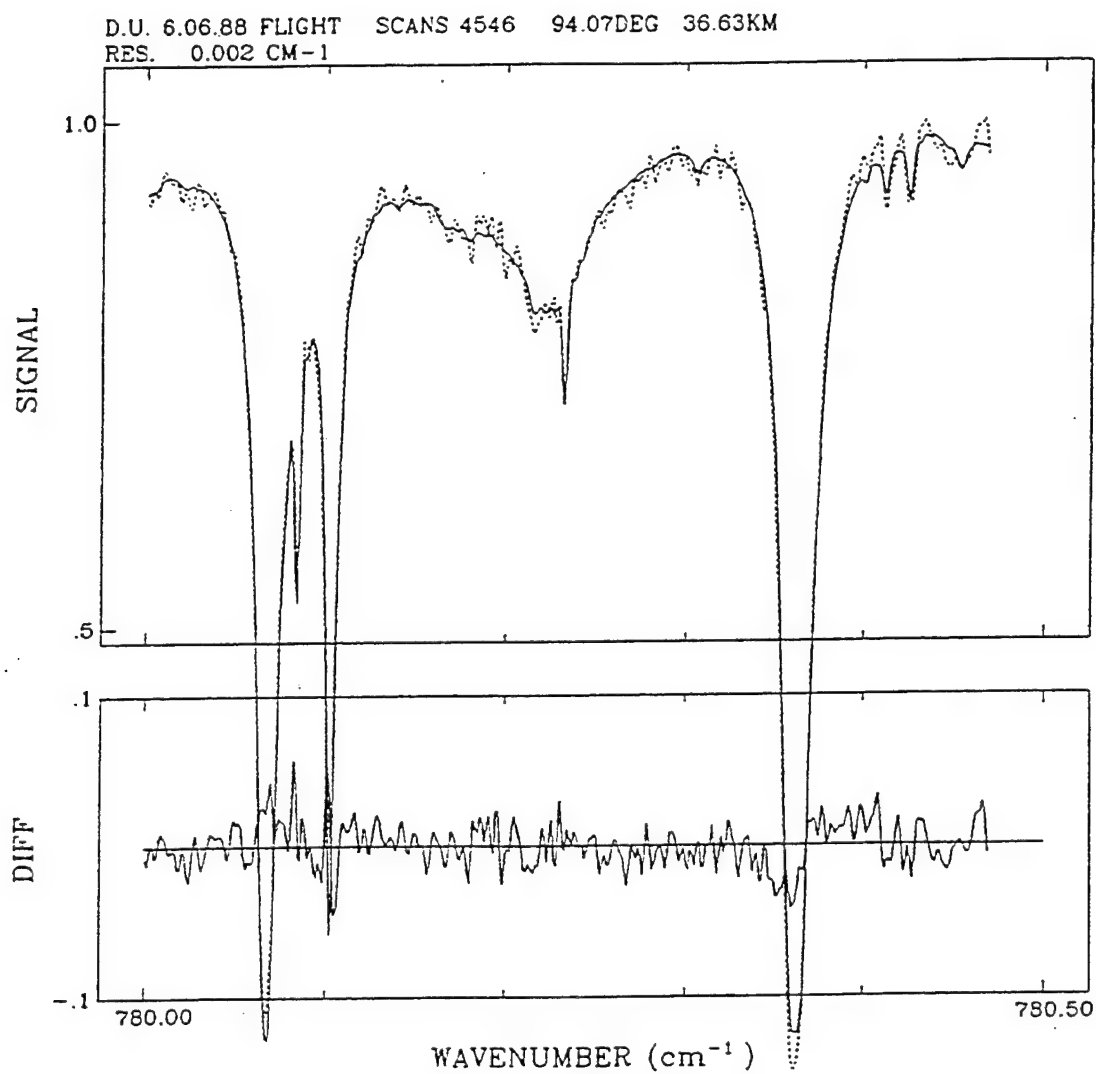


Fig. 6. Sample retrieval of  $\text{ClONO}_2$  by spectral least-squares fitting to balloon-borne solar spectra obtained during University of Denver balloon flight of 6 June 1988.

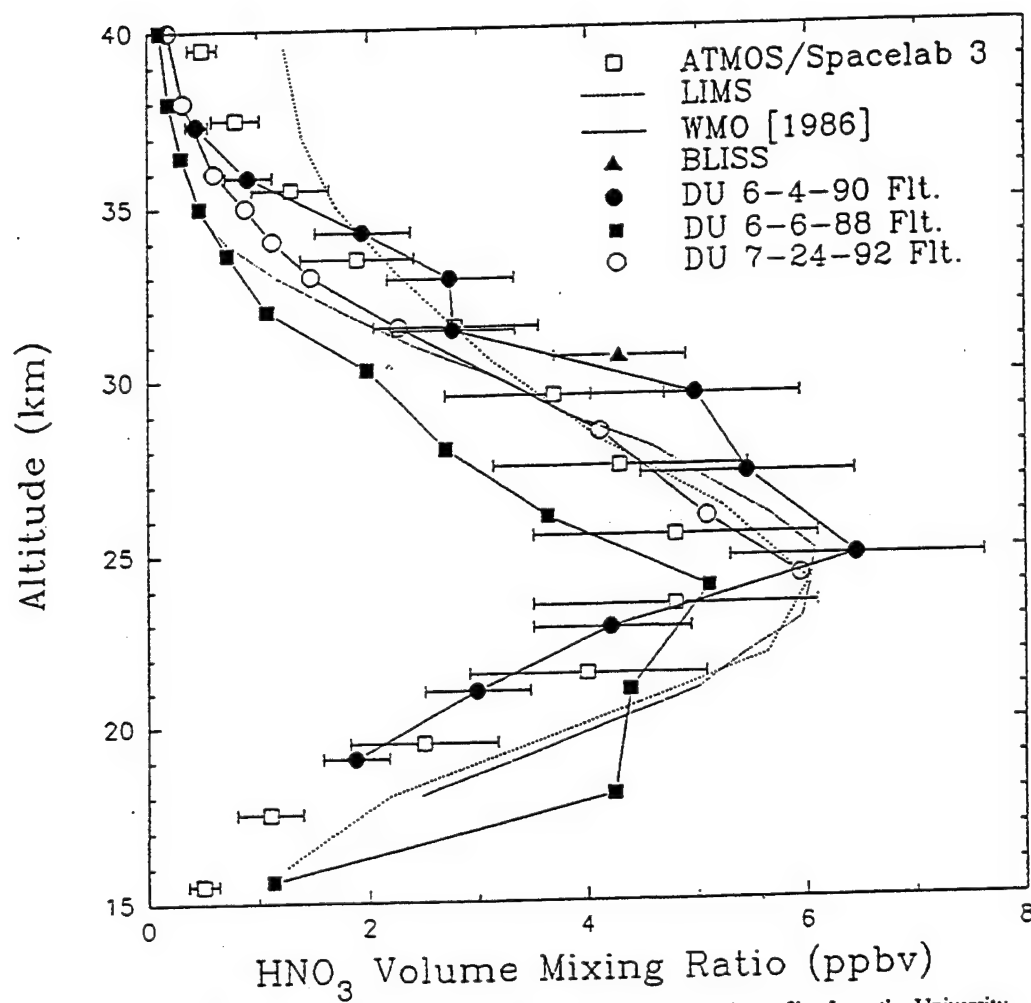


Fig. 7. Comparison of the recent retrievals of  $\text{HNO}_3$  mixing ratio altitude profiles from the University of Denver balloon flights of 6 June 1988 and 24 July 1992. The D.U. 4 June 1990 results were obtained from the  $v_2$  region.<sup>11</sup> The ATMOS, LIMS, WMO (1986) and BLISS results are from Ref. 12-15 respectively.

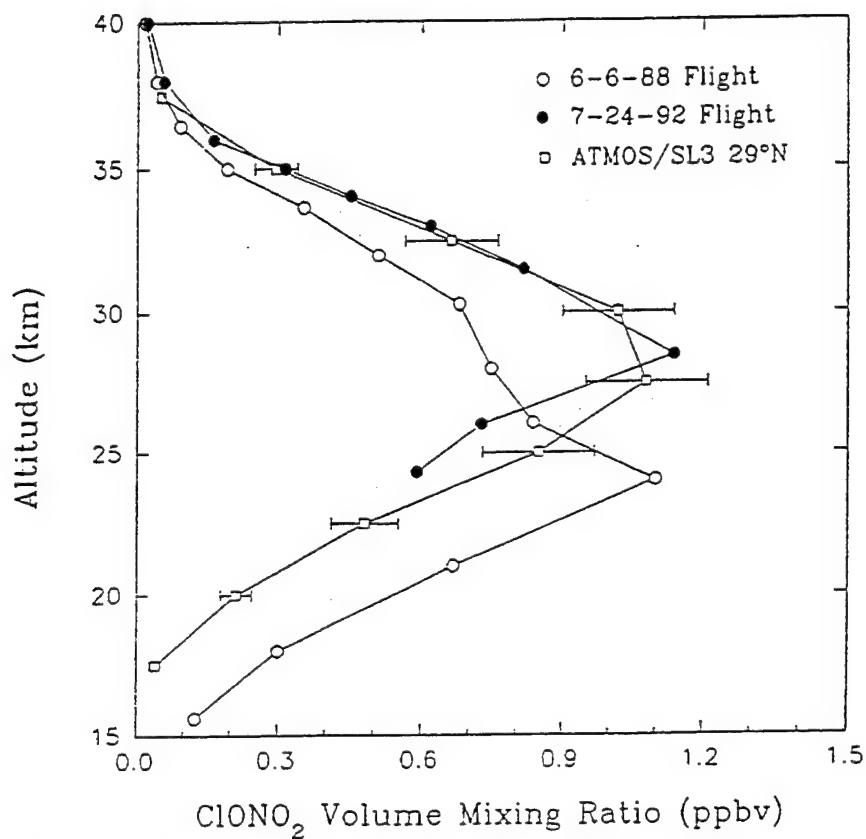


Fig. 8. Comparison of the recent retrievals of  $\text{ClONO}_2$  mixing ratio altitude profiles from the University of Denver balloon flights of 6 June 1988 and 24 July 1992 with previous results of ATMOS.<sup>16</sup>

*Acknowledgements*—This research was supported in part by NSF and in part by NASA. We thank A. G. Maki, J.-M. Flaud, and A. Perrin for providing theoretical results from their HNO<sub>3</sub> studies. Acknowledgement is made to the National Center for Atmospheric Research, which is sponsored by the National Science Foundation, for computer time used in this project.

## REFERENCES

1. A. Goldman, F. J. Murcray, R. D. Blatherwick, J. J. Kusters, F. H. Murcray, D. G. Murcray, and C. P. Rinsland, *J. geophys. Res.* **94**, 14945 (1989).
2. A. Goldman and C. P. Rinsland, *JQSRT* **48**, 653 (1992).
3. A. G. Maki and J. S. Wells, *J. molec. Spectrosc.* **152**, 69 (1992).
4. A. Perrin, V. Jaquen, A. Valentin, J.-M. Flaud and C. Camy-Peyret, *J. molec. Spectrosc.* **157**, 112 (1993); A. Perrin, J.-M. Flaud, C. Camy-Peyret, V. Jaquen, R. Farrenq, F. Guelachvili, Q. Kou, F. Le Roy, M. Morillon-Chapey, J. Orphal, M. Badaoui, J.-Y. Mandin, and V. Dana, *J. molec. Spectrosc.* **160**, 524 (1993).
5. L. P. Giver, F. P. J. Valero, D. Goorvitch, and F. S. Bonomo, *J. opt. Soc. Am. B.* **1**, 715 (1984).
6. J. Ballard, W. B. Johnston, M. R. Gunson, and P. T. Wassel, *J. geophys. Res.* **93**, 1659 (1988).
7. S. T. Massie and A. Goldman, *JQSRT* **48**, 713 (1992).
8. W. Bell, G. Duxbury, and D. D. Stuart, *J. molec. Spectrosc.* **152**, 283 (1992).
9. E. Niple, W. G. Mankin, A. Goldman, D. G. Murcray, and F. J. Murcray, *Geophys. Res. Lett.* **7**, 489 (1980).
10. C. P. Rinsland, A. Goldman, F. J. Murcray, D. G. Murcray, M. A. H. Smith, R. K. Seals Jr., J. C. Larsen, and P. L. Rinsland, *Appl. Opt.* **21**, 4351 (1982).
11. A. Goldman, F. J. Murcray, R. D. Blatherwick, J. J. Kusters, D. G. Murcray, C. P. Rinsland, J.-M. Flaud, and C. Camy-Peyret, *J. geophys. Res.* **97**, 2561 (1992).
12. J. M. Russel III, C. B. Farmer, C. P. Rinsland, R. Zander, L. Froidevaux, G. C. Toon, B. Gao, J. Shaw, and M. Gunson, *J. geophys. Res.* **93**, 1718 (1988).
13. J. C. Gille, J. M. Russel III, P. L. Bailey, E. E. Remsberg, L. L. Gordley, W. F. J. Evans, H. Fischer, B. W. Gandrud, A. Girard, J. E. Harries, and S. A. Beck, *J. geophys. Res.* **89**, 5179 (1984); J. C. Gille, P. L. Bailey, and C. A. Craig, *Adv. Space Res.* **13**, 59 (1993).
14. World Meteorological Organization (WMO), "Atmospheric Ozone 1985—Assessment of our understanding of the processes controlling its present distribution and change", *WMO Rep. 16*, Geneva (1986).
15. R. D. May and C. R. Webster, *J. geophys. Res.* **94**, 16343 (1989).
16. R. Zander, M. R. Gunson, J. C. Foster, C. P. Rinsland, and J. Namkung, *J. geophys. Res.* **95**, 20519 (1990).
17. J. L. Mergenthaler, J. B. Kumer, A. E. Roche, R. W. Nightingale, D. G. Murcray, F. J. Murcray, J. W. Williams, and A. Goldman, AGU 1993 fall meeting, San Francisco, Paper A12D-2 (1993).

### APPENDIX 3

*Journal of Atmospheric Chemistry* 16: 31–40, 1993.  
© 1993 Kluwer Academic Publishers. Printed in the Netherlands.

31

## Stratospheric $\text{N}_2\text{O}_5$ , $\text{CH}_4$ , and $\text{N}_2\text{O}$ Profiles from IR Solar Occultation Spectra

C. CAMY-PEYRET, J.-M. FLAUD, and A. PERRIN

*Laboratoire de Physique Moléculaire et Applications\*, CNRS Université Pierre and Marie Curie,  
Paris, France*

C. P. RINSLAND

*Atmospheric Sciences Division, NASA Langley Research Center, Hampton, Virginia, U.S.A.*

A. GOLDMAN and F. J. MURCRAY

*Department of Physics, University of Denver, Denver, Colorado, U.S.A.*

(Received: 23 January 1992; in final form: 3 June 1992)

**Abstract.** Stratospheric volume mixing ratio profiles of  $\text{N}_2\text{O}_5$ ,  $\text{CH}_4$ , and  $\text{N}_2\text{O}$  have been retrieved from a set of  $0.052\text{ cm}^{-1}$  resolution (FWHM) solar occultation spectra recorded at sunrise during a balloon flight from Aire sur l'Adour, France ( $44^\circ\text{ N}$  latitude) on 12 October 1990. The  $\text{N}_2\text{O}_5$  results have been derived from measurements of the integrated absorption by the  $1246\text{ cm}^{-1}$  band. Assuming a total intensity of  $4.32 \times 10^{-17}\text{ cm}^{-1}/\text{molecule cm}^{-2}$  independent of temperature, the retrieved  $\text{N}_2\text{O}_5$  volume mixing ratios in ppbv (parts per billion by volume,  $10^{-9}$ ), interpolated to 2 km height spacings, are  $1.64 \pm 0.49$  at 37.5 km,  $1.92 \pm 0.56$  at 35.5 km,  $2.06 \pm 0.47$  at 33.5 km,  $1.95 \pm 0.42$  at 31.5 km,  $1.60 \pm 0.33$  at 29.5 km,  $1.26 \pm 0.28$  at 27.5 km, and  $0.85 \pm 0.20$  at 25.5 km. Error bars indicate the estimated  $1-\sigma$  uncertainty including the error in the total band intensity ( $\pm 20\%$  has been assumed). The retrieved profiles are compared with previous measurements and photochemical model results.

**Key words.** Atmospheric composition, middle atmosphere, stratosphere, Fourier transform spectroscopy, balloon measurements, nitrogen oxides, methane.

### 1. Introduction

The odd nitrogen family of molecules (primarily NO,  $\text{NO}_2$ ,  $\text{HNO}_3$ ,  $\text{ClONO}_2$ ,  $\text{HO}_2\text{NO}_2$ , and  $\text{N}_2\text{O}_5$ ) is one of three key chemically-coupled families important in the catalytic destruction of ozone in the stratosphere (Crutzen, 1970) (the others are the odd hydrogen and odd chlorine families). Nitrogen pentoxide ( $\text{N}_2\text{O}_5$ ) is a diurnally-varying reservoir of the odd nitrogen family, and the present work reports the accurate measurement of the profile of this molecule at sunrise.

Only a few measurements of  $\text{N}_2\text{O}_5$  have been reported previously. Roscoe (1982) and Evans (1986) reported tentative observations, based on low-resolution sunrise measurements, which were followed by  $0.015\text{ cm}^{-1}$  resolution solar occultation measurements of the 743,  $1246\text{ cm}^{-1}$ , and  $1720\text{ cm}^{-1}$  bands by the ATMOS Fourier transform spectrometer (FTS) on Spacelab 3 (Toon *et al.*, 1986; Toon,

\* Laboratoire associé aux Universités Pierre et Marie Curie et Paris Sud.

1987; Rinsland *et al.*, 1989), nighttime emission measurements of the  $1246\text{ cm}^{-1}$  band with a balloon-borne FTS (Kunde *et al.*, 1988), and morning emission measurements of the same band with a balloon-borne FTS (Blatherwick *et al.*, 1989).

The present work reports additional measurements of the  $1246\text{ cm}^{-1}$   $\text{N}_2\text{O}_5$  band obtained at sunrise with a high-resolution balloon-borne FTS operating in the solar occultation mode. The  $1246\text{ cm}^{-1}$  band is overlapped by absorption from a number of other atmospheric gases, principally  $\text{CH}_4$  and  $\text{N}_2\text{O}$ , and to a lesser extent molecules such as  $\text{CO}_2$ ,  $\text{H}_2\text{O}$ , and  $\text{COF}_2$ . To obtain accurate corrections for  $\text{CH}_4$  and  $\text{N}_2\text{O}$  interferences, the profiles of both constituents have also been retrieved from the spectra, and those results are also reported.

## 2. Measurements, Data Analysis, and Results

Table I summarizes the most important parameters of the LPMA (Limb Profile Monitor of the Atmosphere) instrument and the balloon flight data of 12 October 1990, which are analyzed here. Instrumental details have been discussed by Camy-Peyret *et al.* (1991); note that a revised set of flight parameters are reported here. Briefly, the LPMA instrument is a rapid-scanning Bomem, Inc. model DA2.01 FTS, which used a HgTdTc detector and a KCl beamsplitter to cover the 800 to  $1400\text{ cm}^{-1}$  region during this balloon flight. The spectral signal-to-rms noise of a single scan exceeded 100 in the region of the  $1246\text{ cm}^{-1}$   $\text{N}_2\text{O}_5$  band. About 40 good spectra were recorded between solar elevation angles of  $-5.42^\circ$  and  $2.47^\circ$  from the float altitude of 40.1 km. This altitude was derived from measurements by an onboard pressure transducer which were converted to altitude from a correlative pressure-temperature profile (discussed below). The effective instrument resolution was about  $0.052\text{ cm}^{-1}$  FWHM (full width half maximum absorption). The field of view (FOV) of the instrument (see Table I) as determined by an iris of 0.6 mm at the detector and by the focal length of the output collimator (100 mm) is  $6 \times 10^{-3}$  rd, i.e. about 2/3 of the angular diameter of the sun. This FOV translates into a vertical span at the limb of about 2.3 km at a tangent height of 30 km. The

Table I. Measurement parameters for the 12 October 1990 balloon flight

Parameter	Value
Launch site	Aire sur l'Adour, France ( $43.7^\circ\text{ N}$ , $359.7^\circ\text{ E}$ )
Float altitude	$40.1 \pm 0.2\text{ km}$
Instrument	Bomem DA2.01 Michelson-type interferometer
Spectral coverage	$800\text{--}1400\text{ cm}^{-1}$ ( $7\text{--}12.5\text{ }\mu\text{m}$ )
Spectral resolution	$0.052\text{ cm}^{-1}$ FWHM
Field of view	6 mrad
Aperture	40 mm diameter (unobscured)
Scan time	50 s
Detector	HgCdTe (cooled to 77 K)
Beam splitter	KCl

vertical resolution is also limited by the time between consecutive zero path difference crossings (in our case  $2 \times 50$ s), which corresponds to a vertical sampling of about 2.5 km at the altitude range of interest.

A pressure-temperature profile calculated by the National Meteorological Center (M. Gelman, private communication, 1991) for the time and location of the balloon flight has been adopted for the analysis. Refracted ray paths for each spectrum were calculated using the FSCATM program (Gallery *et al.*, 1983) and the geometric parameters of the experiment. The time of recording the zero path difference signal was used in computing the solar zenith angles (Park, 1982; Kyle and Blatherwick, 1984).

A nonlinear least-squares spectral fitting procedure (e.g., Rinsland *et al.*, 1982) was used to retrieve the  $\text{CH}_4$  and  $\text{N}_2\text{O}$  profiles. The effective instrument line shape was first determined by least-squares fitting isolated  $\text{CH}_4$  lines in a high signal-to-noise spectrum produced by averaging all of the spectra with zenith angles less than  $90^\circ$ . The retrieved instrument function was held fixed during the subsequent retrievals. Independent onion-peeling retrievals were run using each of the spectral intervals listed in Table II. A sample fit is shown in Figure 1. The final profiles have been obtained by averaging the results from the different intervals. Line parameters from the 1991 HITRAN compilation (L. S. Rothman, unpublished results, 1991) were assumed in the analysis.

Figures 2 and 3 show comparisons of the retrieved profiles with in-situ measurements obtained at the same latitude between 1982 and 1985 (Schmidt *et al.*, 1986) and 2-D photochemical model profiles (M. K. W. Ko, private communication, 1991). Error bars represent the total  $1-\sigma$  uncertainty of the present measurements, about 10% for both gases. The error limits were evaluated from sensitivity studies of the effects of uncertainties in each of the assumed parameters. In these studies, retrievals are repeated with each parameter varied by the amount of its estimated uncertainty while all others remain fixed at the assumed values. The total errors are then calculated from the RSS (square root of the sum of the squares) of the indi-

Table II. Spectral intervals used in the  $\text{CH}_4$  and  $\text{N}_2\text{O}$  retrievals

Interval ( $\text{cm}^{-1}$ )	Notes
1242.00–1247.00	$\text{CH}_4$ profile. $\text{N}_2\text{O}$ below 30 km <sup>a</sup>
1253.00–1255.30	$\text{CH}_4$ profile. $\text{N}_2\text{O}$ below 30 km
1262.63–1262.96	$\text{N}_2\text{O}$ above 30 km
1264.62–1264.84	$\text{N}_2\text{O}$ above 30 km
1270.01–1270.25	$\text{N}_2\text{O}$ above 30 km
1272.73–1273.08	$\text{N}_2\text{O}$ above 30 km
1273.60–1273.85	$\text{N}_2\text{O}$ above 30 km

<sup>a</sup> Significant interference by  $\text{H}_2\text{O}$  and  $\text{CO}_2$  absorptions. The profiles of both gases were adjusted as part of the fitting procedure.



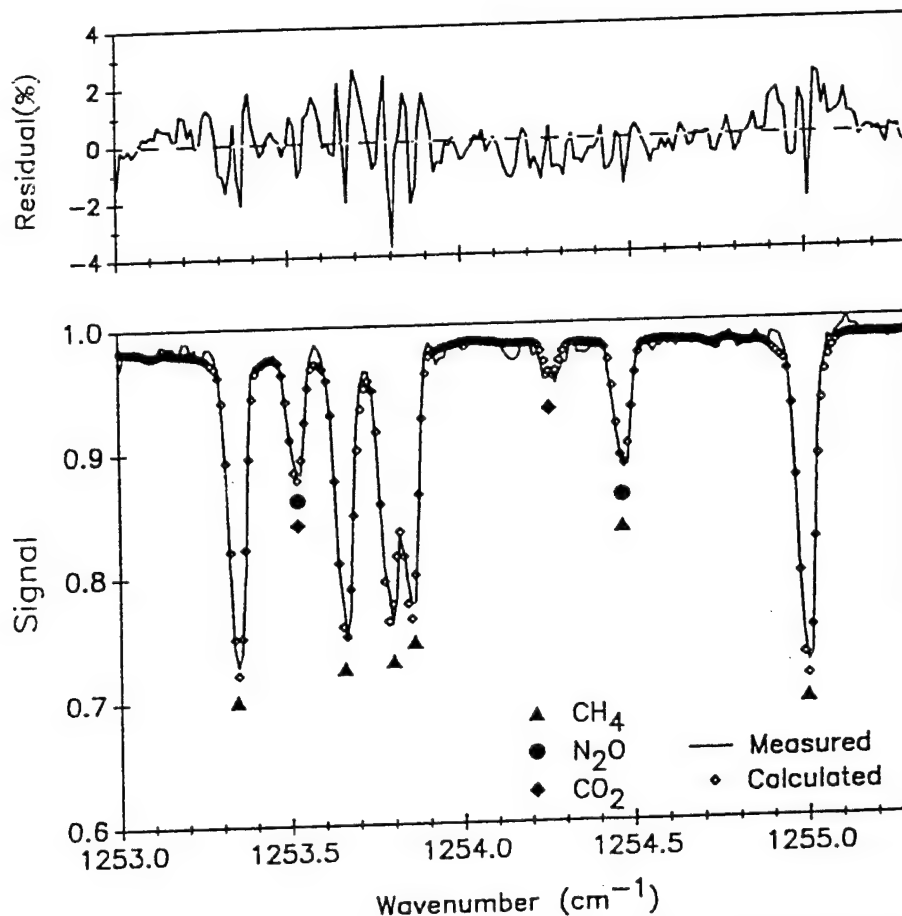


Fig. 1. Sample least-squares fit to a balloon-borne solar spectrum recorded at an astronomical zenith angle of  $92.77^\circ$ , which corresponded to a refracted tangent height of 32.6 km. The bottom panel shows the measured and best-fit calculated spectra while the residuals (measured minus calculated values) are shown on an expanded vertical scale at top. Identifications of the stronger absorption features are given beneath the observed spectrum. No unknown lines appear in this window, and the deviations between measurement and calculation are principally caused by noise and by imperfections in the modeling of the instrument function.

vidual errors. The error sources and the average uncertainty in the retrieved volume mixing ratios resulting from each are (1) uncertainty in the assumed spectroscopic line parameters ( $\pm 4\%$ ), (2) uncertainty in the assumed pressure-temperature profile ( $\pm 2\%$ ), (3) uncertainty in the observational geometry (errors in the pointing angle and balloon float altitude) ( $\pm 5\%$ ), (4) uncertainty due to finite instrument signal-to-noise ( $\pm 5\%$ ), (5) uncertainty in modeling of the instrument line shape function ( $\pm 4\%$ ), and (6) uncertainty due to zero signal level offsets and weak channel spectra ( $\pm 3\%$ ). These last two sources of uncertainty are rather typical of Fourier transform spectra. They are minimal in the present experiment. The

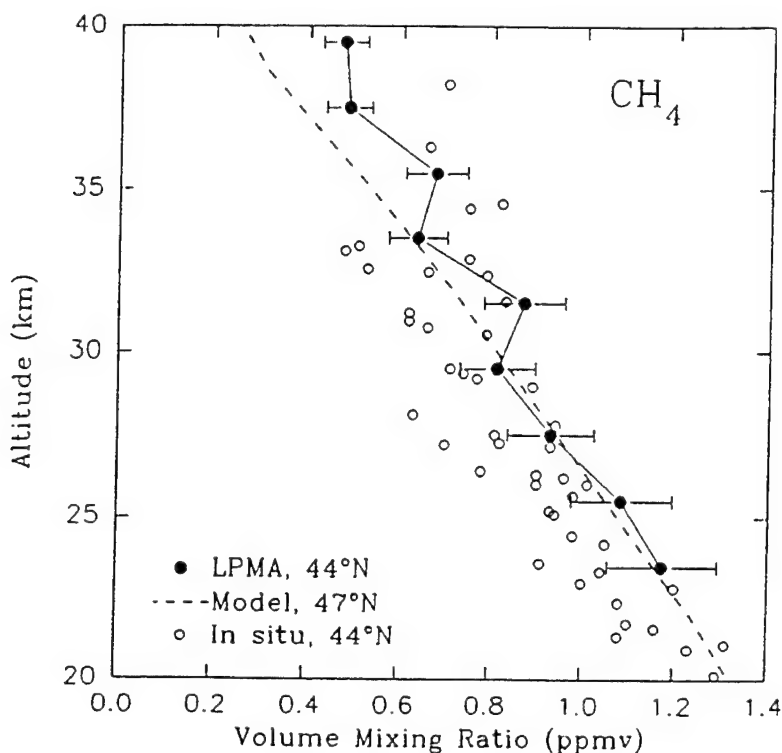


Fig. 2. Comparison of the retrieved LPMA  $\text{CH}_4$  profile with in-situ measurements at  $44^\circ\text{N}$  obtained between 1982 and 1985 (Schmidt *et al.*, 1986) and a 2-D photochemical model profile computed for  $47^\circ\text{N}$  latitude and the date of the LPMA measurements (M. K. W. Ko, private communication, 1991).

zero level can be checked on the edges of the bandpass and at the bottoms of saturated absorption features ( $\text{H}_2\text{O}$  and  $\text{O}_3$  lines). Channel spectra, resulting from the combined effects of using a filter for isolating the spectral region of interest and a germanium window for rejecting the visible-UV part of the solar spectrum, are observable but rather weak. On a relative basis, the agreement between the infrared and in-situ measurements is very good. The mean and the standard deviation of the ratio of the IR volume mixing ratios to the in-situ data are  $1.13 \pm 0.18$  for  $\text{CH}_4$  and  $1.34 \pm 0.47$  for  $\text{N}_2\text{O}$ . The larger standard deviation for  $\text{N}_2\text{O}$  reflects the larger scatter in the in-situ measurements. About half of the offset between the  $\text{CH}_4$  data-sets can be attributed to the long-term increase in  $\text{CH}_4$  between the time of the in-situ measurements (1983–1985) and our flight experiment (1990). The rate of  $\text{CH}_4$  increase at the surface is about 1% per year (e.g., Khalil and Rasmussen, 1990).

Analysis of the spectra to retrieve the  $\text{N}_2\text{O}_5$  profile has followed the procedures described previously (Rinsland *et al.*, 1989). In this method, microwindows spaced about  $1\text{ cm}^{-1}$  apart between  $1210$  and  $1270\text{ cm}^{-1}$ , as given in Table 2 of Rinsland *et al.* (1989), were used to measure the integrated absorption by the  $\text{N}_2\text{O}_5$  band. The

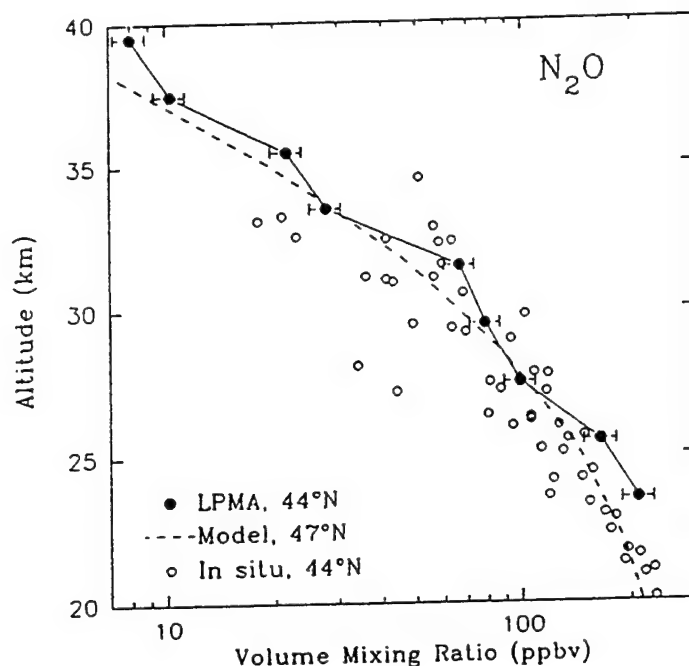


Fig. 3. Comparison of the retrieved LPMA  $\text{N}_2\text{O}$  profile with in-situ measurements at  $44^\circ\text{N}$  obtained between 1982 and 1985 (Schmidt *et al.*, 1986) and a 2-D photochemical model profile computed for  $47^\circ\text{N}$  latitude and the date of the LPMA measurements (M. K. W. Ko, private communication, 1991). Even at the lowest level for which we have retrieved the  $\text{N}_2\text{O}$  mixing ratio, the agreement between our determinations and the in-situ measurements is compatible with the error bars of each technique.

measurements were made on ratio spectra computed by dividing the individual low sun spectra by an average high sun spectrum obtained by coadding all spectra with zenith angles less than  $90^\circ$ . Corrections for residual atmospheric absorption in the microwindows were derived from simulations calculated with the retrieved  $\text{CH}_4$  and  $\text{N}_2\text{O}$  profiles. Reference volume mixing ratio profiles (e.g., the compilation of Smith (1982)) were assumed for calculating the absorption by other gases in this region. All of the species on the 1991 HITRAN compilation (L. S. Rothman, unpublished results, 1991) were included in the calculations.

Figure 4 shows a sequence of microwindow measurements from several of the spectra. The growth of the  $\text{N}_2\text{O}_5$  band absorption with decreasing tangent height is readily apparent. Dashed lines show the fitted 100% transmittance level for two of the spectra. Equivalent widths of the  $\text{N}_2\text{O}_5$  band have been obtained by integrating the absorption between  $1226$  and  $1265\text{ cm}^{-1}$ . The results from spectra with the same zero path difference crossing times agree within the uncertainties and have been averaged. These times correspond to the short period at zero path difference for reverse and forward scans (one sided interferograms) recorded by the present instrument.

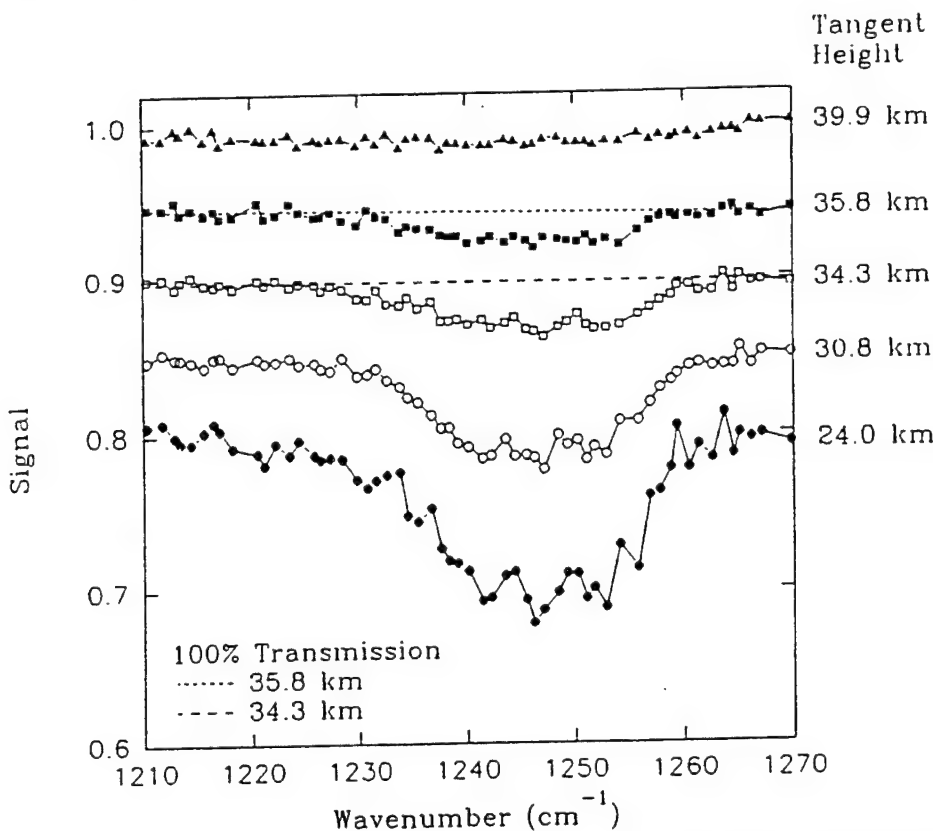


Fig. 4. Examples of microwindow measurements in the region of the  $1246 \text{ cm}^{-1}$  band of  $\text{N}_2\text{O}_5$ . The values from each scan, which have been corrected for residual absorption by other gases, are shown on the same scale, but have been offset vertically for clarity. Refracted tangent heights of the spectra are given at right. Dashed lines show 100% transmission levels determined by fitting the microwindow measurements from  $1210$  to  $1226 \text{ cm}^{-1}$  and  $1265$  to  $1270 \text{ cm}^{-1}$ .

The profile of  $\text{N}_2\text{O}_5$  has been derived from the measured equivalent widths using the onion-peeling retrieval method and an assumed temperature-independent band intensity of  $4.32 \times 10^{-17} \text{ cm}^{-1}/\text{molecule cm}^{-2}$ . This value is the same as adopted previously (Toon *et al.*, 1986; Rinsland *et al.*, 1989). Recently, Roscoe (1991) reviewed the published laboratory and atmospheric measurements of  $\text{N}_2\text{O}_5$  and recommended an integrated  $1246 \text{ cm}^{-1}$   $\text{N}_2\text{O}_5$  band intensity of  $4.01 \times 10^{-17} \text{ cm}^{-1}/\text{molecule cm}^{-2}$ . If this lower value is assumed, the published ATMOS measurements and those reported in this study need to be multiplied by a factor of 1.077.

Figure 5 presents a comparison of our retrieved  $\text{N}_2\text{O}_5$  profile with previous published measurements and two photochemical model calculations performed for conditions corresponding to the ATMOS/Spacelab 3 sunrise measurements at  $47^\circ \text{ S}$  on 1 May 1985. Error bars on the LPMA profile increase with altitude, ranging from 22 to 30%. The uncertainty is dominated by the absolute uncertainty of

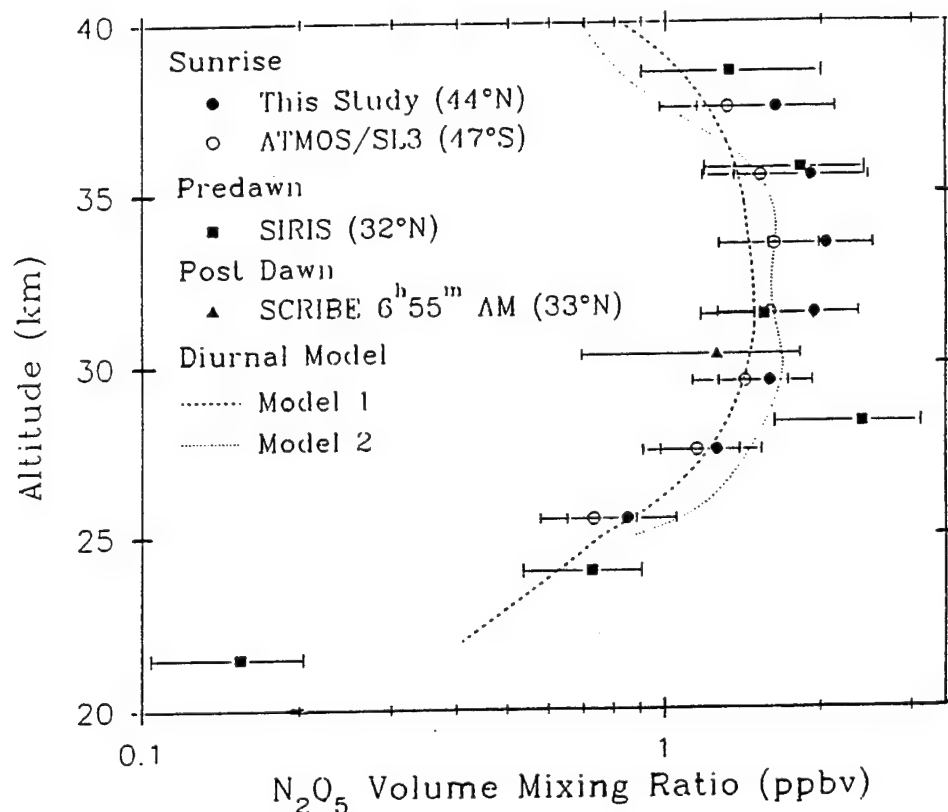


Fig. 5. Comparison of  $\text{N}_2\text{O}_5$  volume mixing ratio profiles measured at sunrise by the LPMA and ATMOS instruments, predawn values retrieved from spectra recorded by the SIRIS instrument (Kunde *et al.*, 1988), a post-sunrise measurement retrieved from a spectrum recorded with the SCRIBE instrument (Blatherwick *et al.*, 1989), and photochemical model calculations generated for the conditions of the ATMOS sunrise measurements (1 May 1985, at 47° S latitude). Error bars indicate the 1-sigma uncertainties of the measurements. Models 1 and 2 denote the model calculations of M. Natarajan (private communication, 1989) and Allen and Delitsky (1990, Fig. 3), respectively. The latter study reported profiles derived with three different values assumed for the  $\text{N}_2\text{O}_5$  absorption cross sections; the curve plotted in this figure (model 2) corresponds to the profile computed with the  $\text{N}_2\text{O}_5$  cross sections recommended by DeMore *et al.* (1987).

20% in the assumed  $\text{N}_2\text{O}_5$  band intensity at stratospheric temperatures. Errors in the equivalent width measurements are also important at the higher tangent altitudes ( $>35$  km), where the  $\text{N}_2\text{O}_5$  absorption is very weak. Below about 31 km, the LPMA profile is in good agreement with the other data. At higher altitudes, the ATMOS volume mixing ratios and photochemical model profiles are lower than the present results, although there is agreement within the measurement errors. A sunrise  $\text{N}_2\text{O}_5$  volume mixing ratio at 30 km has been calculated by Webster *et al.* (1990) from their simultaneous in-situ measurements of  $\text{NO}$ ,  $\text{NO}_2$ ,  $\text{HNO}_3$ ,  $\text{O}_3$ ,  $\text{N}_2\text{O}$ , pressure, and temperature on 13 September 1988, at 32° N latitude. Our measured value of  $1.70 \pm 0.35$  ppbv at the same altitude is significantly lower than

the computed value of  $2.7 \pm 0.4$  ppbv (Webster *et al.*, 1990) (not plotted in the figure). Our measurement results for  $\text{CH}_4$ ,  $\text{N}_2\text{O}$ , and  $\text{N}_2\text{O}_5$  are summarized in Table III. For convenience, the profiles have been interpolated to 2 km altitude spacings. The error limits quoted for all three gases are believed to be conservative.

### 3. Summary and Conclusions

Profiles of  $\text{N}_2\text{O}_5$ ,  $\text{CH}_4$ , and  $\text{N}_2\text{O}$  have been retrieved from  $0.052 \text{ cm}^{-1}$  resolution (FWHM) solar occultation spectra recorded at sunrise near  $44^\circ \text{ N}$  latitude with a balloon-borne Michelson interferometer. The measured profiles have been compared with previous measurements and photochemical model calculations. The agreement is generally good.

The measured spectra contain absorption features of a number of additional stratospheric gases, such as  $\text{HNO}_3$ ,  $^{16}\text{O}_3$ ,  $^{16}\text{O}^{16}\text{O}^{18}\text{O}$ ,  $\text{CCl}_2\text{F}_2$ , and  $\text{CCl}_3\text{F}$ . Work on the analysis of these gases as well as spectra recorded during other balloon flights is in progress.

### Acknowledgements

The authors thank M. K. W. Ko of AER, Inc., Cambridge, Mass., U.S.A., for sending  $\text{CH}_4$  and  $\text{N}_2\text{O}$  photochemical model profiles to compare with the LPMA measurements. Financial support by Programme Atmosphère Moyenne of CNRS together with support from CEC/STEP funding through the SIUBEX project are acknowledged for the balloon flight and instrumentation. Research at the University of Denver is supported by the National Aeronautics and Space Administration.

Table III. Retrieved volume mixing ratio profiles

Altitude (km)	Pressure (mbar)	Temperature (K)	Volume mixing ratio		
			$\text{CH}_4$ (ppmv)	$\text{N}_2\text{O}$ (ppbv)	$\text{N}_2\text{O}_5$ (ppbv)
39.5	3.0	246.2	0.48 (5)	8.0 (7)	—
37.5	4.0	241.7	0.49 (5)	10.3 (10)	1.64 (49)
35.5	5.3	237.0	0.68 (7)	22 (2)	1.92 (56)
33.5	7.1	231.5	0.64 (6)	28 (3)	2.06 (47)
31.5	9.5	226.0	0.87 (9)	66 (6)	1.95 (42)
29.5	12.8	223.0	0.81 (8)	79 (8)	1.60 (33)
27.5	17.5	220.4	0.93 (9)	99 (10)	1.26 (28)
25.5	23.8	217.9	1.08 (11)	165 (17)	0.85 (20)
23.5	32.4	215.6	1.17 (12)	209 (21)	—

ppmv =  $10^{-6}$  per unit volume, ppbv =  $10^{-9}$  per unit volume. Values enclosed in parentheses are 1- $\sigma$  total uncertainties in units of the last quoted digit.

## References

- Allen, M. and Delitsky, M. L., 1990. Stratospheric NO, NO<sub>2</sub>, and N<sub>2</sub>O<sub>5</sub>: A comparison of model results with Spacelab 3 atmospheric trace molecule spectroscopy (ATMOS) measurements. *J. Geophys. Res.* **95**, 14077–14082.
- Blatherwick, R. D., Murcray, D. G., Murcray, F. H., Murcray, F. J., Goldman, A., Vanasse, G. A., Massie, S. T., and Cicerone, R. J., 1989. Infrared emission measurements of morning stratospheric N<sub>2</sub>O<sub>5</sub>. *J. Geophys. Res.* **94**, 18337–18340.
- Camy-Peyret, C., Flaud, J.-M., and Perrin, A., 1991. Balloon-borne solar occultation Fourier transform spectrometry for measurements of stratospheric trace species. *ESA Publ. SP-317*, pp. 179–186.
- Cantrell, C. A., Davidson, J. A., McDaniel, A. H., Shetter, R. E., and Calvert, J. G., 1988. Infrared absorption cross sections for N<sub>2</sub>O<sub>5</sub>. *Chem. Phys. Lett.* **148**, 358–363.
- Crutzen, P. J., 1970. The influence of nitrogen oxides on atmospheric ozone content. *Quart. J. R. Met. Soc.* **96**, 320–325.
- DeMore, W. B., Molina, M. J., Sander, S. P., Golden, D. M., Hampson, R. F., Kurzo, M. J., Howard, C. J., and Ravishankara, A. R., 1987. Chemical kinetics and photochemical data for use in stratospheric modeling. *JPL Publ.* 87-41.
- Evans, W. F. J., 1986. Observation of the 8-μm N<sub>2</sub>O<sub>5</sub> thermal emission feature in the stratosphere. *Appl. Opt.* **25**, 1866–1868.
- Gallery, W. O., Kneizys, F. X., and Clough, S. A., 1981. Air mass computer program for atmospheric transmittance/radiance calculation: FSCATM. AFGL-TR-83-0065. Environmental Research Paper No. 828. Air Force Geophysics Laboratory, Hanscom Air Force Base, Mass.
- Khalil, M. A. K. and Rasmussen, R. A., 1990. Atmospheric methane: Recent global trends. *Environ. Sci. Technol.* **24**, 549–553.
- Kunde, V. G., Brasunas, J. C., Maguire, W. C., Herman, J. R., Massie, S. T., Abbas, M. M., Herath, L. W., and Shaffer, W. A., 1988. Measurement of nighttime stratospheric N<sub>2</sub>O<sub>5</sub> from infrared emission spectra. *Geophys. Res. Lett.* **15**, 1177–1180.
- Kyle, T. G. and Blatherwick, R., 1984. Smearing of interferograms in Fourier transform spectroscopy. *Appl. Opt.* **23**, 261–263.
- Park, J. H., 1982. Effect of interferogram smearing on atmospheric limb sounding by Fourier transform spectroscopy. *Appl. Opt.* **21**, 1356–1366.
- Rinsland, C. P., Goldman, A., Murcray, F. J., Murcray, D. G., Smith, M. A. H., Seals, R. K. Jr., Larsen, J. C., and Rinsland, P. L., 1982. Stratospheric N<sub>2</sub>O mixing ratio profile from high-resolution balloon-borne solar absorption spectra and laboratory spectra near 1880 cm<sup>-1</sup>. *Appl. Opt.* **21**, 4351–4355.
- Rinsland, C. P., Toon, G. C., Farmer, C. B., Norton, R. H., and Namkung, J. S., 1989. Stratospheric N<sub>2</sub>O<sub>5</sub> profiles at sunrise and sunset from further analysis of the ATMOS/Spacelab 3 solar spectra. *J. Geophys. Res.* **94**, 18341–18349.
- Roscoe, H. K., 1982. Tentative observation of stratospheric N<sub>2</sub>O<sub>5</sub>. *Geophys. Res. Lett.* **9**, 901–902.
- Roscoe, H. K., 1991. Review and revision of measurements of stratospheric N<sub>2</sub>O<sub>5</sub>. *J. Geophys. Res.* **96**, 10879–10884.
- Schmidt, U., Jebsen, C., Johnen, F. J., Khedim, A., Klein, E., Knapska, D., Kulesa, G., Rudolph, J., Schumacher, G., and Schunck, E., 1986. Stratospheric observations of long-lived trace gases at midlatitudes 1982–1985 (data report), Kernforschungsanlage Jülich GmbH. Institut für Chemie: Atmosphärische Chemie, Jülich, Germany.
- Smith, M. A. H., 1982. Compilation of atmospheric gas concentration profiles from 0 to 50 km, NASA Tech Memo., TM 83289. (Available as NTIS 82N22822 from the Natl. Tech. Inf. Serv., Springfield, Va.)
- Toon, G., 1987. Reply: Detection of stratospheric nitrogen species. *Nature* **330**, 427.
- Toon, G. C., Farmer, C. B., and Norton, R. H., 1986. Detection of stratospheric N<sub>2</sub>O<sub>5</sub> by infrared remote sounding. *Nature* **319**, 570–571.
- Webster, C. R., May, R. D., Toumi, R., and Pyle, J. A., 1990. Active nitrogen partitioning and the nighttime formation of N<sub>2</sub>O<sub>5</sub> in the stratosphere: Simultaneous in-situ measurements of NO, NO<sub>2</sub>, HNO<sub>3</sub>, O<sub>3</sub>, and N<sub>2</sub>O using the BLISS diode laser spectrometer. *J. Geophys. Res.* **95**, 13851–13866.

## APPENDIX 4

The  $\nu_2$  and  $2\nu_2 - \nu_2$  bands of  $^{14}\text{N } ^{16}\text{O}_2$ : Electron Spin-Rotation and Hyperfine Contact Resonances in the (010) Vibrational StateA. PERRIN,\* J.-M. FLAUD,\* C. CAMY-PEYRET,\* A. GOLDMAN,† F. J. MURCRAY,†  
R. D. BLATHERWICK,† AND C. P. RINSLAND‡

\*Laboratoire de Physique Moléculaire et Applications,<sup>1</sup> CNRS, Université P. et M. Curie, Bte 76,  
4 Place Jussieu, 75252 Paris Cedex 05, France; †Department of Physics, University of Denver,  
Denver, Colorado 80208; and ‡Atmospheric Sciences Division, NASA Langley Research Center,  
Hampton, Virginia 23681-0001

High-resolution Fourier transform spectra covering the 720–920  $\text{cm}^{-1}$  spectral region have been used to perform a reanalysis of the  $\nu_2$  band ((010)–(000) vibrational transition) together with the first analysis of the  $2\nu_2 - \nu_2$  hot band of nitrogen dioxide ((020)–(010) vibrational transition). The high-quality spectra show that, for numerous  $\nu_2$  lines, the hyperfine structure is easily observable in the case of resonances due to the hyperfine Fermi-type operator. By performing a full treatment of the spin-rotation and of the hyperfine operators, a new line list of the  $\nu_2$  band (positions and intensities) has been generated, and it is in excellent agreement with the experimental spectrum. Also, a thorough analysis of the  $2\nu_2 - \nu_2$  hot band has been performed leading to an extended set of new (020) spin-rotation levels. These levels, together with the {(100), (020), (001)} spin-rotation levels deduced previously from the analysis of the  $\nu_1$ ,  $2\nu_2$ , and  $\nu_3$  cold bands performed in the 6.3- to 7.5- $\mu\text{m}$  spectral range [A. Perrin, J.-M. Flaud, C. Camy-Peyret, A.-M. Vasserot, G. Guelachvili, A. Goldman, F. J. Murcray, and R. D. Blatherwick, *J. Mol. Spectrosc.* **154**, 391–406 (1992)] were least-squares fitted, allowing one to derive a new set of vibrational band centers and rotational, spin-rotation, and interaction constants for the {(100)(020)(001)} interacting states of  $^{14}\text{N } ^{16}\text{O}_2$ . © 1993 Academic Press, Inc.

## I. INTRODUCTION

The cold  $\nu_2$  band and the  $2\nu_2 - \nu_2$  first hot band of nitrogen dioxide, located at 13  $\mu\text{m}$ , correspond, respectively, to the (010)–(000) and (020)–(010) vibrational transitions of this molecule; consequently, in order to have accurate line positions it is necessary to have precise parameters for both the upper and the lower vibrational states involved in these transitions.

For the (000) and (010) vibrational states, the most recent spectroscopic parameters were obtained from a simultaneous fit of the available microwave or double resonance data (Refs. (1–8) and (9, 10) for the (000) and (010) state, respectively) and of the infrared spin-rotation energy levels obtained from recent analyses of Fourier transform spectra recorded in the far infrared (11) and in the 13.3- $\mu\text{m}$  (12) spectral regions.

In the analysis of the (000)–(000) band, even at the high resolution of the far-infrared experimental spectra, the hyperfine structure is usually *not* detectable, except in cases of *local* resonances due to the Fermi contact hyperfine operator. Accordingly, the line list (11, 13, 14) of the pure rotation region of  $\text{NO}_2$  ( $\sim 0$ –200  $\text{cm}^{-1}$ ) was generated by explicitly taking into account the spin-rotation and hyperfine structures.

On the other hand, this effect could not be observed so accurately in the 13.3- $\mu\text{m}$  experimental spectrum which was used in Ref. (12) for the analysis of the  $\nu_2$  band,

<sup>1</sup> Laboratoire associé aux Universités P. et M. Curie et Paris-Sud.



and consequently the line list (12-14) generated in the 13.3- $\mu\text{m}$  spectral range did not include the hyperfine structure.

For the (020) vibrational state, the most recent spectroscopic parameters were obtained from a recent analysis (15) of the  $\nu_1$ ,  $2\nu_2$ , and  $\nu_3$  bands ((100)-(000), (020)-(000), and (001)-(000) vibrational transitions, respectively) using Fourier transform spectra (15, 16) covering the 6.3- $\mu\text{m}$  region. Actually the (001) state is involved in a strong Coriolis interaction with the (020) and (100) states, and the very weak  $2\nu_2$  band borrows its intensity from the strong  $\nu_3$  band. In fact, only the  $K_a = 0-2$  subbands for  $N \leq 46$  (because they appear in a clear window between  $\nu_1$  and  $\nu_3$ ) and the  $K_a = 6$  subband for  $19 \leq N \leq 62$  (because the corresponding (020) levels are strongly resonating with levels of (001) state) could be analyzed at 6.7  $\mu\text{m}$  (15-17). Finally, it must be pointed out that for the energy level calculations of the {(100), (020), (001)} interacting vibrational states, both the spin-rotation and the vibrational Coriolis-type interactions were explicitly taken into account, but that the hyperfine structure was not considered:

(i) For the  $A$ -type  $\nu_3$  band, which is by far the strongest band at 6.3  $\mu\text{m}$ , the hyperfine resonances affect only some  $\nu_3$  nonresolved doublets, the spin splittings of which vanish in the upper and lower levels of the transition. In this case, the hyperfine structure is blended within the total line width, and the hyperfine components cannot be observed.

(ii) Because of the weakness of the  $\nu_1$  and  $2\nu_2$  bands the hyperfine structures cannot be precisely measured on the spectra and consequently the hyperfine resonances were not considered for these bands.

Using new high-resolution Fourier transform spectra recorded in the 13.3- $\mu\text{m}$  spectral region, we report in this paper a reanalysis of the  $\nu_2$  band (with a full treatment of the hyperfine structure), together with a first analysis of the hot  $2\nu_2 - \nu_2$  band of  $^{14}\text{N } ^{16}\text{O}_2$ .

## II. EXPERIMENTAL DETAILS

The spectra were recorded in the 720-960  $\text{cm}^{-1}$  spectral range at 0.002  $\text{cm}^{-1}$  resolution with the BOMEM Fourier transform spectrometer of the University of Denver. The optical path length was 1 m, and two spectra were recorded at  $\text{NO}_2$  pressures of 1 and 2 Torr. The calibration of the spectra was performed by means of  $\text{N}_2\text{O}$  absorption lines (18, 19) in the 1150-1250  $\text{cm}^{-1}$  region, and the accuracy of the positions of unblended lines is estimated to be  $\sim 0.0002 \text{ cm}^{-1}$ .

## III. ANALYSIS AND LINE POSITION CALCULATIONS

### *The $\nu_2$ Band*

The analysis was started by comparing the experimental line positions to the line list calculated in Ref. (12). Overall, the agreement was excellent except for transitions in which the upper or the lower state are involved in a hyperfine Fermi resonance. Consequently, a new line list was generated for the  $\nu_2$  band, taking into account not only the electron spin-rotation interaction, but also, as described in Ref. (11) for the (000) state, the magnetic hyperfine hamiltonian (i.e., the Fermi contact operator together with the spin-spin dipolar interaction operators) and the nuclear quadrupole interaction. For this calculation we used the vibrational band center, rotational, spin-rotation, and hyperfine constants of Ref. (12) and Ref. (11), respectively, for the upper and lower state of the transition.

The agreement this time proved to be excellent for all the lines. However, we observed a  $-0.0004 \text{ cm}^{-1}$  global shift of the observed line positions relative to the calculated

ones, which is due to a slightly different calibration of the spectra used in the present work (18, 19) compared to that used (20) in 1988. This leads to a different vibrational band center of the  $\nu_2$  band:  $E_{(010)} = 749.652561 \text{ cm}^{-1}$  (instead of  $749.652961 \text{ cm}^{-1}$  obtained previously in Ref. (12)).

To show the quality of the experimental spectra and of the calculations performed in the present work, we show in Figs. 1 and 2 portions around  $771.8$  and  $758.0 \text{ cm}^{-1}$  of the experimental spectra together with line-by-line calculations performed using either the line list generated in Ref. (12) (no hyperfine structure) or the line list derived here (full treatment of the hyperfine operators). In both regions, the improvement brought by the new calculation is very clear.

In the first spectral region, the complex hyperfine structure appears clearly in the  $N = \text{even } {}^RQ_{K_a=1}$  subband. At  $771.30$  and  $771.64 \text{ cm}^{-1}$  it is due to a strong hyperfine resonance involving the  $(010)[22\ 2\ 20]$  and  $(010)[20\ 2\ 18]$  rotational levels. At  $772 \text{ cm}^{-1}$ , since the resonance is weaker, one observes mainly a broadening of the  $N = 18$  doublet structure. The same hyperfine effect can be clearly observed in Fig. 2 around  $758 \text{ cm}^{-1}$  for lines belonging to the  ${}^RQ_{K_a=0}$  subband. It is worth stressing that in both cases the new calculation, which involves the hyperfine operators, reproduces the experimental spectrum with high accuracy.

### *The $2\nu_2 - \nu_2$ Band*

Lines from the  $2\nu_2 - \nu_2$  band were already observed in the experimental spectrum (12) which was used in 1988 for the analysis of the  $13.3\text{-}\mu\text{m}$  band of nitrogen dioxide. However, because this hot band is weak and because the  $(020)$  spectroscopic parameters available at that time were not precise enough (only the  $K_a = 0, 1, 2$   $(020)$  series were derived from the analysis of the  $2\nu_2$  band performed at  $6.6 \mu\text{m}$  (17)), only a few lines involving the  $K_a = 0, 1, 2$   $(020)$  rotational series could be analyzed at  $13.3 \mu\text{m}$ .

The  $(020)$  parameters were recently significantly improved from a new analysis of the  $\{\nu_1, 2\nu_2, \nu_3\}$  interacting bands (15). Indeed, more lines involving the  $K_a = 0, 1, 2$  series were assigned; also, lines involving the  $K_a = 6$  rotational series of  $(020)$ , which borrow their intensities from  $\nu_3$  through a Coriolis interaction, were observed (15, 16).

Consequently, from the  $\{(100), (020), (001)\}$  and  $(010)$  parameters obtained in Ref. (15) and Ref. (12) respectively, it has been possible to better predict the  $2\nu_2 - \nu_2$  line positions, as performed in the present analysis.

Because the  $2\nu_2 - \nu_2$  band is rather weak, only transitions of this band involving  $N \leq 30$  rotational quantum number could be identified in the spectrum. For transitions involving the  $K_a = 0-2$  and  $K_a = 6$   $(020)$  energy levels, the agreement between the observed and the predicted line positions was excellent, but this was not completely the case for lines involving the  $K_a = 3-5$   $(020)$  rotational levels since small discrepancies (up to  $0.0030 \text{ cm}^{-1}$ ) were observed. Using these new data, we then determined the vibrational band centers, rotational, spin-rotation, and coupling constants of the  $\{(100), (020), (001)\}$  resonating states. As in Ref. (15) the Hamiltonian matrix explicitly takes into account both the Coriolis and the spin-rotation interactions. For this least-squares fit calculation, the 164  $(020)$  new spin-rotation energy levels obtained in the present work for  $K_a \leq 6$  and  $N \leq 30$  were combined to the 3230  $(100)$   $(001)$  and  $(020)$  energy levels obtained in Ref. (15).

Table I gives the list of vibrational energies and rotational, spin-rotation, and coupling constants deduced from the fit, together with their estimated uncertainty. The

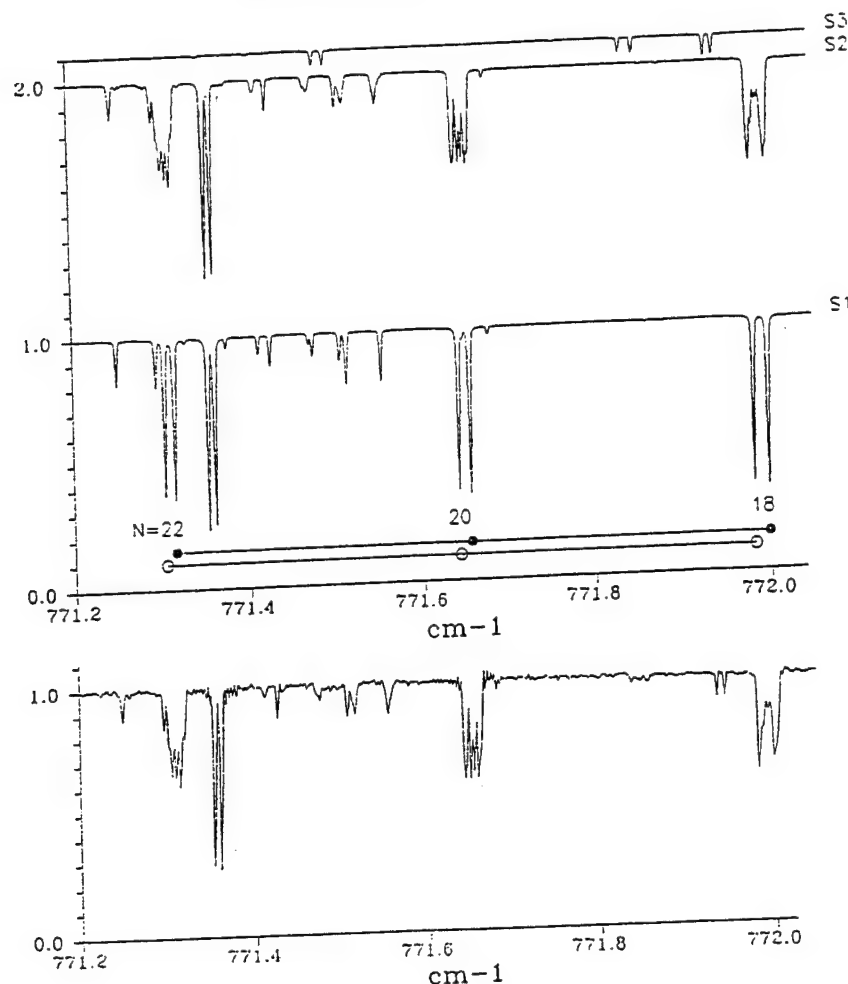


FIG. 1. Experimental spectrum (bottom trace) of nitrogen dioxide around  $771\text{ cm}^{-1}$  and calculated spectra of the absorption due to the  $^{14}\text{N } ^{16}\text{O}_2$  isotopic species: trace S1 and S2 are for the  $\nu_2$  band, respectively, without and with taking into account the hyperfine structure; trace S3 is for the  $2\nu_2 - \nu_2$  hot band (no calculation of the hyperfine structure). All spectra have the same vertical scale but are displaced for clarity. On trace S1 we have marked the rotational transitions belonging to the  $^2Q_{K_a-1}$  subband (black dots and open circles correspond to  $J = N + \frac{1}{2}$  and  $J = N - \frac{1}{2}$ , respectively). The agreement between observation and calculation is excellent.

corresponding statistical analysis of the results is given in Table II. It is clear that significant improvements were obtained in the present calculation for the (020) spin-rotation levels and to a lesser extent for the (001) levels compared with the results obtained previously (15): the percentages of experimental energy levels which are reproduced within  $0.001\text{ cm}^{-1}$  are now 84.5 and 79.1% instead of 69.5 and 77% for (020) and (001), respectively.

#### IV. SYNTHETIC SPECTRA

This section presents the calculations<sup>2</sup> which have been performed in order to generate a precise line list of absorption lines of  $^{14}\text{N } ^{16}\text{O}_2$  in the  $13.3\text{-}\mu\text{m}$  region.

<sup>2</sup> Both calculations were performed for a reference temperature of 296 K using a  $Z(296\text{ K}) = 13\,617.9$  partition function (this value includes the nitrogen nuclear degeneracy).

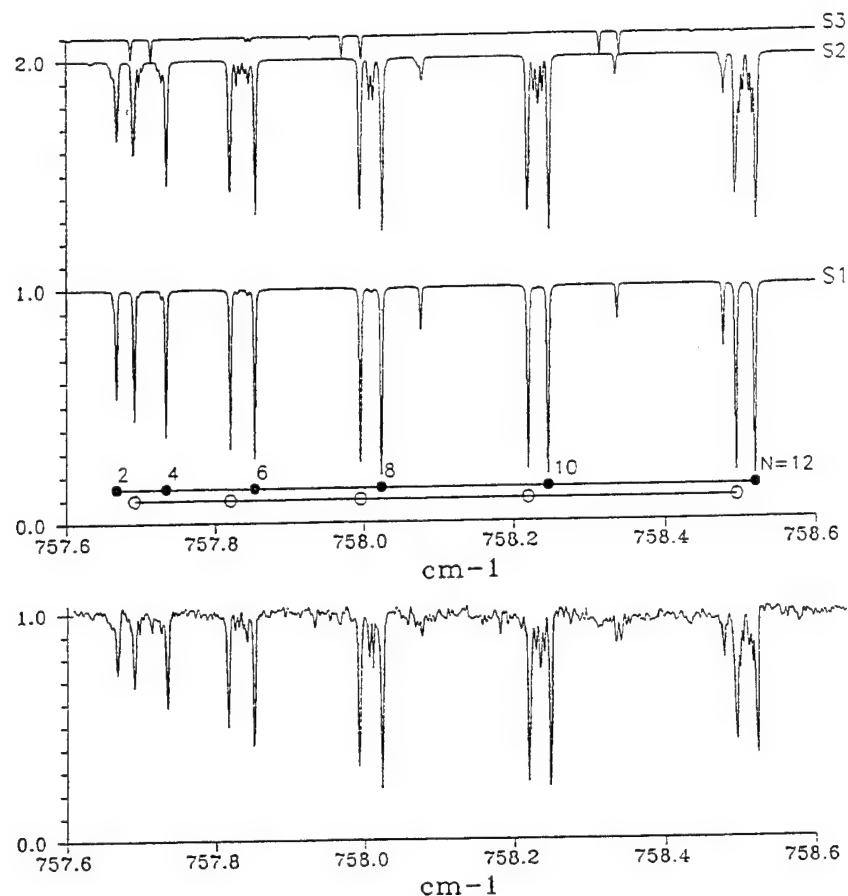


FIG. 2. Experimental spectrum (bottom trace) of nitrogen dioxide around  $758\text{ cm}^{-1}$  and calculated spectra of absorption due to the  $^{14}\text{N}^{16}\text{O}_2$  isotopic species: trace S1 and S2 are for the  $\nu_2$  band, respectively, *without* and *with* taking into account the hyperfine structure; trace S3 is for the  $2\nu_2 - \nu_2$  hot band (no calculation of the hyperfine structure). All spectra have the same vertical scale but are displaced for clarity. On trace S1, we have marked the rotational transitions belonging to the  $^RQ_{K'_2=0}$  subband, (black dots and open circles are for  $J = N + \frac{1}{2}$  and  $J = N - \frac{1}{2}$ , respectively). The agreement between observation and calculation is excellent.

### $\nu_2$ Band

For the calculation of the  $\nu_2$  band we used the  $\nu_2$  transition moment operator obtained in Ref. (21):

$${}^{(000)(010)}\mu'_z = -0.04272\varphi_x + 0.403 \times 10^{-3}\{i\varphi_y, N_z\} + 0.1083 \times 10^{-3}\{\varphi_z, iN_y\}. \quad (1)$$

Also, for this calculation the effect of the hyperfine structure was *explicitly* taken into account, as described in Ref. (11), through the standard tensorial formalism using a  $\mathbf{F} = \mathbf{J} + \mathbf{I}$  and  $\mathbf{J} = \mathbf{N} + \mathbf{S}$  coupling scheme.

Finally, 30 620 line intensities were calculated with an intensity cutoff of  $0.1 \times 10^{-24}\text{ cm}^{-1}/\text{molecule cm}^{-2}$  and the following ranges of quantum numbers and energies:

$$\begin{aligned} N &\leq 65 & K'_a &\leq 13 \\ E' &\leq 2600\text{ cm}^{-1} & E'' &\leq 2000\text{ cm}^{-1} \end{aligned}$$

TABLE I  
Vibrational Energies and Rotational, Spin-Rotation, and Coupling Constants for the  
{(100), (020), (001)} Interacting Vibrational States of  $^{14}\text{N } ^{16}\text{O}_2$

	1 0 0	0 2 0	0 0 1
$E_v$	1319.76589 $\pm$ 0.00012	1498.34688 $\pm$ 0.00027	1616.84918 $\pm$ 0.00089
$A_v$	8.0932898 $\pm$ 0.000082	8.778705 $\pm$ 0.00054	7.7742509 $\pm$ 0.000080
$B_v$	0.43133685 $\pm$ 0.0000067	0.4335453 $\pm$ 0.000015	0.43092954 $\pm$ 0.0000022
$C_v$	0.40928232 $\pm$ 0.0000037	0.4086528 $\pm$ 0.000017	0.40637082 $\pm$ 0.0000018
$\Delta_v^x$	(0.285392 $\pm$ 0.00015) $\times 10^{-2}$	(0.43885 $\pm$ 0.00037) $\times 10^{-2}$	(0.252448 $\pm$ 0.00018) $\times 10^{-2}$
$\Delta_{K_N}^x$	(-0.20710 $\pm$ 0.00012) $\times 10^{-4}$	(-0.24104 $\pm$ 0.00011) $\times 10^{-4}$	(-0.18874 $\pm$ 0.00010) $\times 10^{-4}$
$\Delta_N^x$	(0.30118 $\pm$ 0.00071) $\times 10^{-6}$	(0.29919 $\pm$ 0.00043) $\times 10^{-6}$	(0.30278 $\pm$ 0.00074) $\times 10^{-6}$
$\delta_N^x$	(0.518 $\pm$ 0.012) $\times 10^{-5}$	(0.861 $\pm$ 0.063) $\times 10^{-5}$	(0.4657 $\pm$ 0.0070) $\times 10^{-5}$
$\delta_K^x$	(0.2987 $\pm$ 0.0040) $\times 10^{-7}$	(0.3111 $\pm$ 0.0024) $\times 10^{-7}$	(0.3417 $\pm$ 0.0037) $\times 10^{-7}$
$H_N^x$	(0.33722 $\pm$ 0.00011) $\times 10^{-5}$	(0.7503 $\pm$ 0.0067) $\times 10^{-5}$	(0.27939 $\pm$ 0.00013) $\times 10^{-5}$
$H_K^x$	(-0.2823 $\pm$ 0.0014) $\times 10^{-7}$	-0.44346 $\times 10^{-7}$	(-0.2596 $\pm$ 0.0013) $\times 10^{-7}$
$H_{K_N}^x$	(0.220 $\pm$ 0.087) $\times 10^{-10}$	-0.8928 $\times 10^{-10}$	(0.1044 $\pm$ 0.0072) $\times 10^{-9}$
$h_N^x$	(0.330 $\pm$ 0.071) $\times 10^{-12}$	0.1777 $\times 10^{-12}$	(0.350 $\pm$ 0.013) $\times 10^{-12}$
$h_K^x$	(0.378 $\pm$ 0.029) $\times 10^{-7}$		(0.562 $\pm$ 0.028) $\times 10^{-7}$
$h_{K_N}^x$	-0.2571 $\times 10^{-10}$		(0.21 $\pm$ 0.14) $\times 10^{-10}$
$h_N^y$	0.10727 $\times 10^{-12}$		(0.1277 $\pm$ 0.0067) $\times 10^{-12}$
$L_K^x$	(-0.55356 $\pm$ 0.00027) $\times 10^{-8}$	-0.13633 $\times 10^{-7}$	(-0.48653 $\pm$ 0.00031) $\times 10^{-8}$
$L_{K_N}^x$	(0.3250 $\pm$ 0.0041) $\times 10^{-10}$		(0.3482 $\pm$ 0.0064) $\times 10^{-10}$
$L_{K_N}^y$	(0.325 $\pm$ 0.041) $\times 10^{-12}$		(0.87 $\pm$ 0.27) $\times 10^{-13}$
$P_K^x$	0.867 $\times 10^{-11}$		0.867 $\times 10^{-11}$
$Q_K^x$	-0.8439 $\times 10^{-14}$		-0.8439 $\times 10^{-14}$
$\epsilon_{K_a}^x$	0.183418 $\pm$ 0.000052	0.21947 $\pm$ 0.00037	0.172433 $\pm$ 0.000044
$\epsilon_{K_b}^x$	(0.230 $\pm$ 0.013) $\times 10^{-3}$	(0.176 $\pm$ 0.018) $\times 10^{-3}$	(0.2660 $\pm$ 0.0043) $\times 10^{-3}$
$\epsilon_{K_c}^x$	(-0.332 $\pm$ 0.0013) $\times 10^{-2}$	(-0.334 $\pm$ 0.0015) $\times 10^{-2}$	(-0.31510 $\pm$ 0.00041) $\times 10^{-2}$
$\Delta_{K_N}^{xS}$	(-0.18430 $\pm$ 0.00036) $\times 10^{-3}$	(-0.306 $\pm$ 0.012) $\times 10^{-3}$	(-0.16757 $\pm$ 0.00031) $\times 10^{-3}$
$\Delta_{K_N}^{xS} + \Delta_{K_N}^{yS}$	0.6005 $\times 10^{-6}$		0.6005 $\times 10^{-6}$
$\Delta_{K_N}^{yS}$	0.1678 $\times 10^{-5}$		0.1678 $\times 10^{-5}$
$\Delta_{K_N}^{zS}$	0.6322 $\times 10^{-9}$		0.6322 $\times 10^{-9}$
$\delta_N^{yS}$	0.3769 $\times 10^{-6}$		0.3769 $\times 10^{-6}$
$\delta_N^{zS}$	0.244 $\times 10^{-9}$		0.244 $\times 10^{-9}$
$H_N^{yS}$	0.29673 $\times 10^{-6}$		0.29673 $\times 10^{-6}$
$L_K^{yS}$	-0.3568 $\times 10^{-9}$		-0.3568 $\times 10^{-9}$

$$h_{(001)(020)}^{\text{C}} = (-0.294552 \pm 0.000088) \times 10^{-1}$$

$$h_{(001)(020)}^{\text{C}} = (0.736 \pm 0.031) \times 10^{-7}$$

$$h_{(001)(100)}^{\text{C}} = -0.656287 \pm 0.000064$$

$$h_{(001)(100)}^{\text{C}} = (-0.9193 \pm 0.0096) \times 10^{-4}$$

$$h_{(001)(100)}^{\text{C}} = (0.256 \pm 0.033) \times 10^{-5}$$

Note. All the results are in  $\text{cm}^{-1}$  and the quoted errors correspond to one standard deviation. The constants with no errors were held fixed during the fit.

The total band intensity was found to be  $S_{(010)-(000)} = 0.542 \times 10^{-18} \text{ cm}^{-1}/\text{molecule cm}^{-2}$  at 296 K.

Because of the rather high proportion of so-called  $\Delta F \neq \Delta J \neq \Delta N$  "forbidden" transitions which were not considered in the 1988 calculation (12), the present calculated lines are more numerous than those in 1988 (30 620 instead of  $8065 \times 3$ , taking into account the  $(2I + 1) = 3$  nitrogen nuclear degeneracy).

### $2\nu_2 - \nu_2$ Band

For the hot  $2\nu_2 - \nu_2$  band, only the spin-rotation fine structure was considered and its vibrational transition moment constant was determined using the following relation, valid up to the second order of approximation:

$$(020)(010)\mu_z' = \sqrt{2} \times (010)(000)\mu_z' \quad (2)$$

The  $2\nu_2 - \nu_2$  line intensities were calculated in the following ranges:

TABLE II  
Statistical Analysis of the Results for the Energy Levels Calculation

	(100)	(020)	(001)
Number of experimental spin-rotation levels	1187	374	1833
$0 \leq \delta E < 1 \times 10^{-3}$	65.8%	84.5%	79.1%
$1 \times 10^{-3} \leq \delta E < 2 \times 10^{-3}$	26.7%	12.8%	15.4%
$2 \times 10^{-3} \leq \delta E < 7.0 \times 10^{-3}$	7.4%	2.7%	5.6%

$$\delta E = |E_{\text{obs}} - E_{\text{calc}}| \text{ in cm}^{-1}$$

$$N \leq 60 \quad K'_a \leq 10$$

$$E' \leq 3200 \text{ cm}^{-1} \quad E'' \leq 2600 \text{ cm}^{-1}$$

Also, in order to be consistent with the  $\nu_2$  calculation, the intensity cutoff was chosen to be  $0.3 \times 10^{-24} \text{ cm}^{-1}/\text{molecule cm}^{-2}$  at 296 K, taking into account the  $3I + 1 = 3$  nitrogen nuclear degeneracy.

Finally, 4388 lines were calculated for the  $2\nu_2 - \nu_2$  band and the sum of all the intensities was found to be  $S_{(020)-(010)} = 0.2735 \times 10^{-19} \text{ cm}^{-1}/\text{molecule cm}^{-2}$  at 296 K.

#### V. CONCLUSION

Using high-resolution Fourier transform spectra, a new analysis of the  $\nu_2$  band of  $^{14}\text{N } ^{16}\text{O}_2$  involving the hyperfine structure has been performed for the first time together with the first extensive analysis of the  $2\nu_2 - \nu_2$  band of this molecule, leading to a very accurate representation of the absorption of  $^{14}\text{N } ^{16}\text{O}_2$  in the  $13.3\text{-}\mu\text{m}$  region. It must be mentioned that lines of the  $\nu_2$  band of  $\text{NO}_2$  are visible in the University of Denver balloon flight spectra of June 1988 (22), and knowledge of their parameters (and lines of the hot band) may be important in attempts to detect the weakly absorbing lines of stratospheric ClO in the infrared (23).

RECEIVED: January 27, 1993

#### REFERENCES

1. G. R. BIRD, J. C. BAIRD, A. W. JACHE, J. A. HODGENSON, R. F. CURL, Jr., A. C. KUNKLE, J. W. BRANSFORD, J. RASTRUP-ANDERSON, AND J. ROSENTHAL, *J. Chem. Phys.* **40**, 3378-3390 (1964).
2. R. M. LEE, R. F. CURL, AND J. C. BAKER, *J. Chem. Phys.* **45**, 2037-2040 (1966).
3. P. A. BARON, P. D. GODFREY, AND D. O. HARRIS, *J. Chem. Phys.* **60**, 3723-3724 (1974).
4. W. C. BOWMAN AND F. C. DE LUCIA, *J. Chem. Phys.* **77**, 92-107 (1982).
5. O. I. BASKAKOV, M. V. MOSKIENKO, AND S. F. DYUBKO, *Opt. Spectrosc. (USSR)* **53**, 270-272 (1982).
6. T. TANAKA, A. D. ENGLISH, R. W. FIELDS, D. A. JENNINGS, AND D. O. HARRIS, *J. Chem. Phys.* **59**, 5217-5218 (1973).
7. J. M. BROWN, T. C. STEIMLE, M. E. COLES, AND R. F. CURL, Jr., *J. Chem. Phys.* **74**, 3668-3672 (1981).
8. N. SEMMOUD-MONNANTEUIL, J.-M. COLMONT, A. PERRIN, J.-M. FLAUD, AND C. CAMY-PEYRET, *J. Mol. Spectrosc.* **134**, 176-182 (1989).
9. L. W. HRUBESH AND R. F. CURL, *J. Mol. Spectrosc.* **61**, 144-146 (1976).

10. Y. MORINO, M. TANIMOTO, S. SAITO, E. HIROTA, R. AWATA, AND T. TANAKA, *J. Mol. Spectrosc.* **98**, 331-348 (1983).
11. A. PERRIN, J.-M. FLAUD, C. CAMY-PEYRET, B. CARLI, AND M. CARLOTTI, *Mol. Phys.* **63**, 791-810 (1988).
12. A. PERRIN, C. CAMY-PEYRET, J.-M. FLAUD, AND J. KAUPPINEN, *J. Mol. Spectrosc.* **130**, 168-182 (1988).
13. A. PERRIN, C. CAMY-PEYRET, AND J.-M. FLAUD, *J. Quant. Spectrosc. Radiat. Transfer* **48**, 645-651 (1992).
14. L. S. ROTHMAN, R. R. GAMACHE, R. H. TIPPING, C. P. RINSLAND, M. A. H. SMITH, D. CHRIS BENNER, V. MALATHY-DEVI, J.-M. FLAUD, C. CAMY-PEYRET, A. PERRIN, A. GOLDMAN, S. T. MASSIE, L. R. BROWN, AND R. A. TOTH, *J. Quant. Spectrosc. Radiat. Transfer* **48**, 469-507 (1992).
15. A. PERRIN, J.-M. FLAUD, C. CAMY-PEYRET, A.-M. VASSEROT, G. GUELACHVILI, A. GOLDMAN, F. J. MURCRAY, AND R. D. BLATHERWICK, *J. Mol. Spectrosc.* **154**, 391-406 (1992).
16. R. A. TOTH, *J. Opt. Soc. Amer. B* **9**, 433-461 (1992).
17. A. PERRIN, J.-M. FLAUD, AND C. CAMY-PEYRET, *J. Mol. Spectrosc.* **118**, 174-179 (1986).
18. R. A. TOTH, *J. Opt. Soc. Amer. B* **3**, 1263-1281 (1986).
19. A. G. MAKI AND J. S. WELLS, "Wavenumber Calibration Tables from Heterodyne Frequency Measurements," NIST Special Publication 821, 1992.
20. G. GUELACHVILI AND K. NARAHARI RAO, "Handbook of Infrared Standards," Academic Press, Orlando, 1986.
21. V. MALATHY DEVI, P. P. DAS, A. BANO, K. NARAHARI RAO, J.-M. FLAUD, C. CAMY-PEYRET, AND J.-P. CHEVILLARD, *J. Mol. Spectrosc.* **88**, 251-258 (1981).
22. A. GOLDMAN, F. J. MURCRAY, R. D. BLATHERWICK, J. J. KOSTERS, F. H. MURCRAY, F. G. MURCRAY, AND C. P. RINSLAND, *J. Geophys. Res. D* **94**, 14945-14955 (1989).
23. C. P. RINSLAND AND A. GOLDMAN, *J. Quant. Spectrosc. Radiat. Transfer* **48**, 685-692 (1992).

# APPENDIX 5

## Stratospheric HNO<sub>3</sub> Measurements From 0.002-cm<sup>-1</sup> Resolution Solar Occultation Spectra and Improved Spectroscopic Line Parameters in the 5.8-μm Region

A. GOLDMAN, F. J. MURCRAY, R. D. BLATHERWICK, J. J. KOSTERS, AND D. G. MURCRAY

*Department of Physics, University of Denver, Colorado*

C. P. RINSLAND

*Atmospheric Sciences Division, NASA Langley Research Center, Hampton, Virginia*

J.-M. FLAUD AND C. CAMY-PEYRET

*Laboratoire de Physique Moléculaire et Applications, CNRS, Université Pierre and Marie Curie, Paris, France*

Measurements of stratospheric HNO<sub>3</sub> are presented based on new very high resolution (0.002-cm<sup>-1</sup> full width at half maximum (FWHM)) solar occultation spectra recorded at 32°N latitude with a balloon-borne interferometer in the region of the HNO<sub>3</sub> ν<sub>2</sub> band at 5.8 μm and improved spectroscopic line parameters generated for this HNO<sub>3</sub> band and the interfering bands of O<sub>3</sub> and H<sub>2</sub>O. The line parameters for HNO<sub>3</sub>, computed from the spectroscopic constants reported by Maki, are a significant improvement in that the calculated positions are more accurate than previous data and the line list now includes higher *J* and *K<sub>a</sub>* transitions needed to account for weaker HNO<sub>3</sub> absorption features observable in the stratospheric spectra. Verifications of the new line parameters based on the stratospheric spectra and a 0.002-cm<sup>-1</sup> resolution HNO<sub>3</sub> laboratory spectrum are presented along with comparisons generated with the parameters from the 1986 HITRAN compilation. Significant improvements are apparent for all the updated bands. Finally, the stratospheric HNO<sub>3</sub> profile retrieved from the stratospheric solar spectra using a nonlinear least squares fitting algorithm and the new line parameters is reported and compared with previously reported measurements.

### 1. INTRODUCTION

The need for improvements in the precision and accuracy of remote sounding measurements of key minor constituents in the Earth's atmosphere has motivated a wide variety of recent field and laboratory investigations. A Michelson interferometer capable of recording broadband spectra in the mid-infrared at an unapodized full width at half maximum (FWHM) resolution of 0.002 cm<sup>-1</sup> has recently become operational for field and laboratory use at the University of Denver [Murcray *et al.*, 1990]. This instrument has been flown successfully in several stratospheric balloon flights and has yielded high-quality measurements of a number of important trace constituents [Goldman *et al.*, 1989a, b].

The present investigation focuses on the quantitative measurement of stratospheric HNO<sub>3</sub> through the analysis of the absorption by its intense ν<sub>2</sub> fundamental band in the 5.8-μm region of solar occultation spectra recorded with the new University of Denver instrument. Because of the high resolution and high signal-to-rms noise (>100) of the present spectra, the HNO<sub>3</sub> profile can be measured accurately up to 37 km, an altitude seldom reached in previous investigations. Below tangent heights of 30 km the HNO<sub>3</sub> ν<sub>2</sub> band features are prominent in the spectra, but their absorption is overlapped by strong lines from the ν<sub>1</sub> + ν<sub>2</sub> and ν<sub>2</sub> + ν<sub>3</sub> combination bands of O<sub>3</sub>, less numerous but occasionally strong features produced by H<sub>2</sub>O, weak lines of CH<sub>4</sub> and

N<sub>2</sub>O, and lines of the Δ*v* = 1 sequence of solar CO. Despite the complexity of the absorption this spectral region has frequently been used for quantifying stratospheric HNO<sub>3</sub> from high-resolution solar spectra [e.g., Goldman *et al.*, 1980; Coffey *et al.*, 1981, 1989; Russell *et al.*, 1988]. As shown by the present analysis, much of the available spectroscopic line parameters for such work is in need of improvement. Line parameters derived from recent high-resolution laboratory work on HNO<sub>3</sub>, O<sub>3</sub>, and H<sub>2</sub>O have been used and are shown to greatly improve the quality of retrievals from the stratospheric spectra. Based on the new spectroscopic parameters, a stratospheric HNO<sub>3</sub> profile is derived from the new solar spectra and compared with other measurements including a HNO<sub>3</sub> total column amount retrieved from IR solar spectra recorded on the same day at Kitt Peak, about 1500 km due west of the balloon-borne measurements [Rinsland *et al.*, 1991]. To further verify the HNO<sub>3</sub> profile results, we also analyzed the balloon-borne spectra to retrieve CO<sub>2</sub> volume mixing ratios (VMRs) and an O<sub>3</sub> profile which are compared with other data.

### 2. OBSERVATIONS

The stratospheric spectral measurements were recorded during a balloon flight conducted from the National Scientific Balloon Facility (NSBF) in Palestine, Texas, on June 4, 1990. Spectra were recorded both prior to and during sunset from a float altitude of 37.0 ± 0.2 km, as estimated from readings of on-board pressure transducers converted to altitude based on the 1966 U.S. Standard Atmosphere 30°N

Copyright 1992 by the American Geophysical Union.

Paper number 91JD02850.  
0148-0227/92/91JD-02850\$05.00



TABLE 1. Geometry for the June 4, 1990, Balloon Flight Spectra Analyzed in This Study

Observation Altitude, km	Solar Astronomical Zenith Angle, deg	Refracted Tangent Altitude, km
37.08	90.64	36.68
36.98	91.42	35.02
37.00	92.20	32.30
37.05	92.97	28.52
36.95	93.73	23.69
36.76	94.49	18.14

profile and a NSBF calibration. The geographic coordinates of the balloon gondola at sunset were 31°25'N latitude and 95°44'W longitude. Measurements were recorded at the full instrument resolution (maximum optical path difference of 250 cm) both prior to sunset and during sunset. Geometric parameters, the observational altitude, the solar astronomical zenith angle, and the refracted tangent altitude, are given in Table 1 for the scans used in the present study. In addition, a few very low Sun scans (also at full resolution) were obtained, but due to the large change in solar zenith angle during the recording time, the data are less useful for quantitative analysis. See *Murcray et al.* [1990] for a detailed description of the instrumentation and its use for balloon-borne measurements.

### 3. SPECTROSCOPIC LINE PARAMETERS

An updated calculation of the  $\nu_2$  band of HNO<sub>3</sub> was generated for this investigation based on the spectroscopic parameters reported by *Maki* [1988]. A total of 32,340 lines were computed with a maximum  $J$  and  $K$  value of 74. The lower and upper wavenumber limits of the file are 1650 and 1770 cm<sup>-1</sup>, respectively. The calculated line positions do not differ by more than 0.00001 cm<sup>-1</sup> from a recent independent calculation by A. Maki (private communication, 1990). An integrated intensity of 1087 cm<sup>-1</sup> atm<sup>-1</sup> at 296 K corresponding to  $4.381 \times 10^{-17}$  cm<sup>-1</sup>/molecule cm<sup>-2</sup> at 296 K has been assumed for the sum of all  $\nu_2$  band transitions. This value has been derived by *Maki* [1988] based on the integrated band intensity measurement of 1412 cm<sup>-1</sup> atm<sup>-1</sup> at 296 K [*Giver et al.*, 1984]. Hot bands and other isotopic bands are assumed to produce the additional absorption. The room temperature tunable diode laser intensity measurements by *May et al.* [1987] imply a total band intensity 0.97 times the *Giver et al.* [1984] value. The difference between the results is well within the quoted experimental errors of the two investigations. For a discussion of the comparison of these results with earlier intensity measurements, see *May et al.* [1987].

*Maki* [1988] noted that his analysis indicates that the  $\nu_2$  band of HNO<sub>3</sub> is remarkably free of perturbations. This contrasts sharply with the spectrum in the other two regions of strong absorption by HNO<sub>3</sub> in the infrared. At 11.3  $\mu$ m the  $\nu_5$  and  $2\nu_9$  bands are strongly coupled by Fermi resonance [*Maki and Wells*, 1984]; at 7.5  $\mu$ m the  $\nu_3$  and  $\nu_4$  bands are coupled through Fermi and Coriolis resonances, and in addition, levels of both states are perturbed by interactions with unobserved levels from other vibrational states [*Perrin et al.*, 1989]. These interactions make accurate calculations of line parameters much more difficult than in the  $\nu_2$  band region. Unfortunately, at present the agreement between

measurement and calculation is not completely satisfactory in the regions of the perturbed bands [cf. *Goldman et al.*, 1984, 1989b]. Since both *May et al.* [1987] and *Maki* [1988] have found no evidence for intensity perturbations in their studies of the  $\nu_2$  band, we have neglected a Herman-Wallis-like term in our intensity calculations.

It should be noted that the previous HNO<sub>3</sub>  $\nu_2$  band parameters were based on the work of *Maki and Wells* [1980]. These parameters appear on the 1986 HITRAN line parameters compilation, but with an incorrect intensity normalization [*Rothman et al.*, 1987]. The new work provides a corrected intensity normalization, as described above, and extends the calculations to higher  $J$  and  $K$ . Also, the wavelength calibration scale has been improved due to recent heterodyne frequency measurements [*Wells et al.*, 1981a, b, 1983], which include higher rotational levels obtained with a tunable diode laser system. According to *Maki* [1988] the calculated line positions are accurate to about  $\pm 0.0005$  cm<sup>-1</sup> between 1680 and 1738 cm<sup>-1</sup>.

A Lorentz air-broadening coefficient of 0.11 cm<sup>-1</sup> atm<sup>-1</sup> at 295 K and a  $T^{-0.75}$  temperature dependence of the Lorentz air-broadening coefficient have been assumed for all HNO<sub>3</sub> lines. These average values were reported by *May and Webster* [1989a] based on their tunable diode laser laboratory measurements of HNO<sub>3</sub> lines in the 7.5- $\mu$ m spectral region. The IR results are within 5% of calculated linewidths derived from recent millimeter wave pressure-broadening measurements between 100 and 400 K [*Goyette et al.*, 1991]. Note, however, that a dependence of HNO<sub>3</sub> pressure-broadening coefficients on the quantum numbers has been measured [e.g., *Goyette et al.*, 1988] and is predicted by the Anderson-Tsao-Curnutte theory calculations performed by *Tejwani and Yeung* [1978]. The new air-broadening parameters replace the constant value of 0.13 cm<sup>-1</sup> atm<sup>-1</sup> at 296 K and a  $T^{-0.5}$  temperature dependence of the air-broadened Lorentz coefficient which were assumed for all HNO<sub>3</sub> lines on the 1986 HITRAN compilation [*Rothman et al.*, 1987]. A constant HNO<sub>3</sub> self-broadened Lorentz coefficient of 0.73 cm<sup>-1</sup> atm<sup>-1</sup> at 296 K [*Goldman et al.*, 1980] was introduced in the new linelist. The linelist, which is in the 1986 HITRAN compilation format, may be obtained by writing to the authors.

To verify the new line parameters, two room temperature HNO<sub>3</sub> laboratory spectra covering the 1400- to 1900-cm<sup>-1</sup> region were recorded at 0.002-cm<sup>-1</sup> resolution with a 22-cm path length absorption cell and sample pressure of 0.4 and 1.0 torr. Broad residual H<sub>2</sub>O background absorptions formed at ambient atmospheric pressure and small, narrow NO<sub>2</sub> features from the sample (NO<sub>2</sub> partial pressure less than 5% of the HNO<sub>3</sub> amount) are present in the spectra in addition to the HNO<sub>3</sub> absorption. The NO<sub>2</sub> absorptions are due to high  $J$ ,  $R$  branch lines of the strong  $\nu_3$  band, centered at 1616.85 cm<sup>-1</sup>, outside the HNO<sub>3</sub> region. The background absorptions have been partially removed by dividing the sample spectra by a background (empty cell) spectrum.

With the new line parameters the calculated and measured HNO<sub>3</sub> lines agree very well in position and intensity throughout the entire region of the  $\nu_2$  band (about 1680 to 1740 cm<sup>-1</sup>). However, many weak lines observed in the extreme  $P$  branch of the laboratory spectrum are not included in the synthetic spectrum calculations, and these lines are attributed to "hot" band transitions yet to be analyzed. Fewer hot band lines are encountered in the  $R$

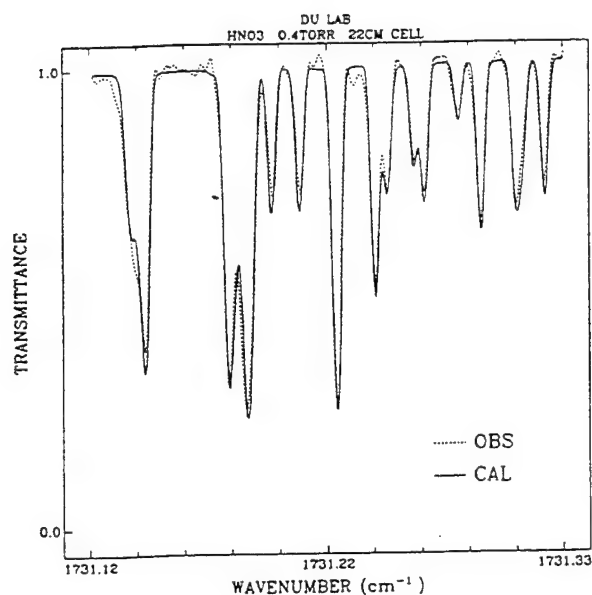


Fig. 1. Spectral least squares fit of a HNO<sub>3</sub> laboratory spectrum in the 1731-cm<sup>-1</sup> region.

branch. The hot band lines limit the accuracy of the spectral fittings. However, in narrow intervals with less interference, both P and R branch features yield retrieved gas amounts close (within  $\pm 5\%$ ) to the nominal HNO<sub>3</sub> amount in the cell. An example of such a fit is shown in Figure 1. Our results indicate no measurable vibration-rotation effect on the line intensities and that our assumed normalization of the line intensities is correct. These conclusions are consistent with the results reported by May *et al.* [1987]. Comparisons of the measured spectra and simulations also indicate that the calculated line positions at the  $\nu_2$  band manifold heads (overlapping lines  $J'' = N - i$ ,  $K''_a = i$ , or  $i + 1$ ,  $K''_c = N - (i + 1)$  with  $N$ ,  $i$  integers) are not fully consistent with those outside the manifold heads, which limits the agreement that can be obtained in the spectral least squares fitting. This effect and isolated disagreements between the positions of measured and calculated features justify a new spectroscopic constant analysis of the  $\nu_2$  band in the future. Also, as expected, fewer hot band lines are observed in the stratospheric spectra because of the low temperatures.

Figure 2 demonstrates the type of improvements obtained with the new HNO<sub>3</sub>  $\nu_2$  band line parameters. The figure presents comparisons of the laboratory data near 1729 cm<sup>-1</sup> with simulations generated with both the HITRAN 1986 lines and the new lines. The calculations include a normalization of  $4.381/2.014$  to correct the 1986 HITRAN line intensities to the value of  $4.381 \times 10^{-17}$  cm<sup>-1</sup>/molecule cm<sup>-2</sup> at 296 K. The improvement is particularly important toward the wings of the band, above 1725 cm<sup>-1</sup> and below 1680 cm<sup>-1</sup>, where the 1986 HITRAN linelist does not include many of the high  $J$ ,  $K$  lines which show significant absorption in the atmospheric spectrum. Refinements in the line positions of the new linelist are also noticeable. The improvements are less dramatic in other parts of the band.

The ozone line positions and intensities have been calculated from the results reported by Malathy Devi *et al.* [1987] and Rinsland *et al.* [1990b] (see Flaud *et al.* [1990a] for a listing of the parameters of the stronger lines). In addition to improving the positions and intensities of the two main

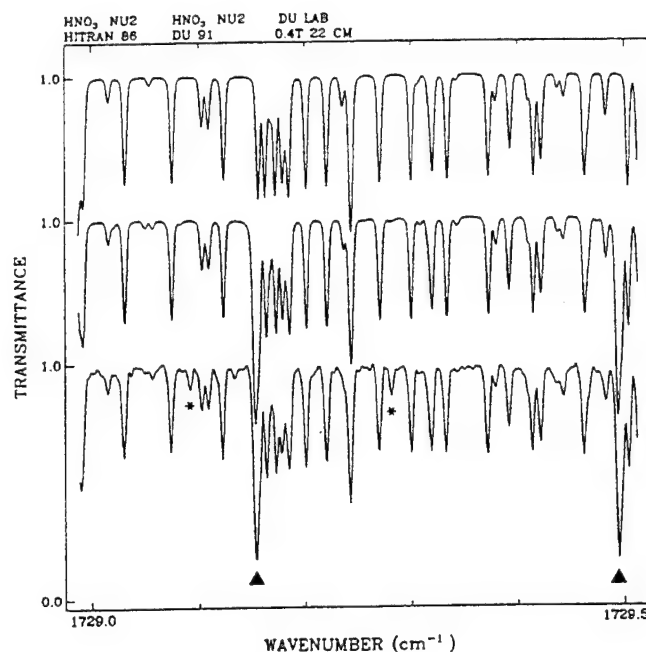


Fig. 2. Comparison of a section of the 0.4 torr HNO<sub>3</sub> laboratory spectrum (bottom) with simulations generated using the 1986 HITRAN compilation (top) and the new HNO<sub>3</sub>  $\nu_2$  band line parameters (middle). The solid triangles beneath the measured spectrum mark features that are missing in the simulation with the 1986 HITRAN compilation [Rothman *et al.*, 1987] but included in the simulation with the new linelist. Features missing in both simulations, marked by asterisks beneath the measured spectrum, are probably hot band lines. The spectra are offset vertically for clarity.

bands,  $\nu_2 + \nu_3$  (band center = 1726.5225 cm<sup>-1</sup>) and  $\nu_1 + \nu_2$  (band center = 1796.2619 cm<sup>-1</sup>), the new linelist includes the two strongest hot bands  $2\nu_2 + \nu_3 - \nu_2$  and  $2\nu_2 + \nu_1 - \nu_2$ , with band centers at 1707.0034 and 1785.6456 cm<sup>-1</sup>, respectively. The two hot bands were not included in the 1986 HITRAN line parameters compilation [Rothman *et al.*, 1987]. The assumed air-broadened O<sub>3</sub> line widths have been calculated with an empirical expression derived from a fit to air-broadened line widths measured from room temperature laboratory spectra [Flaud *et al.*, 1990b]. A  $T^{-0.77}$  temperature dependence has been adopted for the O<sub>3</sub> air-broadened widths based on theoretical calculations performed for N<sub>2</sub> broadening [Gamache, 1985].

Line parameters for the four strongest H<sub>2</sub>O bands in the 6- $\mu$ m region (excluding HDO) have been taken from the work of Toth [1989, 1991]. The bands are the  $\nu_2$  and the  $2\nu_2 - \nu_2$  bands of H<sub>2</sub><sup>16</sup>O, the  $\nu_2$  bands of H<sub>2</sub><sup>18</sup>O, and the  $\nu_2$  band of H<sub>2</sub><sup>17</sup>O. Line parameters from the 1986 HITRAN compilation [Rothman *et al.*, 1987] have been adopted for the weaker H<sub>2</sub>O bands and all lines of HDO. The air-broadened half widths on the 1986 HITRAN compilation have been adopted for all H<sub>2</sub>O lines along with a  $T^{-0.68}$  temperature dependence [Gamache and Rothman, 1988]. Line parameters for other gases were taken from the 1986 HITRAN compilation [Rothman *et al.*, 1987].

Figure 3 shows two narrow spectral intervals of the flight data dominated by absorption lines of HNO<sub>3</sub>, O<sub>3</sub>, and H<sub>2</sub>O. In each region the stratospheric spectrum is compared with two simulations, one generated with the new spectroscopic parameters and the other with the 1986 HITRAN compilation parameters [Rothman *et al.*, 1987]. This comparison

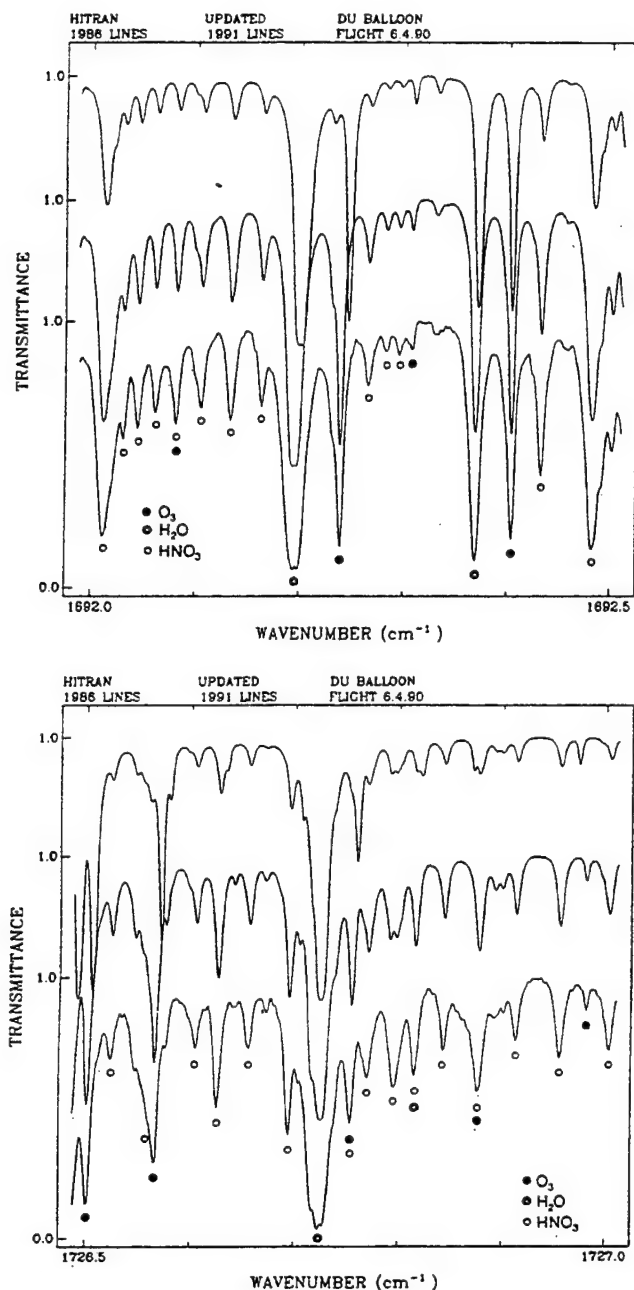


Fig. 3. The 1692 (upper panel) and 1726- $\text{cm}^{-1}$  (lower panel) regions of a stratospheric solar spectrum recorded at an astronomical solar zenith angle of  $93.73^\circ$  (tangent height of 23.69 km) and simulations of the data. The spectra are offset vertically for clarity with the simulation computed from the 1986 HITRAN compilation [Rothman *et al.*, 1987] at top, the simulation generated from the new line parameters in the middle, and the measured solar spectrum at bottom in each panel. The selected intervals show spectral features of  $\text{O}_3$ ,  $\text{H}_2\text{O}$ , and  $\text{HNO}_3$ , which are identified beneath the lowest spectrum. Note that two closely spaced  $\text{HNO}_3$  features near  $1726.79 \text{ cm}^{-1}$  are resolved in the simulations but appear as a single feature in the observation. This is an example of the isolated discrepancies that have been noted between the measured and calculated  $\text{HNO}_3$  line positions.

demonstrates the improvements that have been achieved in reproducing the atmospheric absorption of the three gases with the new set of line parameters. The better agreement is in part the result of the corrected normalization of the  $\text{HNO}_3$  line intensities; however, other improvements are readily

apparent (e.g., corrected line positions, simulation of lines missing in the 1986 HITRAN compilation [Rothman *et al.*, 1987]). Simulations and spectral fittings in other regions also consistently show significant improvements resulting from the higher accuracy of the new  $\text{HNO}_3$ ,  $\text{O}_3$ , and  $\text{H}_2\text{O}$  line parameters.

The new  $\text{HNO}_3$ ,  $\text{O}_3$ , and  $\text{H}_2\text{O}$  line parameters noted above have been included in the 1991 HITRAN line parameters compilation. A detailed description of the 1991 HITRAN data base is in preparation (L. S. Rothman, private communication, 1991).

#### 4. DATA ANALYSIS AND RESULTS

Multiscan onion-peeling using nonlinear least squares spectral fitting followed by simultaneous multiscan spectral fitting has been used to analyze the balloon-borne data. Details and examples of the application of the least squares technique to derive gas concentration profiles from IR solar occultation spectra are presented in various papers [cf. Niple, 1980; Niple *et al.*, 1980; Goldman *et al.*, 1980; Rinsland *et al.*, 1990a]. The retrieval algorithms used in this study allow for the simultaneous fitting of the volume mixing ratios of up to eight gases along with instrumental parameters (e.g., parameters to model the 100% transmission level and a wavelength shift between the measured and calculation spectra) from the analysis of each spectral interval. Because of the complexity of the absorption, typically two or three gases have been fitted in analyzing each region. Also, it was necessary in most cases to model the absorption by solar  $\text{CO}$  lines; we used the method described by Rinsland *et al.* [1982].

The zero levels in the observed spectra are shifted 4–6% above the instrumental zero signals with some frequency dependence. Rather than fitting the zero level as part of the spectral least squares analysis, which can yield unreliable results if the lines are weak, we used completely absorbed lines (in other spectral regions or scans) to establish the corrections.

A pressure-temperature profile calculated by the National Meteorological Center (NMC) for the location, date, and time of the balloon flight was adopted in the ray-tracing calculations (M. Gelman, NMC, private communication, 1990). Gas concentration profiles from the reference compilation of Smith [1982] were taken as initial guesses in the  $\text{HNO}_3$ ,  $\text{O}_3$ , and  $\text{H}_2\text{O}$  profile retrievals and in the calculation of the absorption by the other, less strongly absorbing gases in the retrieval intervals.

The spectral intervals studied are listed in Table 2. In addition to selecting intervals to retrieve the  $\text{HNO}_3$  profile, we included intervals to retrieve the  $\text{CO}_2$  VMR and the  $\text{O}_3$  profile. The results from spectral regions dominated by  $\text{CO}_2$ , such as near  $1333 \text{ cm}^{-1}$ , indicate that 335 ppmv (parts per million by volume)  $\text{CO}_2$  is consistent with the data (no detailed profile has been retrieved). This is in agreement with the value of 337 ppmv anticipated from the values adopted previously [Rinsland *et al.*, 1990a] and a  $\text{CO}_2$  trend of  $1.42 \text{ ppmv yr}^{-1}$  measured at Mauna Loa [Thoning *et al.*, 1989]. The ozone profile, obtained from intervals dominated by  $\text{O}_3$  lines such as near  $1803 \text{ cm}^{-1}$ , is very similar in shape to those retrieved from the May 1985 ATMOS/Spacelab 3 data at  $28^\circ\text{N}$  latitude [Gunson *et al.*, 1990] and SAGE II monthly mean measurements at  $32^\circ\text{N}$  in May and July 1990 (J. C.

TABLE 2. Spectral Regions Investigated in the Present Study

Spectral Region, cm <sup>-1</sup>	Target Molecules	Primary Interfering Molecules
1686.00–1688.00	HNO <sub>3</sub>	O <sub>3</sub> , solar CO
1690.45–1692.15	HNO <sub>3</sub>	O <sub>3</sub> , solar CO
1692.90–1693.20	HNO <sub>3</sub>	O <sub>3</sub>
1802.80–1804.60	O <sub>3</sub>	solar CO
1805.40–1807.40	O <sub>3</sub>	H <sub>2</sub> O, NO, solar CO
1933.60–1933.90	CO <sub>2</sub>	
1950.55–1950.95	CO <sub>2</sub>	O <sub>3</sub> , COF <sub>2</sub> , solar CO
1952.15–1952.50	CO <sub>2</sub>	solar CO, O <sub>3</sub> , COF <sub>2</sub>
1955.40–1955.70	CO <sub>2</sub>	...
1957.10–1957.50	CO <sub>2</sub>	O <sub>3</sub> , COF <sub>2</sub> , solar CO

Larsen, private communication, 1990), but our results are consistently lower by about 12%.

The onion-peeling analysis was begun by fitting the highest tangent altitude solar spectrum (37.08 km). Absorption by the strongest HNO<sub>3</sub> manifolds appears clearly in that spectrum. The fit from each spectral region was used to retrieve individual profile scaling factors which converted the target molecule's first guess VMR into an absolute value in every layer with a lower boundary altitude at or above the tangent height of the spectrum. VMRs were then retrieved for altitude ranges defined by the tangent heights of successively lower Sun spectra. To further improve the derived profile, the simultaneous multiscan spectral fitting with additional intermediate layers was then performed. The results were adopted as the final profile.

Figure 4 presents a sample multiscan least squares fit showing the 1693-cm<sup>-1</sup> region which is dominated by medium-J HNO<sub>3</sub>  $\nu_2$  band, *P* branch lines and weaker absorption lines of O<sub>3</sub> (mostly from the  $\nu_2 + \nu_3$  band). Absorption by

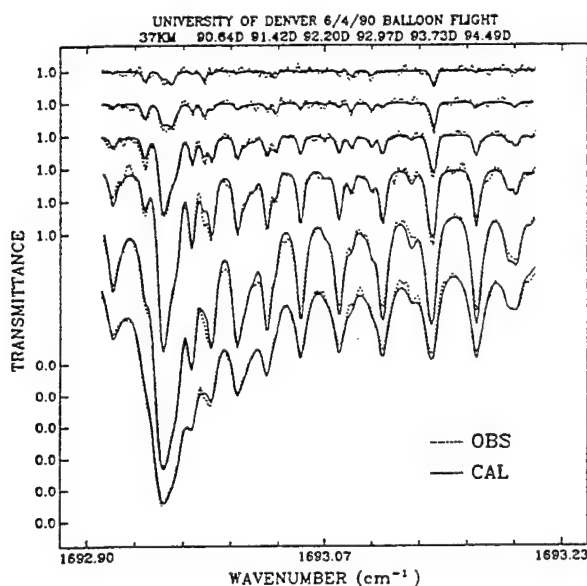


Fig. 4. Simultaneous multiscan spectral least squares fitting of the balloon-borne solar spectra in the 1693-cm<sup>-1</sup> region. The spectra, plotting in order of increasing solar zenith angle, are offset vertically for clarity. The zero and 100% transmission level for each spectrum are shown on the ordinate axis. The astronomical zenith angles of the scans are listed at top.

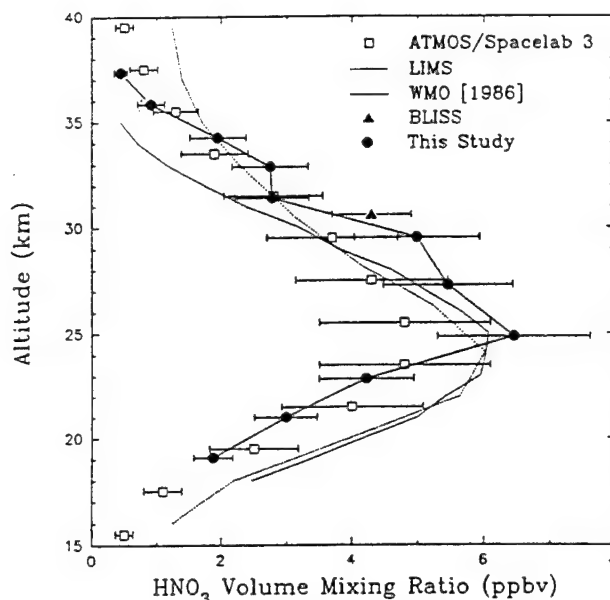


Fig. 5. HNO<sub>3</sub> VMR versus altitude profile retrieved from the fitting results shown in Figure 4 along with profiles measured near the same latitude. The ATMOS/Spacelab 3 measurements are from Russell *et al.* [1988], the LIMS data are from Gille *et al.* [1984], the WMO data are from WMO [1986], and BLISS data are from May and Webster [1989b].

solar CO lines is negligible in this region as shown by high Sun balloon spectra from the same flight and the ATMOS solar atlas [Farmer and Norton, 1989]. The standard deviation of the residuals (1.80%) is close to that expected from the signal-to-rms noise ratio of the spectra.

Figure 5 presents the retrieved HNO<sub>3</sub> volume mixing ratio profile, which is also given in numerical form in Table 3. Error bars are the estimated 1-sigma total uncertainties, which range from 16 to 23%. The error sources and the estimated uncertainty in the HNO<sub>3</sub> VMR resulting from each are (1) uncertainty due to instrumental effects (the finite signal-to-noise ratio, channeling, and zero signal level offsets) ranging from 10% below 30 km to 20% at 37 km; (2) uncertainty in the assumed tangent pressures, 5% at all altitudes; (3) uncertainty in the assumed temperature profile, 1% at all altitudes; (4) uncertainty in the assumed HNO<sub>3</sub> line parameters, 10% at all altitudes (mostly from the uncertainty in the absolute band intensity); and (5) the uncertainty in the simulation of overlapping lines, 5% at all altitudes. The total

TABLE 3. Retrieved HNO<sub>3</sub> Volume Mixing Ratio Profile

Altitude, km	Pressure, mbar	Volume Mixing Ratio, ppb, 10 <sup>-9</sup>
19.1	70.8	1.88 ± 0.30
21.0	51.3	2.99 ± 0.48
22.8	38.3	4.22 ± 0.72
24.8	28.3	6.46 ± 1.16
27.3	19.7	5.46 ± 0.98
29.5	14.0	4.99 ± 0.95
31.4	10.6	2.78 ± 0.56
32.9	8.53	2.75 ± 0.58
34.3	7.06	1.95 ± 0.43
35.8	5.67	0.92 ± 0.21
37.3	4.61	0.44 ± 0.10

errors have been computed from the square root of the sum of the squares of the individual errors. The relative errors are largest at high altitude because of the weakness of the HNO<sub>3</sub> absorption.

Figure 5 also shows HNO<sub>3</sub> profiles retrieved from data collected at about the same latitude as the present measurements and, in addition, the "most likely" 32°N profile reported in *World Meteorological Organization (WMO)* [1986, Figures 10–13], based on a synthesis of balloon-borne measurements. The present results and the ATMOS/Spacelab 3 29°N latitude zonal mean HNO<sub>3</sub> profile [Russell *et al.*, 1988] agree very well except between 25 and 30 km, where the ATMOS VMRs are systematically lower. The largest discrepancy occurs at the VMR peak near 25 km where the ATMOS HNO<sub>3</sub> mixing ratio is  $4.8 \pm 1.3$  ppbv, significantly lower than the present measured value of  $6.5 \pm 1.2$  ppbv and the other data in Figure 5. The Limb Infrared Monitor of the Stratosphere (LIMS) experiment on the Nimbus 7 satellite measured HNO<sub>3</sub> profiles from the time of its launch, October 24, 1978, until May 28, 1979 [Gille *et al.*, 1984]. The reported zonal mean LIMS profile for May 1979 at 28°N latitude, taken from Figure 16 of Russell *et al.* [1988], agrees fairly well with present measurements. Above about 34 km the LIMS profile decreases more slowly with increasing altitude than the present profile and the ATMOS measurements [Russell *et al.*, 1988]. As mentioned by Russell *et al.* [1988], the LIMS investigators attributed this effect to an instrumental anomaly. Jackman *et al.* [1985] noted that the LIMS measurements above about 5 mbar are inconsistent with HNO<sub>3</sub> values calculated using LIMS H<sub>2</sub>O, O<sub>3</sub>, NO<sub>2</sub>, and temperature measurements. The HNO<sub>3</sub> VMR of  $4.3 \pm 0.6$  ppbv at 30.6 km retrieved from 0.0005-cm<sup>-1</sup> resolution spectra recorded by the balloon-borne laser in situ sensor (BLISS) at 32°N latitude in September 1988 [May and Webster, 1989b] is very close to the present measurement at the same altitude.

A HNO<sub>3</sub> total column of  $5.74 \times 10^{15}$  molecules cm<sup>-2</sup> has been derived by integrating the measured profile from 18.14 to 55.0 km. This value can be compared with a total column retrieved from 0.0053-cm<sup>-1</sup> resolution IR solar spectra recorded on the same day from Kitt Peak (altitude 2.1 km, latitude 31.9°N, 111.6°W), which is located about 70 km west of Tucson, Arizona, and about 1500 km west of the Palestine, Texas, launch site. The 868.8- to 870.0-cm<sup>-1</sup> region, which contains a sequence of three P branch manifolds of the HNO<sub>3</sub>  $\nu_3$  band, was analyzed in four Kitt Peak solar spectra [Rinsland *et al.*, 1991]. The line parameters from the 1986 HITRAN compilation [Rothman *et al.*, 1987] were assumed along with a correlative pressure-temperature profile from NMC global satellite and radiosonde measurements (M. Gelman, private communication, 1990). The mean retrieved Kitt Peak HNO<sub>3</sub> total column,  $7.66 \times 10^{15}$  molecules cm<sup>-2</sup>, is 1.33 times the total column deduced from the balloon-borne measurements. It should be noted that the integrated HNO<sub>3</sub> column between 2 and 18 km obtained with the reference profile of Smith [1982] is 0.30 times the total. Therefore after accounting for the 30% contribution to the total column from layers below 18 km, the Kitt Peak and the balloon-borne total columns are consistent.

## 5. SUMMARY AND CONCLUSIONS

In the present work we have reported the calculation and verification of improved HNO<sub>3</sub> spectroscopic line param-

eters in the 5.8- $\mu$ m spectral region and the use of these parameters along with improved parameters for O<sub>3</sub> and H<sub>2</sub>O to retrieve a stratospheric HNO<sub>3</sub> profile extending to an altitude of 37 km. In general, the retrieved profile is consistent with previously published satellite and balloon-borne measurements obtained near the same latitude. Our direct measurements confirm the bias in the high-altitude LIMS measurements noted previously [e.g., Gille *et al.*, 1984; Jackman *et al.*, 1985]. The excellent agreement between the positions and strengths of HNO<sub>3</sub> features in simulations and in the very high resolution stratospheric and laboratory spectra (e.g., Figures 1 to 4) confirms the quality of the new line parameters and their suitability for use in the quantification of HNO<sub>3</sub> stratospheric profiles from IR spectroscopic measurements.

**Acknowledgments.** Research at the University of Denver was supported by NASA and NSF. Acknowledgment is made to the National Center for Atmospheric Research, which is supported by NSF, for computer time used in this research. The National Solar Observatory (NSO) FTS on Kitt Peak is operated by the Association of Universities for Research in Astronomy, Inc. (AURA), under cooperative agreement with NSF. The McMath FTS solar observations were partially supported by NASA. The Laboratory of Molecular Physics and Applications is associated with the Universités Pierre et Marie Curie et Paris Sud.

## REFERENCES

- Coffey, M. T., W. G. Mankin, and A. Goldman, Simultaneous spectroscopic determination of the latitudinal, seasonal, and diurnal variability of stratospheric N<sub>2</sub>O, NO, NO<sub>2</sub> and HNO<sub>3</sub>, *J. Geophys. Res.*, **86**, 7331–7341, 1981.
- Coffey, M. T., W. G. Mankin, and A. Goldman, Airborne measurements of stratospheric constituents over Antarctica in the austral spring, 1987, 2, Halogen and nitrogen trace gases, *J. Geophys. Res.*, **94**, 16,597–16,613, 1989.
- Farmer, C. B., and R. H. Norton, A high-resolution atlas of the infrared spectrum of the sun and the earth atmosphere from space: A compilation of ATMOS spectra of the region from 650 to 4800 cm<sup>-1</sup> (2.3 to 16  $\mu$ m), *The Sun, NASA Ref. Publ.* 1224, vol. 1, 1989.
- Flaud, J.-M., C. Camy-Peyret, C. P. Rinsland, M. A. H. Smith, and V. Malathy Devi, *Atlas of Ozone Spectral Parameters from Microwave to Medium Infrared*, Academic, San Diego, Calif., 1990a.
- Flaud, J.-M., C. Camy-Peyret, C. P. Rinsland, V. Malathy Devi, M. A. H. Smith, and A. Goldman, Improved line parameters for ozone bands in the 10- $\mu$ m spectral region, *Appl. Opt.*, **29**, 1860–1863, 1990b.
- Gamache, R. R., Temperature dependence of N<sub>2</sub>-broadened half-widths of ozone, *J. Mol. Spectrosc.*, **114**, 31–41, 1985.
- Gamache, R. R., and L. S. Rothman, Temperature dependence of N<sub>2</sub>-broadened halfwidths of water vapor: The pure rotation and  $\nu_2$  bands, *J. Mol. Spectrosc.*, **128**, 360–369, 1988.
- Gille, J. C., et al., Accuracy and precision of the nitric acid concentrations determined by the Limb Infrared Monitor of the Stratosphere experiment on NIMBUS 7, *J. Geophys. Res.*, **89**, 5179–5190, 1984.
- Giver, L. P., F. P. J. Valero, D. Goorvitch, and F. S. Bonomo, Nitric acid band intensities and band-model parameters from 610 to 1760 cm<sup>-1</sup>, *J. Opt. Soc. Am. B*, **1**, 715–722, 1984.
- Goldman, A., D. G. Murcray, F. J. Murcray, and E. Niple, High resolution IR balloon-borne solar spectra and laboratory spectra in the HNO<sub>3</sub> 1720-cm<sup>-1</sup> region: An analysis, *Appl. Opt.*, **19**, 3721–3724, 1980.
- Goldman, A., J. R. Gillis, C. P. Rinsland, F. J. Murcray, and D. G. Murcray, Stratospheric HNO<sub>3</sub> quantification from line-by-line nonlinear least squares analysis of high-resolution balloon-borne solar absorption spectra in the 870-cm<sup>-1</sup> region, *Appl. Opt.*, **23**, 3252–3255, 1984.
- Goldman, A., F. J. Murcray, D. G. Murcray, J. J. Kusters, C. P.



- Rinsland, C. Camy-Peyret, J.-M. Flaud, and A. Barbe, Isotopic abundance of stratospheric ozone from balloon-borne high resolution infrared solar spectra, *J. Geophys. Res.*, **94**, 8467–8473, 1989a.
- Goldman, A., F. J. Murcray, R. D. Blatherwick, J. J. Kusters, F. H. Murcray, and D. G. Murcray, and C. P. Rinsland, New spectral features of stratospheric trace gases identified from high resolution infrared balloon-borne and laboratory spectra, *J. Geophys. Res.*, **94**, 14,945–14,955, 1989b.
- Goyette, T. M., W. L. Ebenstein, F. C. De Lucia, and P. Helminger, Pressure broadening of the millimeter and submillimeter wave spectra of nitric acid by oxygen and nitrogen, *J. Mol. Spectrosc.*, **128**, 108–116, 1988.
- Goyette, T. M., W. Guo, F. C. De Lucia, and P. Helminger, Variable temperature pressure broadening of  $\text{HNO}_3$  in the millimeter wave spectral region, *J. Quant. Spectrosc. Radiat. Transfer*, in press, 1991.
- Gunson, M. R., C. B. Farmer, R. H. Norton, R. Zander, C. P. Rinsland, J. H. Shaw, and B.-C. Gao, Measurements of  $\text{CH}_4$ ,  $\text{N}_2\text{O}$ ,  $\text{CO}$ ,  $\text{H}_2\text{O}$ , and  $\text{O}_3$  in the middle atmosphere by the atmospheric trace molecule spectroscopy experiment on Spacelab 3, *J. Geophys. Res.*, **95**, 13,867–13,882, 1990.
- Jackman, C. H., J. A. Kaye, and P. D. Guthrie, LIMS  $\text{HNO}_3$  data above 5 mbar: Corrections based on simultaneous observations of other species, *J. Geophys. Res.*, **90**, 7923–7930, 1985.
- Maki, A. G., High-resolution measurements of the  $\nu_2$  band of  $\text{HNO}_3$  and the  $\nu_3$  band of trans-HONO, *J. Mol. Spectrosc.*, **127**, 104–111, 1988.
- Maki, A. G., and J. S. Wells, High-resolution measurement and analysis of the infrared spectrum of nitric acid near  $1700\text{ cm}^{-1}$ , *J. Mol. Spectrosc.*, **82**, 427–434, 1980.
- Maki, A. G., and J. S. Wells, High resolution spectrum of the  $\nu_3$  band of nitric acid ( $\text{HNO}_3$ ) near  $880\text{ cm}^{-1}$ , *J. Mol. Spectrosc.*, **108**, 17–30, 1984.
- Malathy Devi, V., J.-M. Flaud, C. Camy-Peyret, C. P. Rinsland, and M. A. H. Smith, Line positions and intensities for the  $\nu_1 + \nu_2$  and  $\nu_2 + \nu_3$  bands of  $^{16}\text{O}_3$ , *J. Mol. Spectrosc.*, **125**, 174–183, 1987.
- May, R. D., and C. R. Webster, In situ stratospheric measurements of  $\text{HNO}_3$  and  $\text{HCl}$  near 30 km using the balloon-borne laser in situ sensor tunable diode laser spectrometer, *J. Geophys. Res.*, **94**, 16,343–16,350, 1989a.
- May, R. D., and C. R. Webster, Measurements of line positions, intensities, and collisional air-broadening coefficients in the  $\text{HNO}_3$   $7.5\text{-}\mu\text{m}$  band using a computer-controlled tunable diode laser system, *J. Mol. Spectrosc.*, **138**, 383–388, 1989b.
- May, R. D., C. R. Webster, and L. T. Molina, Tunable diode laser measurements of absolute line strengths in the  $\text{HNO}_3$   $\nu_2$  band near  $5.8\text{ }\mu\text{m}$ , *J. Quant. Spectrosc. Radiat. Transfer*, **38**, 381–388, 1987.
- Murcray, F. J., J. J. Kusters, R. D. Blatherwick, J. Olson, and D. G. Murcray, High resolution solar spectrometer system for measuring atmospheric constituents, *Appl. Opt.*, **29**, 1520–1525, 1990.
- Niple, E., Nonlinear least squares analysis of atmospheric absorption spectra, *Appl. Opt.*, **19**, 3481–3490, 1980.
- Niple, E., W. G. Mankin, A. Goldman, D. G. Murcray, and F. J. Murcray, Stratospheric  $\text{NO}_2$  and  $\text{H}_2\text{O}$  mixing ratio profiles from high resolution infrared solar spectra using nonlinear least squares, *Geophys. Res. Lett.*, **7**, 489–492, 1980.
- Perrin, A., O. Lado-Bordowsky, and A. Valentin, The  $\nu_3$  and  $\nu_4$  interacting bands of  $\text{HNO}_3$  line positions and intensities, *Mol. Phys.*, **67**, 249–270, 1989.
- Rinsland, C. P., A. Goldman, F. J. Murcray, D. G. Murcray, M. A. H. Smith, R. K. Seals, Jr., J. C. Larsen, and P. L. Rinsland, Stratospheric  $\text{N}_2\text{O}$  mixing ratio profile from high-resolution balloon-borne solar absorption spectra and laboratory spectra near  $1880\text{ cm}^{-1}$ , *Appl. Opt.*, **21**, 4351–4355, 1982.
- Rinsland, C. P., A. Goldman, F. J. Murcray, R. D. Blatherwick, J. J. Kusters, D. G. Murcray, N. D. Sze, and S. T. Massie, Long-term trends in the concentrations of  $\text{SF}_6$ ,  $\text{CHClF}_2$ , and  $\text{COF}_2$  in the lower stratosphere from analysis of high-resolution infrared solar occultation spectra, *J. Geophys. Res.*, **95**, 16,477–16,490, 1990a.
- Rinsland, C. P., M. A. H. Smith, V. Malathy Devi, J.-M. Flaud, and C. Camy-Peyrot, the  $2\nu_2 + \nu_3$  and  $2\nu_2 + \nu_1$  bands of  $^{16}\text{O}_3$  at  $4.1\text{ }\mu\text{m}$ : Line positions and intensities, *J. Mol. Spectrosc.*, **139**, 343–352, 1990b.
- Rinsland, C. P., R. Zander, and P. Demoulin, Ground-based infrared measurements of  $\text{HNO}_3$  total column abundances: Long-term trend and variability, *J. Geophys. Res.*, **96**, 9379–9389, 1991.
- Rothman, L. S., et al., The HITRAN database: 1986 edition, *Appl. Opt.*, **26**, 4058–4097, 1987.
- Russell, J. M., III, C. B. Farmer, C. P. Rinsland, R. Zander, L. Froidevaux, G. C. Toon, B. Gao, J. Shaw, and M. Gunson, Measurements of odd nitrogen compounds in the stratosphere by the ATMOS experiment on Spacelab 3, *J. Geophys. Res.*, **93**, 1718–1736, 1988.
- Smith, M. A. H., Compilation of atmospheric gas concentration profiles from 0 to 50 km, *NASA Tech. Memo.*, TM83289, 1982. (Available as NTIS 82N22822 from the Natl. Tech. Inf. Serv., Springfield, Va.)
- Tejwani, G. D. T., and E. S. Yeung, Pressure-broadened linewidths of  $\text{HNO}_3$ , *J. Chem. Phys.*, **68**, 2012–2013, 1978.
- Thoning, K. W., P. P. Tans, and W. D. Komhyr, Atmospheric carbon dioxide at Mauna Loa Observatory, 2, Analysis of the NOAA GMCC data, 1974–1985, *J. Geophys. Res.*, **94**, 8549–8565, 1989.
- Toth, R. A., New measurements and analysis of  $\text{H}_2^{16}\text{O}$ ,  $\text{H}_2^{17}\text{O}$ , and  $\text{H}_2^{18}\text{O}$  in the  $6.2\text{ }\mu\text{m}$  region, paper presented at Forty-Fourth Symposium on Molecular Spectroscopy, Ohio State Univ., Columbus, 1989.
- Toth, R. A., The  $\nu_2$  band of  $\text{H}_2^{16}\text{O}$ —line strengths and transition frequencies, *J. Opt. Soc. Am. B*, in press, 1991.
- Wells, J. S., F. R. Petersen, A. G. Maki, and D. J. Sukle, Heterodyne frequency measurements on the  $11.6\text{-}\mu\text{m}$  band of OCS: New frequency/wavelength calibration tables for  $11.6\text{-}$  and  $5.8\text{-}\mu\text{m}$  OCS bands, *Appl. Opt.*, **20**, 1676–1684, 1981a.
- Wells, J. S., F. R. Petersen, A. G. Maki, and D. J. Sukle, Heterodyne frequency measurements on the  $11.6\text{-}\mu\text{m}$  band of OCS: New frequency/wavelength calibration tables for  $11.6\text{-}$  and  $5.8\text{-}\mu\text{m}$  OCS bands: Erratum, *Appl. Opt.*, **20**, 2874, 1981b.
- Wells, J. S., F. R. Petersen, and A. G. Maki, Heterodyne frequency measurements of carbonyl sulfide transitions at 26 and 51 Thz, Improved OCS,  $\text{O}^{13}\text{CS}$ , and  $\text{OC}^{34}\text{S}$  molecular constants, *J. Mol. Spectrosc.*, **98**, 404–412, 1983.
- World Meteorological Organization (WMO) Atmospheric ozone 1985—Assessment of our understanding of the processes controlling its present distribution and change, *WMO Rep. 16*, Geneva, 1986.
- R. D. Blatherwick, A. Goldman, J. J. Kusters, D. G. Murcray, and F. J. Murcray, Department of Physics, University of Denver, 2112 East Wesley, Denver, CO 80208.
- J.-M. Flaud and C. Camy-Peyret, Laboratoire de Physique Moléculaire et Applications, CNRS, Tour 13, Bte 76, 3<sup>e</sup> étage, Université Pierre et Marie Curie, 4 place Jussieu, 75252 Paris Cedex 05 France.
- C. P. Rinsland, Atmospheric Sciences Division, NASA Langley Research Center, Mail Stop 401A, Hampton, VA 23665-5225.

(Received August 28, 1991;  
revised November 8, 1991;  
accepted November 8, 1991.)

## APPENDIX 6

### High-resolution studies of atmospheric IR emission spectra

F.J. Murcray, F.H. Murcray, A. Goldman  
R.D. Blatherwick and D.G. Murcray  
Department of Physics, University of Denver  
Denver, Colorado 80208

#### 1. INTRODUCTION

The Network for the Detection of Stratospheric Change (NDSC) will consist of at least five sites located at different latitudes. Current sites include a site at Lauder, New Zealand; Mauna Loa, Hawaii; Jungfrauoch, Switzerland and two proposed high latitude sites in the Arctic and Antarctic. The instrumentation proposed for these sites includes a Fourier Transform Spectrometer (FTS) system to obtain very high resolution solar spectra in the mid infrared. One problem with the high latitude sites is that the sun does not get above the horizon during a significant portion of the year. Atmospheric emission spectroscopy offers an alternative way of obtaining data on several of the constituents of interest. The technique has the advantage that data can be obtained at any time of day or night. The major disadvantage is that the atmosphere is a much weaker source of radiation than the sun. Therefore in order to achieve the same spectral resolution at a given signal-to-noise ratio, one must integrate for a much longer time. The time required depends on the spectral region being covered and the spectral resolution one is trying to achieve. At shorter wavelengths and higher resolutions the integration times become prohibitive. At longer wavelengths it is possible to achieve an adequate signal-to-noise ratio in the spectrum with relatively short integration times by sacrificing a modest amount of spectral resolution. The trade off between spectral resolution and integration time obviously depends on the measurement objectives. These also dictate the instrumentation required to make the measurement. In this paper we present some preliminary results obtained with two different systems. These systems, which were designed with different experimental objectives, are used to illustrate the potential of the technique.

#### 2. INSTRUMENTATION

##### A. ANTARCTIC EMISSION RADIOMETER

The first system was designed for almost automatic operation at the South Pole. It is based on the BOMEM Michelson interferometer with  $1\text{ cm}^{-1}$  resolution. The Michelson system is a full 4 port interferometer, which provides some advantages in stability. A mercury-cadmium-telluride detector, a reference blackbody, a calibration blackbody, and an elevation scan mechanism were added to the stripped commercial instrument. The interferometer, detector, scan mechanism, and blackbodies were mounted outside the building, and had to be appropriately insulated to maintain the various components at their correct operating temperatures. Due to logistical constraints, the detector was operated with a Joule-Thompson cooler. Gas consumption precluded continuous operation, so data were recorded for 2 one-half hour periods each day, although the interferometer itself ran continuously.

Data were recorded on floppy discs by a personal computer, and a partial backup copy generated on the hard disk. The computer ran a scheduling program, which controlled the Joule-Thompson cooler and the elevation scan mechanism. It also monitored the instrument status for possible errors. Operator maintenance was required once per week to change the floppy disk, monitor gas consumption, check for computer generated error messages, and verify that the instrument optics were free of snow.

The instrument was installed in the Skylab building at the Amundsen-Scott South Pole station and began collecting data on December 5, 1989. It was turned over to the NSF winter over technician in late December. The system operated almost continuously until it was removed in late January of 1991. One of the instrument power supplies shut down, causing data loss for about 10 days. This was apparently a result of some electrical glitch in the building, but the supply restarted after being powered off and on. Gas consumption for the cooler was larger than expected, so the observing schedule had to be reduced during part of the year.

The instrument was designed to operate in the 500 to 1500  $\text{cm}^{-1}$  region. The primary purpose was to monitor atmospheric chemistry, with a strong secondary interest in the radiation budget. The instrument was set up to view two different angles (+15 and +45 degrees elevation). An initial concern was with the stability and calibration of an interferometer for radiometric purposes. For this reason, the instrument was calibrated during each observing sequence by devoting almost half of the time to viewing the calibration blackbody.

#### B. NDSC SOLAR SPECTROMETER

The second system is a modified Bruker Instruments IFS120 very high spectral resolution interferometer, under test for the Network for Detection of Stratospheric Change (NDSC). It is intended to observe the solar spectrum in the mid infrared, and is capable of 0.002  $\text{cm}^{-1}$  unapodized resolution.

The modifications consist primarily of removing the sample and detector compartments from the standard laboratory instrument, and installing the detectors in the beamsplitter compartment. The system is equipped with two detectors, a MCT for 5 to 15 microns and an InSb for 2 to 5 microns. A solar tracking system is usually installed to bring sunlight into the instrument, but for the emission observations it was removed, and skylight was directed into the interferometer by a set of mirrors.

Since the atmosphere is a weak source of radiation, the system resolution was reduced to 0.06  $\text{cm}^{-1}$  (apodized) for the emission measurements, allowing a larger field aperture and thus higher throughput. Scans were also coadded for about 20 minutes to improve the signal-to-noise ratio.

Data were taken from Denver on a number of clear days in the fall of 1990. The system was set to view low elevation angles to enhance the atmospheric path. No attempt was made to calibrate the spectra radiometrically.



### 3. RESULTS AND ANALYSIS

#### A. ANTARCTIC SPECTRA

As we have only had the data since January, the results reported here are from a limited sample and are preliminary. A check of the instrument calibrations showed a sudden change of about 20% in the fall, then all calibrations fall within 2% during the winter and spring. 2% is roughly the accuracy of the temperature measurements, so there was no measurable change in sensitivity after the one time shift. We are still trying to determine the source of the step change.

A sample spectrum is shown in Figure 1. This particular spectrum was taken on September 7, 1990 at the 15 degree elevation view. The 15 micron  $\text{CO}_2$  band is the predominate feature of the spectrum. It has an unusual appearance here, because of the strong temperature inversion just above the surface. This inversion is persistent in the winter data, and complicates fitting the  $\text{CO}_2$  band theoretically because the standard radiosonde data has one point at the surface and one point at the inversion height. One of our continuing projects is to try to extract temperature profile information from the spectra. The features around  $1050\text{ cm}^{-1}$  are the 9.6 micron ozone band. The region from about  $1250\text{ cm}^{-1}$  to  $1500\text{ cm}^{-1}$  is predominately water vapor and methane. Figure 2 shows the spectrum near  $1400\text{ cm}^{-1}$  along with a theoretical calculation including only water vapor. The fit required 200 microns of precipitable water, but may be modified slightly if a more accurate temperature profile can be obtained from the  $\text{CO}_2$  region.

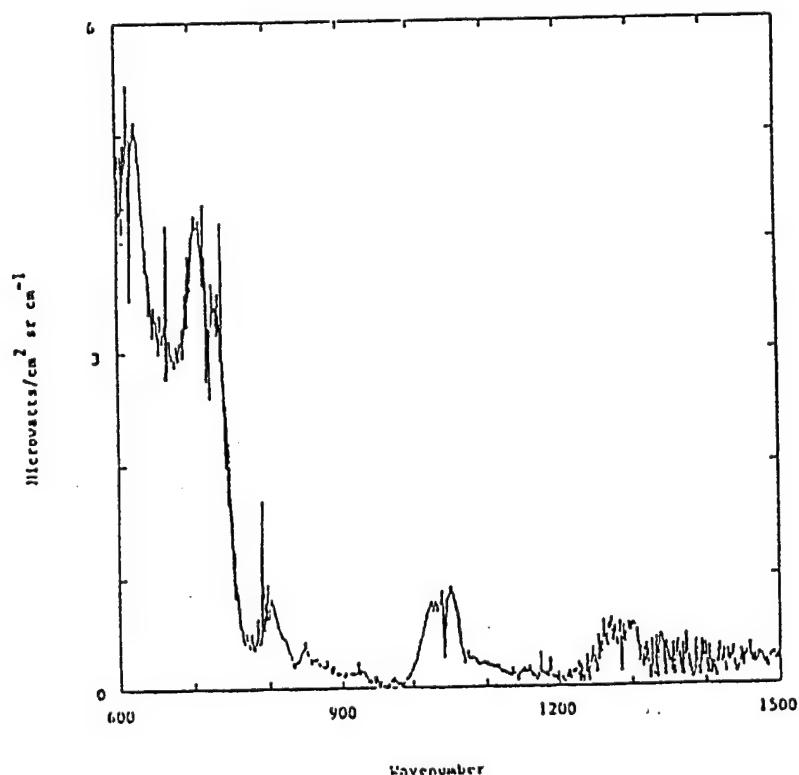


Figure 1. Spectrum taken with the atmospheric emission radiometer from the South Pole on September 7, 1990. The instrument was viewing  $15^\circ$  elevation.

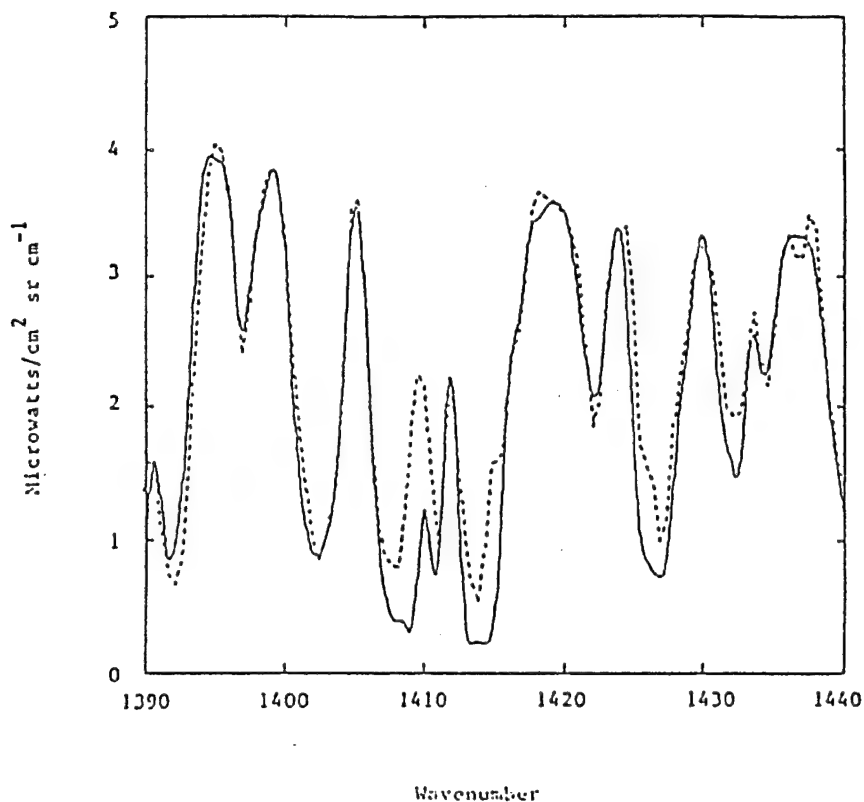


Figure 2. Expanded region of the 15° elevation spectrum of Sept. 7, 1990. Most of the features in this area are due to water vapor.

#### B. VERY HIGH RESOLUTION SPECTRA

A portion of an emission spectrum obtained with the NDSC instrument is shown in Figure 3. This covers a section of the  $\nu_5$  and  $2\nu_9$  bands of  $\text{HNO}_3$ . The strong features are weak water vapor lines. A calculated emission spectrum is also shown, using a standard temperature and water vapor profile. The ordinate scale applies to the calculated spectrum, the observed spectrum was linearly scaled and a zero subtracted to match the calculation. The agreement is very good except for the line at  $875.7 \text{ cm}^{-1}$ , which may have an incorrect strength listed in the data base. Another discrepancy is at  $876.6 \text{ cm}^{-1}$  which is probably due to  $\text{HNO}_3$ .

Figure 4 is an expanded view of the  $865$  to  $870 \text{ cm}^{-1}$  spectral interval. The upper spectrum (A) in this figure is a solar absorption spectrum taken at the same resolution as the emission data and plotted upside-down. The second spectrum (B) is the atmospheric emission in the same interval. The bottom (C) spectrum is a calculation. The emission features are mainly due to  $\text{HNO}_3$ . The broad feature in the experimental data in the  $867$  to  $868 \text{ cm}^{-1}$  and  $869$  to  $870 \text{ cm}^{-1}$  area is a channel spectrum due to a non-wedged filter. Some weak  $\text{HNO}_3$  lines appear in the observed spectra but are not in the calculation. The emission spectrum also shows a feature near  $868 \text{ cm}^{-1}$ , which is probably due to  $\text{NH}_3$ .  $\text{NH}_3$  is highly variable in concentration near the surface, and shows considerable enhancement in the emission spectrum compared to  $\text{HNO}_3$  because it is warmer since it is near the surface.

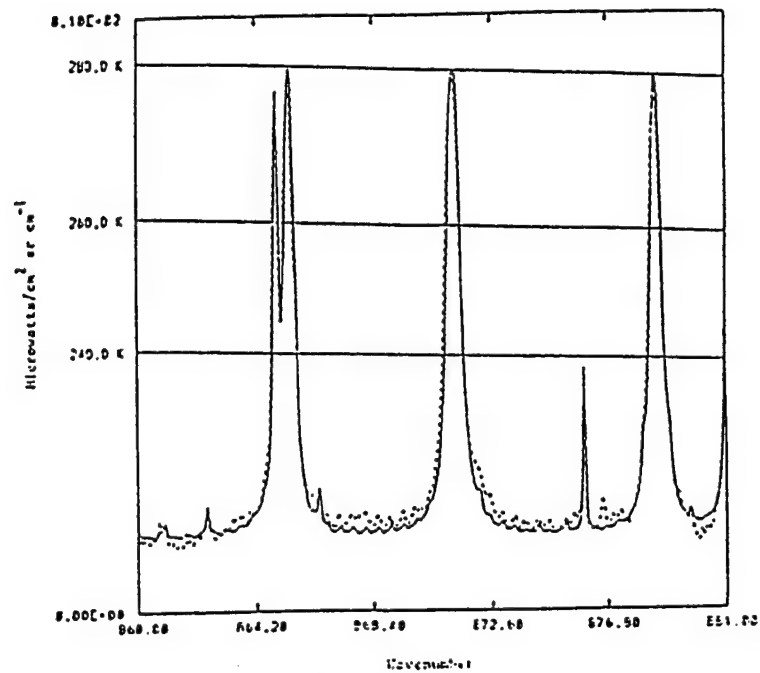


Figure 3. Portion of an atmospheric emission spectrum obtained at an elevation angle of  $15^\circ$ . This is compared with a spectrum calculated using a standard atmospheric temperature profile. The observed spectra is shown on the dashed line and has been adjusted to fit the water vapor features in the calculated spectra.

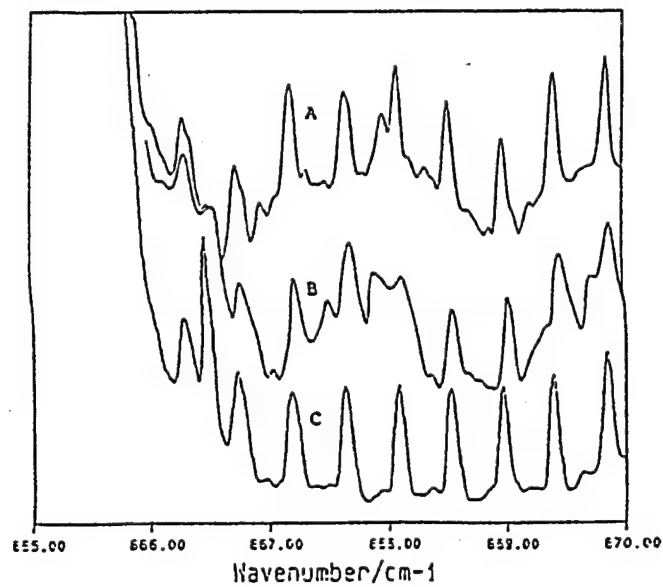


Figure 4. Enlarged portion of the emission spectrum given in Figure 3 (Curve B). This spectrum is compared with a solar spectrum (Curve A) obtained with the same instrument at about the same elevation angle. Also shown (Curve C) is a theoretical spectrum for the same spectral interval.

#### 4. CONCLUSIONS

We have presented atmospheric emission spectra obtained with two different spectrometer systems. The first system was designed for emission work. Spectra were obtained under adverse conditions in the Antarctic, and are still of good absolute accuracy. The second system demonstrates the sensitivity that can be achieved even at higher spectral resolution. Although the system was not calibrated, and is not particularly well designed for emission work, it still shows that mid infrared atmospheric emission spectra can be obtained with good signal-to-noise in a reasonable length of time at relatively high resolution. A properly designed high resolution system should achieve high accuracy, sensitivity and resolution, thereby permitting measurements of many atmospheric constituents when solar spectra can not be obtained.

#### 5. ACKNOWLEDGEMENTS

This research was supported in part by the National Science Foundation and in part by the National Aeronautics and Space Administration. Acknowledgement is made to the National Center for Atmospheric Research, which is supported by the National Science Foundation, for computer time used in this research.

## APPENDIX 7

The Fundamental Quadrupole Band of  $^{14}\text{N}_2$ : Line Positions from High-Resolution Stratospheric Solar Absorption Spectra

The purpose of this note is to report accurate measurements of the positions of *O*- and *S*-branch lines of the (1-0) vibration-rotation quadrupole band of molecular nitrogen ( $^{14}\text{N}_2$ ) and improved Dunham coefficients derived from a simultaneous least-squares analysis of these measurements and selected infrared and far infrared data taken from the literature. The new measurements have been derived from stratospheric solar occultation spectra recorded with Fourier transform spectrometer (FTS) instruments operated at unapodized spectral resolutions of 0.002 and 0.01  $\text{cm}^{-1}$ .

The motivation for the present investigation is the need for improved  $\text{N}_2$  line parameters for use in IR atmospheric remote sensing investigations. The *S* branch of the  $\text{N}_2$  (1-0) quadrupole band is ideal for calibrating the line-of-sight airmasses of atmospheric spectra since the strongest lines are well placed in an atmospheric window, their absorption is relatively insensitive to temperature and is moderately strong (typical line center depths of 10 to 50% in high-resolution ground-based solar spectra and in lower stratospheric solar occultation spectra), and the volume mixing ratio of nitrogen is constant in the atmosphere and well known. However, a recent investigation has shown the need to improve the accuracies of the  $\text{N}_2$  line positions, intensities, air-broadened half-widths, and their temperature dependences to fully exploit this calibration capability (1). The present investigation addresses the problem of improving the accuracy of the  $\text{N}_2$  line positions.

Nitrogen is a homonuclear diatomic molecule, and therefore electric dipole pure rotation and vibration-rotation transitions within the  $^1\Sigma_g^+$  ground electronic state are forbidden. For this reason, the vibrational and rotational constants of the ground electronic state have remained poorly determined with most of the reported values derived from medium-resolution Raman spectra recorded in the far infrared (2-4) and infrared (3-5) regions. Reuter *et al.* (6) used a White cell to achieve an absorption path length of 434 m and a FTS to obtain measurements of line positions in the *O* and *S* branches of the (1-0) vibration-rotation quadrupole band. The positions derived in Ref. (6) were significantly more precise than achieved previously, and the use of standard IR calibration techniques yielded a wavenumber calibration superior to those of the Raman investigations. Measurements with line position accuracies of 0.003 to 0.010  $\text{cm}^{-1}$  were reported from analysis of a spectrum recorded at 0.01- $\text{cm}^{-1}$  resolution. The results were limited in accuracy by the weakness of the  $\text{N}_2$  lines in the measured spectrum (maximum line center absorption of a few tenths of one percent).

The stratospheric measurements reported here were obtained from solar spectra recorded during flights by two different instruments. The first set of data was acquired from orbit on April 30-May 1, 1985, by the atmospheric trace molecule spectroscopy (ATMOS) instrument, a high speed FTS operating at an unapodized spectral resolution of 0.01  $\text{cm}^{-1}$  during its first Shuttle mission onboard Spacelab 3. For an overview of the ATMOS instrument and experiment and the Spacelab 3 results, see the review paper by Farmer (7). ATMOS-related data processing and science analysis methods are described in a paper by Norton and Rinsland (8). The other set of measurements was obtained with a FTS achieving an unapodized resolution of 0.002  $\text{cm}^{-1}$  onboard a balloon platform. The instrument is a modified commercial interferometer operated by the atmospheric spectroscopy group at the University of Denver. Solar observations were recorded both prior to and during sunset from a float altitude of  $36.6 \pm 0.5$  km during a flight from the National Scientific Balloon Facility in Palestine, Texas, on June 4, 1990. A description of the instrumentation and examples of spectra from several balloon flights can be found in the paper by Murcray *et al.* (9).

The positions of unblended  $\text{N}_2$  lines between *S*(4) and *S*(20) (2373 to 2492  $\text{cm}^{-1}$  region) have been measured from ATMOS spectra recorded with a filter covering approximately 1580 to 3400  $\text{cm}^{-1}$ . The continuum signal-to-rms noise in the  $\text{N}_2$  *S*-branch region is  $\sim 100$  in an individual spectrum. The stronger  $\text{N}_2$  *S*-branch lines first appear above the noise level at a tangent altitude of  $\sim 40$  km (10). Because the atmospheric density increases exponentially with decreasing altitude, the nitrogen lines strengthen rapidly

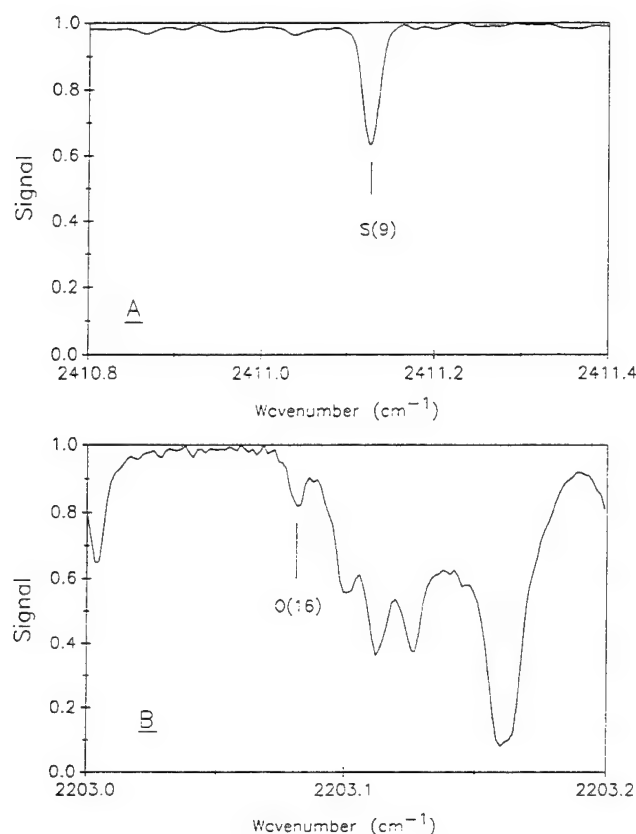


FIG. 1. Examples of  $^{14}\text{N}_2$  (1-0) band quadrupole lines in the ATMOS and University of Denver infrared stratospheric solar occultation spectra. The upper panel (A) shows the region of the  $S(9)$  line in a zonal average ATMOS spectrum with tangent altitude of 19.7 km. The slight decrease in signal to lower wavenumbers is caused by continuous absorption produced by the  $\text{N}_2$  pressure-induced (1-0) band and sub-Lorentzian absorption by the overlapping far wings of the intense  $\text{CO}_2$   $\nu_3$  fundamental band (11). The region of the  $O(16)$  line is plotted in the lower panel (B). The spectrum was recorded at a tangent altitude of 23.4 km with the University of Denver FTS. The nitrogen lines are identified and marked with vertical ticks in both panels.

with decreasing tangent altitude. The most accurate measurements are obtained from spectra recorded near a tangent altitude of 20 km where the stronger  $S$ -branch lines are prominent features in the ATMOS spectra (10).<sup>1</sup> At that altitude, the atmospheric pressure is  $\sim 40$  Torr, so that the effect of pressure-induced line shifts should be small. At lower tangent altitudes, the signal-to-noise ratio is decreased by continuum absorption resulting from the collision-induced fundamental vibration-rotation band of  $\text{N}_2$  and sub-Lorentzian absorption produced by the superposition of the far wings of the intense  $\text{CO}_2$   $\nu_3$  fundamental band (11). Also, the absorption by other telluric gases generally increases with decreasing tangent altitude so that interference effects become more of a limitation. For the present work, to improve the signal-to-noise ratio, we derived the line positions from zonal average ATMOS spectra obtained by coadding nearly equal tangent altitude spectra recorded during four sunset occultations near  $30^\circ\text{N}$  latitude. The line positions were measured with

a second derivative line finder algorithm and calibrated using accurate line positions reported for the  $N_2O$   $\nu_3$  (12) or  $\nu_1 + 2\nu_2$  bands (13). Nitrogen line positions from 1 to 4 ATMOS zonal spectra have been averaged for use in the subsequent analysis; the corresponding uncertainties were estimated on the basis of the standard deviation of the individual measurements and the calculated uncertainty derived from the formula given by Reuter *et al.* (6). A minimum uncertainty limit of  $0.0002 \text{ cm}^{-1}$  was adopted to account for the uncertainty in the absolute wavenumber calibration.

The balloon-borne solar spectra were recorded with a filter covering the  $1580$  to  $2230 \text{ cm}^{-1}$  region and hence provide measurements of only high- $J$   $N_2$  lines in the  $O$  branch. A total of 6  $N_2$  lines between  $O(13)$  and  $O(19)$  were selected for measurement based on comparisons of the solar spectra with synthetic spectrum calculations. All of the measured transitions are calculated to be free of significant blending by other telluric lines. The  $O(20)$   $N_2$  line also appears to be present, but it is at the limit of detection and was not included in the analysis. As the  $N_2$  lines occur near the edge of the band-pass filter, the continuum signal-to-rms noise ratio of a single spectrum decreases from  $\sim 100$  at the  $O(19)$  line to  $\sim 50$  at the  $O(13)$  line. The positions of the  $N_2$  lines were measured from one to three spectra recorded between tangent altitudes of  $28.1$  and  $18.0 \text{ km}$ . Mean values were used in the subsequent analysis. Calibration of the individual solar spectra was achieved by comparing measured positions of strong, isolated lines (e.g.,  $H_2O$  and  $CO_2$  transitions) with values derived from stratospheric spectra recorded with the same instrument during an earlier balloon flight. The calibration of this earlier dataset, which covers  $1400$  to  $1960 \text{ cm}^{-1}$ , is based on  $H_2O$  standard positions (14), scaled by the multiplicative factor recommended by Brown and Toth (15). The frequency scale of the new flight data was also checked using accurate  $NO_2$   $\nu_3$  band line positions (16), as well as direct comparisons of measured  $H_2O$  line center positions with the data of Brown and Toth (15). A second derivative line finder was used here to determine the location of the line centers. Uncertainties were estimated as described earlier. Figure 1 presents examples of the  $N_2$  lines in the ATMOS (A) and University of Denver (B) stratospheric solar spectra.

The line position measurements were analyzed with the Dunham formula for the upper and lower state term values (17)

$$F(v, J) = \sum_{ij} Y_{ij}(v + \frac{1}{2})^i [J(J+1)]^j \quad (1)$$

TABLE I  
Dunham Coefficients<sup>a</sup> for  $^{14}N_2$

Dunham Coefficient	This Study		Ref. 6	Ref. 5
	Case A	Case B		
$Y_{01}$	1.9982673(43)	1.9982369(56)	1.998286(13)	
$Y_{02} \times 10^6$	-5.761(10)	-5.747(14)	-5.763(40)	
$Y_{03} \times 10^{12}$	0.	4.78 <sup>b</sup>	0.	
$Y_{10}$	2329.91170(20)	2329.91156(21)	2329.91239(70)	
$Y_{11} \times 10^2$	-1.73717(9)	-1.73030(19)	-1.73121(67)	1.72978
$Y_{12} \times 10^8$	0.	-1.01(56)	0.	-0.832
$Y_{21} \times 10^5$	0.	-3.28(20) <sup>c</sup>	-3.28(20) <sup>c</sup>	-4.15
Weighted Error	$2.72 \times 10^{-4}$	$2.67 \times 10^{-4}$	$1.99 \times 10^{-3}$	

a) Values in parentheses are standard deviations in units of the last quoted digit of the coefficient.

b) Calculated from case A Dunham coefficients and Eq. 2 of Reuter *et al.* (6); value was held fixed in the analysis.

c) Taken from Lofthus and Krupenie (18); value was held fixed in the analysis.

with the coefficients  $Y_{ij}$  obtained from a weighted linear least-squares fit of the stratospheric measurements and additional data selected from reported laboratory experiments. Each weight was given by  $1/\sigma^2$ , where  $\sigma$  is the estimated uncertainty. The additional data were required because the stratospheric dataset covers only a limited range of transitions in the  $O$  and  $S$  branches. Three additional datasets were included: the ground state Raman measurements of Bendtsen (3), the Raman (1-0) band  $O$ -branch measurements of Bendtsen (3), and the quadrupole  $O$ - and  $S$ -branch (1-0) band measurements of Reuter *et al.* (6). The  $Q$ - and  $S$ -branch (1-0) band Raman measurements of Bendtsen (3) were excluded from the fit because they show a bias of about  $+0.009 \text{ cm}^{-1}$  with respect to our measured line positions and our fitting results; this offset was noted previously by Reuter *et al.* (6). Similarly, the calibrated coherent anti-Stokes Raman (CARS) (1-0) band  $Q$ -branch measurements of Gilson *et al.* (5) were excluded from the fit because of a calibration bias in the data (also about  $+0.009 \text{ cm}^{-1}$ ). No obvious offset was noted between our measurements and the  $O$ -branch (1-0) band positions from Ref. (3) so we retained those data in the analysis.

Table I presents the two sets of Dunham coefficients obtained from the least-squares analysis. Set A was obtained by fitting the coefficients  $Y_{10}$ ,  $Y_{01}$ ,  $Y_{11}$ , and  $Y_{02}$  with all other Dunham coefficients constrained to zero. For set B, the coefficient  $Y_{12}$  was fitted in addition to the same four Dunham coefficients. Also,  $Y_{21}$  was fixed at the value  $-3.28 \times 10^{-5}$ , as determined by Lofthus and Krupenie (18), and  $Y_{03}$  was set to  $4.78 \times 10^{-12}$ , a value estimated from Dunham's theory (17) by substituting the  $Y_{01}$  and  $Y_{11}$  values from set A and the  $Y_{10}$  value of  $2358.5665 \text{ cm}^{-1}$  from Ref. (5) into Eq. (2) of Reuter *et al.* (6). The  $Y_{10}$  value from our analysis was not used in these calculations because only two vibrational states were studied in this work.

TABLE II  
Experimental Line Positions<sup>a</sup> for  $^{14}\text{N}_2$

$v'$	$J'$	$v''$	$J''$	Measured Position	R	U	$v'$	$J'$	$v''$	$J''$	Measured Position	R	U
0	2	0	0	11.9344 <sup>b</sup>	-2.9	10.0	1	9	0	11	2244.8345 <sup>c</sup>	-5.2	3.0
0	3	0	1	19.8941 <sup>b</sup>	-0.9	10.0	1	8	0	10	2253.0967 <sup>c</sup>	-0.1	3.0
0	4	0	2	27.8517 <sup>b</sup>	-0.3	10.0	1	7	0	9	2261.3203 <sup>b</sup>	-1.5	10.0
0	5	0	3	35.8084 <sup>b</sup>	0.4	10.0	1	6	0	8	2269.5146 <sup>c</sup>	0.2	3.0
0	6	0	4	43.7629 <sup>b</sup>	0.0	10.0	1	5	0	7	2277.6737 <sup>b</sup>	-0.6	10.0
0	7	0	5	51.7163 <sup>b</sup>	0.2	10.0	1	4	0	6	2285.8056 <sup>b</sup>	4.3	10.0
0	8	0	6	59.6658 <sup>b</sup>	-1.8	10.0	1	3	0	5	2293.8986 <sup>b</sup>	3.5	10.0
0	9	0	7	67.6162 <sup>b</sup>	-0.9	10.0	1	2	0	4	2301.9561 <sup>b</sup>	0.7	10.0
0	10	0	8	75.5643 <sup>b</sup>	0.1	10.0	1	1	0	3	2309.9851 <sup>b</sup>	3.2	10.0
0	11	0	9	83.5061 <sup>b</sup>	-2.5	10.0	1	0	0	2	2317.9750 <sup>b</sup>	0.7	10.0
0	12	0	10	91.4513 <sup>b</sup>	1.1	10.0	1	6	0	4	2372.9433	-1.6	2.4
0	13	0	11	99.3881 <sup>b</sup>	-0.5	10.0	1	8	0	6	2388.3288	0.2	0.2
0	14	0	12	107.3242 <sup>b</sup>	0.7	10.0	1	9	0	7	2395.9652	-0.2	0.2
0	15	0	13	115.2546 <sup>b</sup>	-0.1	10.0	1	10	0	8	2403.5651	0.0	0.2
0	16	0	14	123.1839 <sup>b</sup>	2.0	10.0	1	11	0	9	2411.1273	-0.0	0.3
0	17	0	15	131.1061 <sup>b</sup>	1.2	10.0	1	12	0	10	2418.6519	-0.1	0.2
0	18	0	16	139.0205 <sup>b</sup>	-2.8	10.0	1	13	0	11	2426.1389	0.2	0.2
0	19	0	17	146.9378 <sup>b</sup>	1.0	10.0	1	14	0	12	2433.5871	-0.1	0.2
0	20	0	18	154.8418 <sup>b</sup>	-3.5	10.0	1	15	0	13	2440.9973	0.0	0.2
1	17	0	19	2177.6601	1.1	1.0	1	16	0	14	2448.3709 <sup>c</sup>	2.4	3.0
1	16	0	18	2186.1621	-1.2	0.8	1	17	0	15	2455.7008	0.1	0.2
1	15	0	17	2194.6277 <sup>b</sup>	-9.9	30.0	1	18	0	16	2462.9934	-0.2	0.3
1	14	0	16	2203.0818	0.1	0.4	1	19	0	17	2470.2474 <sup>c</sup>	0.5	7.0
1	13	0	15	2211.4956	0.2	0.5	1	20	0	18	2477.4619 <sup>c</sup>	1.6	3.0
1	12	0	14	2219.8781	-0.2	0.5	1	21	0	19	2484.6349	1.4	1.9
1	11	0	13	2228.2309	0.7	0.9	1	22	0	20	2491.7658	-0.5	1.3
1	10	0	12	2236.5481 <sup>c</sup>	-2.6	3.0							

a) Measured line positions are in  $\text{cm}^{-1}$ , R is the residual (measured minus calculated) in  $10^{-3} \text{ cm}^{-1}$  obtained with the set B constants given in Table I, and U is the estimated uncertainty in  $10^{-3} \text{ cm}^{-1}$ . Uncertainties for transitions from Refs. (3,6) are taken from Table I of Ref. (6). Uncertainties from the present work have been estimated as described in the text.

b) These measurements are taken from Ref. (3).

c) These measurements are taken from Ref. (6).



and all higher-order pure vibrational Dunham coefficients were constrained to values of zero. This procedure produces a fitted coefficient that is an underestimate of  $Y_{10}$ . In Table I, we also give the weighted fitting error  $(N \sum w_i \delta_i^2 / m \sum w_i)^{1/2}$ , where  $N$  is the number of lines,  $m$  is the number of degrees of freedom, and  $\delta_i$  is the observed minus calculated wavenumber for line  $i$  (6).

Examination of the values in Table I indicates that the uncertainties in the case A coefficients are slightly smaller than those of case B. The case A and case B values are consistent among themselves, but the coefficients from the two solutions are sometimes slightly outside the range of the calculated uncertainties. Table I also lists previously reported values for the Dunham coefficients. The accuracies of  $Y_{01}$ ,  $Y_{02}$ ,  $Y_{10}$ , and  $Y_{11}$  have been improved by about a factor of 3 compared to the results in Ref (6). No error estimates were given for the Dunham coefficients listed in Ref. (5), but the present values are generally consistent with those results. The  $Y_{12}$  coefficient determined in case B has an uncertainty of  $\sim 50\%$ . Within this uncertainty, the measured value of  $-1.01 \times 10^{-8}$  agrees with a value of  $-7.9 \times 10^{-9}$  calculated from Eq. (3) of Reuter *et al.* (6), the case B values of  $Y_{11}$  and  $Y_{01}$ , and the values of  $Y_{10}$  and  $Y_{20}$  reported by Gilson *et al.* (5).

Table II presents the measurement results and the residuals of the case B weighted least-squares best fit to the data. The case A results, which are not reported, are very similar. For most lines, the residual (measured minus calculated) position is less than the estimated uncertainty. The residuals of both the far infrared and infrared data show no obvious trend with  $J$ . Reuter *et al.* (6) noted that the pure rotational lines showed a slight negative bias in the residuals of their fit, but this offset does not appear in the present results nor is it obvious in ground state combination differences computed from the stratospheric infrared line positions.

We examined published  $0.0033\text{-cm}^{-1}$  resolution stratospheric emission spectra for the presence of the ground state  $v = 0-0$  quadrupole lines of  $\text{N}_2$ . The  $7-40\text{ cm}^{-1}$  interval covered in the atlas of Baldecchi *et al.* (19, 20) and the few small higher wavenumber intervals in Refs. (21-23) show only the  $S(1)$  and  $S(4)$  lines at  $19.895$  and  $43.763\text{ cm}^{-1}$  in regions nearly free of interfering telluric features (see Fig. 13 of Ref. (19) and Fig. 2 of Ref. (23)). The absence of any significant features at the predicted positions of these transitions indicates that the  $\text{N}_2$  pure rotational quadrupole band is extremely weak.

#### ACKNOWLEDGMENTS

Research at the Jet Propulsion Laboratory (JPL), California Institute of Technology, was performed under contract to the National Aeronautics and Space Administration. Research at the University of Denver was funded by NASA and the National Science Foundation (NSF). The Ministère de l'Éducation Nationale, Belgium, partially supported the investigations at the University of Liège.

#### REFERENCES

1. PH. DEMOULIN, C. B. FARMER, C. P. RINSLAND, AND R. ZANDER, *J. Geophys. Res.*, accepted for publication.
2. R. J. BUTCHER, D. V. WILLETTS, AND W. J. JONES, *Proc. R. Soc. London A* **324**, 231-245 (1971).
3. J. BENDTSEN, *J. Raman Spectrosc.* **2**, 133-145 (1974).
4. B. P. STOICHEFF, *Can. J. Phys.* **32**, 630-634 (1954).
5. T. R. GILSON, I. R. BEATTIE, J. D. BLACK, D. A. GREENHALGH, AND S. N. JENNY, *J. Raman Spectrosc.* **9**, 361-368 (1980).
6. D. REUTER, D. E. JENNINGS, AND J. W. BRAULT, *J. Mol. Spectrosc.* **115**, 294-304 (1986).
7. C. B. FARMER, *Mikrochim. Acta [Wien]* **III**, 189-214 (1987).
8. R. H. NORTON AND C. P. RINSLAND, *Appl. Opt.* **30**, 389-400 (1991).
9. F. J. MURCRAY, J. J. KOSTERS, R. D. BLATHERWICK, J. OLSON, AND D. G. MURCRAY, *Appl. Opt.* **29**, 1520-1525 (1990).
10. C. B. FARMER AND R. H. NORTON, unpublished.
11. C. P. RINSLAND, R. ZANDER, J. S. NAMKUNG, C. B. FARMER, AND R. H. NORTON, *J. Geophys. Res.* **94**, 16,303-16,322 (1989).
12. R. A. TOTH, *J. Opt. Soc. Am. B Opt. Phys.* **4**, 357-374 (1987).
13. R. A. TOTH, unpublished results, 1991.
14. G. GUELACHVILI AND K. NARAHARI RAO, "Handbook of Infrared Standards," Academic Press, Orlando, FL, 1986.

15. L. R. BROWN AND R. A. TOTH, *J. Opt. Soc. Am. B Opt. Phys.* **2**, 842-856 (1985).
16. L. R. ZINK, M. VANEK, AND J. S. WELLS, unpublished.
17. J. L. DUNHAM, *Phys. Rev.* **41**, 721-731 (1932).
18. A. LOFTHUS AND P. H. KRUPENIE, *J. Phys. Chem. Ref. Data* **6**, 113-307 (1977).
19. M. G. BALDECCHI, B. CARLI, F. MENCARAGLIA, A. BONETTI, AND M. CARLOTTI, *J. Geophys. Res.* **89**, 11,689-11,704 (1984).
20. M. G. BALDECCHI, B. CARLI, F. MENCARAGLIA, A. BARBIS, A. BONETTI, AND M. CARLOTTI, *J. Geophys. Res.* **93**, 5303-5318 (1988).
21. B. CARLI, F. MENCARAGLIA, AND A. BONETTI, *Int. J. Infrared Millimeter Waves* **3**, 385-394 (1982).
22. B. CARLI, F. MENCARAGLIA, A. BONETTI, B. M. DINELLI, AND F. FORNI, *Int. J. Infrared Millimeter Waves* **4**, 475-488 (1983).
23. B. CARLI AND J. H. PARK, *J. Geophys. Res.* **93**, 3851-3865 (1988).

C. P. RINSLAND

NASA Langley Research Center  
Atmospheric Sciences Division  
Mail Stop 401A  
Hampton, Virginia 23665-5225

R. ZANDER

Institute of Astrophysics  
University of Liège  
4200 Liège-Ougrée  
Belgium

Department of Physics  
University of Denver  
Denver, Colorado

A. GOLDMAN  
F. J. MURCRAY  
D. G. MURCRAY

M. R. GUNSON  
C. B. FARMER

Jet Propulsion Laboratory  
California Institute of Technology  
Mail Stop 183-301  
4800 Oak Grove Drive  
Pasadena, California  
Received March 4, 1991

## APPENDIX 8

### Analysis of Atmospheric Trace Constituents from High Resolution Infrared Balloon-Borne and Ground-Based Solar Absorption Spectra

A. Goldman, F.J. Murcray, C.P. Rinsland\*, R.D. Blatherwick,  
F.H. Murcray, and D.G. Murcray

Department of Physics, University of Denver  
Denver CO 80208

\*Atmospheric Sciences Division, NASA Langley Research Center  
Hampton VA 23665

#### ABSTRACT

Recent results and ongoing studies of high resolution solar absorption spectra will be presented. The analysis of these spectra is aimed at the identification and quantification of trace constituents important in atmospheric chemistry of the stratosphere and upper troposphere.

Analysis of balloon-borne and ground-based spectra obtained at  $0.0025\text{ cm}^{-1}$  covering the  $700\text{--}2200\text{ cm}^{-1}$  interval will be presented. Results from ground-based  $0.02\text{ cm}^{-1}$  solar spectra, from several locations such as Denver, South Pole, M. Loa, and New Zealand will also be shown. The  $0.0025\text{ cm}^{-1}$  spectra show many new spectroscopic features. The analysis of these spectra, along with corresponding laboratory spectra, improves the spectral line parameters, and thus the accuracy of trace constituents quantification. The combination of the recent balloon flights, with earlier flights data since 1978 at  $0.02\text{ cm}^{-1}$  resolution, provides trends analysis of several stratospheric trace species. Results for  $\text{COF}_2$ , F22,  $\text{SF}_6$  and other species will be presented. Analysis of several ground-based solar spectra provides trends for HCl, HF and other species.

The retrieval methods used for total column density and altitude distribution for both ground-based and balloon-borne spectra will be presented. These are extended for the analysis of the ground-based spectra to be obtained by the high resolution interferometers of the Network for Detection of Stratospheric Change (NDSC). Progress of the University of Denver studies for the NDSC will be presented. This will include intercomparison of solar spectra and trace gases retrievals obtained from simultaneous scans by the high resolution ( $0.0025\text{ cm}^{-1}$ ) interferometers of BRUKER and BOMEM.

#### 1. INTRODUCTION

The technique of infrared solar spectra has been used for many years to obtain information about the column abundance and vertical distribution of atmospheric gases. To maximize retrieval of this information, nonlinear multiparameters spectral least squares fitting methods have been developed, and since 1980 became an important tool in our research.<sup>1-4</sup> Subsequent studies (see below), conducted with higher resolution and signal to noise spectra, allowed to further enhance these analysis methods.

The spectral least square programs can fit simultaneously several spectral regions of several spectral scans, with three kinds of parameters: (i) instrumental parameters, such as resolution and background contours with channel and phase corrections, (ii) atmospheric (or laboratory) parameters such as the temperature and gas amounts in isothermal layers, and (iii) spectral line parameters such as line positions, intensities and half widths. The programs allow the initial parameters to remain fixed or vary within a constrained range of a priori values. The fitted parameters include the scaling of the initial mixing ratio distribution functions which determine the gas amount.

The atmospheric spectroscopy group at the University of Denver has been studying atmospheric infrared absorption with several types of balloon-borne, aircraft and ground-based spectrometers for many years. The instrumentation used in recent experiments includes  $0.002\text{--}0.003\text{ cm}^{-1}$  (unapodized) resolution FTS systems<sup>5</sup> and  $0.0005\text{ cm}^{-1}$  resolution tunable diode LHS system<sup>6</sup> for atmospheric solar absorption spectra. Ground-based measurements have been made from various

locations, e.g. Denver, New Mexico, Hawaii, New Zealand, the South Pole, and McMurdo, during several seasons over the last few years. Balloon flights were made from several locations in the U.S. and Europe. The field measurements are supplemented by extensive laboratory spectra, mostly taken with the field spectrometers. The analysis of these spectra has been very successful in the identification and quantification of atmospheric trace gases, some monitored since 1980, and upgrading the theoretical capabilities of atmospheric spectroscopy. Analysis of the data includes detailed atlases with complete identifications of the individual atmospheric and solar lines, molecular spectroscopic constants and line parameters analysis of selected bands, theoretical line-by-line and cross sections simulations of emission and absorption spectra, and spectral least-squares fitting using the most current atmospheric absorption parameters. These show good agreement with the data in many spectral intervals and also many new spectral features in the stratospheric spectrum. In this paper, samples of our recent 0.002-0.003  $\text{cm}^{-1}$  data and analysis leading to advances in atmospheric spectroscopy will be discussed. Quantification of several trace gases since 1980 will be summarized from 0.02  $\text{cm}^{-1}$  and 0.002  $\text{cm}^{-1}$  data.

Work in progress with new BRUKER and BOMEM interferometer systems towards the NDSC (Network for Detection of Stratospheric Change) will be presented, including intercomparisons, and further developments in the retrieval methods.

## 2. RESULTS

### 2.1 Balloon-borne spectra

We have studied the new infrared spectroscopic observations of several important stratospheric trace gases obtained with a 0.002  $\text{cm}^{-1}$  resolution interferometer system now covering the 700-2200  $\text{cm}^{-1}$  region.<sup>7-8</sup> Most stratospheric species are measurable in these spectra. The main molecules studied are  $\text{O}_3$ ,  $\text{HNO}_3$ ,  $\text{ClONO}_2$ ,  $\text{HO}_2\text{NO}_2$ ,  $\text{NO}_2$ ,  $\text{COF}_2$ ,  $\text{SF}_6$  and  $\text{CHClF}_2$ . The stratospheric solar spectra, ground-based solar spectra, and laboratory spectra reveal new details of the absorption by these molecules which are important in determining the photochemistry and the heat balance of the atmosphere. It has been possible to assign numerous previously unidentified features to these gases in the stratospheric spectra and to incorporate several new sets of spectral line parameters and cross sections from their simulation.

Many of these features were not accounted for in the previous line parameters compilations, and will be included in future data bases, HITRAN91 and GEISA91. A number of spectral regions have been atlased in detail.<sup>9</sup> Fig. 1 shows a sample from the atlas. The high resolution 10  $\mu\text{m}$  spectra have been analyzed with the new ozone line parameters<sup>10</sup> to determine the isotopic ratios of  $^{16}\text{O}^{16}\text{O}^{18}\text{O}$  and  $^{16}\text{O}^{18}\text{O}^{16}\text{O}$  in the stratosphere.

The excellent agreement between the highly precise laboratory and stratospheric spectra provided significant new evidence for absorption by the  $\text{HO}_2\text{NO}_2$  802.7  $\text{cm}^{-1}$  Q branch in the lower stratosphere. The improved resolution of the flights measurements reveals additional details of the interference in the  $\text{ClONO}_2$  780.2  $\text{cm}^{-1}$   $\nu_4$  Q branch region, including the identification of overlapping  $\text{HNO}_3$   $\nu_8$  features. New analysis of the  $\text{COF}_2$   $\nu_6$  band and the  $\nu_4$  band, and recent analysis of the  $\text{HNO}_3$   $\nu_8$  and  $\nu_8+\nu_9$  bands have been applied to both laboratory and stratospheric spectra. New features of other trace gases (e.g.  $\text{ClONO}_2$ ,  $\text{HNO}_3$  and  $\text{CF}_4$  in the 1280  $\text{cm}^{-1}$  region) have been identified in the stratospheric spectra and are currently under study with new line parameters and cross-sections.

The 5-7  $\mu\text{m}$  spectra are also being studied for numerous new  $\text{O}_3$  features. Updated line parameters of  $\text{HNO}_3$   $\nu_2$ ,  $\text{O}_3$  5 $\mu$  bands, and  $\text{H}_2\text{O}$   $\nu_2$  bands are now used for new retrievals of  $\text{HNO}_3$ . The  $\text{NO}_2$  spectral lines in the 6  $\mu\text{m}$  region show the need for further update. The combination of the high resolution flight data with other solar spectral data allows improvements in the spectral line parameters of the reference gases  $\text{O}_2$  and  $\text{N}_2$ , but further studies are needed.<sup>11-12</sup>

The long time span covered by medium and high resolution infrared atmospheric absorption measurements generated considerable interest in studying trends of atmospheric trace gases. Thus, an analysis of both recent 0.002  $\text{cm}^{-1}$  spectra and previous 0.02  $\text{cm}^{-1}$  spectra provided long term trends for  $\text{SF}_6$ ,  $\text{CHClF}_2$ , and  $\text{COF}_2$  over the last decade. Exponential increase rates of  $(7.4 \pm 1.9)\%$ ,  $(9.4 \pm 1.3)\%$  and  $(10.3 \pm 1.8)\%$   $\text{year}^{-1}$  were found.<sup>13</sup>

### 2.2 Ground-based spectra

We have performed quantitative analysis of the absorption by a number of minor and trace constituents in 0.02  $\text{cm}^{-1}$

resolution solar absorption spectra geographical locations.<sup>13-20</sup> In addition to various measurements from Denver, these include the total vertical column amounts of H<sub>2</sub>O (and isotopes), CO<sub>2</sub>, O<sub>3</sub>, N<sub>2</sub>O, CH<sub>4</sub>, CHClF<sub>2</sub>, NO, NO<sub>2</sub>, HCl, and HNO<sub>3</sub> from M. Loa, Hawaii, in February 1987; O<sub>3</sub>, N<sub>2</sub>O, HNO<sub>3</sub>, CO<sub>2</sub>, CH<sub>4</sub>, and CF<sub>2</sub>Cl<sub>2</sub> in December 1980 and November-December 1986 from the South Pole; HCl, NO, NO<sub>2</sub>, and C<sub>2</sub>H<sub>6</sub> in December 1986 from the S. Pole, and HCl, HNO<sub>3</sub>, O<sub>3</sub>, ClONO<sub>2</sub>, and NO<sub>2</sub> from McMurdo, Antarctica during the spring 1987 ozone hole. In the M. Loa measurements it was found that the average tropospheric concentrations deduced for CO<sub>2</sub>, N<sub>2</sub>O and CH<sub>4</sub> are very consistent with correlative NOAA GMCC surface data.

Of particular interest is the observed increase in the CF<sub>2</sub>Cl<sub>2</sub> column amount above the S. Pole over the 6 year period, corresponding to  $(3.6 \pm 2.1)\%$  year<sup>-1</sup>. The column amount of HNO<sub>3</sub> for both 1980 and 1986 were not significantly different. Other data sets, such as from the National Solar Observatory (NSO) at Kitt Peak were used for monitoring trends of HF and HCl from 0.02-0.005 cm<sup>-1</sup> spectra obtained during the 1977-1990 period. Linear increase rates of  $(10.7 \pm 1.1)\%$  year<sup>-1</sup> and  $(4.9 \pm 0.7)\%$  year<sup>-1</sup> have been obtained for HF and HCl respectively.

We have also been conducting 0.002-0.003 cm<sup>-1</sup> resolution solar absorption ground-based measurements, for periodic observations and monitoring of the atmosphere from Denver. The initial measurements were made with the balloon-borne BOMEM FTS system.<sup>5</sup> Typical results are shown in Figures 2-5. More recently, dedicated BOMEM and BRUKER FTS have been used, one of which will be moved to Mauna Loa as soon as the NDSC station becomes operational. Preliminary results are shown in Figures 6-10.

The analysis of the ground-based spectra shows that the trace gases of interest to the NDSC can be well monitored from selected spectral intervals of multiscans measurements, with temperatures and geometry and instrumental performance monitored from reference gases. It is apparent that no more than scale height vertical resolution can usually be expected for the altitude distribution of the trace gases, and in some cases only the tropospheric and stratospheric components could be separated. The translation of the statistical errors of the spectral least squares fitting to absolute errors estimates from a priori constraints and accuracies requires further studies.

### 3. CONCLUSIONS

High resolution stratospheric spectra show many new spectral features not observed in previous lower resolution spectra. This requires new analysis of laboratory and atmospheric spectra and improved theoretical calculations for many molecular bands of atmospheric interest. Atmospheric spectra remain a powerful source for observing and monitoring our changing atmosphere.

Retrieval methods based on spectral least squares are best suited for spectroscopic quantification, but further development are desired.

### 4. ACKNOWLEDGMENTS

Research was at the University of Denver supported in part by NSF and in part by NASA. Acknowledgement is made to the National Center for Atmospheric Research, which is sponsored by the National Science Foundation, for computer time used in this work. We thank A. Maki, L.R. Brown, J.-M. Flaud, and C. Camy-Peyret, and others for collaboration on new spectral line parameters, and to N.D. Sze, M. Ko, R. Cicerone and others for providing photochemical modeling.

### 5. REFERENCES

1. E. Niple, W.G. Mankin, A. Goldman, D.G. Murcray, and F.J. Murcray, "Stratospheric NO<sub>2</sub> and H<sub>2</sub>O Mixing Ratio Profiles from High Resolution Infrared Solar Spectra Using Nonlinear Least Squares," *Geophys. Res. Lett.*, 7, 489-492, 1980.
2. A. Goldman, D.G. Murcray, F.J. Murcray, and E. Niple, "High Resolution IR Balloon-Borne Solar and Laboratory Spectra in the HNO<sub>3</sub> 1720-cm<sup>-1</sup> Region: An Analysis," *Appl. Opt.*, 19, 3721-3724, 1980.
3. C.P. Rinsland, A. Goldman, F.J. Murcray, D.G. Murcray, M.A. H. Smith, R.K. Scals, Jr., J.C. Larsen, and P.L. Rinsland, "Stratospheric N<sub>2</sub>O Mixing Ratio Profile from High-Resolution Balloon-Borne Solar Absorption Spectra and

Laboratory Spectra Near  $1880\text{ cm}^{-1}$ ," *Appl. Opt.*, 21, 4351-4355, 1982.

4. A. Goldman, F.G. Fernald, F.J. Murcray, F.H. Murcray, and D.G. Murcray, "Spectral Least Squares Quantification of Several Atmospheric Gases from High Resolution Infrared Solar Spectra Obtained at the South Pole," *J. Quant. Spectrosc. Radiat. Transfer*, 29, 189-204, 1983.

5. F.J. Murcray, J.J. Kusters, R.D. Blatherwick, J. Olson, and D.G. Murcray, "High Resolution Solar Spectrometer System for Measuring Atmospheric Constituents," *Appl. Opt.*, 29, 1520-1525, 1990.

6. C.T. McElroy, A. Goldman, P.F. Fogel, and D.G. Murcray, "Heterodyne Spectrophotometry of Ozone in the  $9.6\text{-}\mu\text{m}$  Band using a Tunable Diode Laser," *J. Geophys. Res.*, 95, D5, 5567-5575, 1990.

7. A. Goldman, F.J. Murcray, D.G. Murcray, J.J. Kusters, C.P. Rinsland, C. Camy-Peyret, J.-M. Flaud, and A. Barbe, "Isotopic Abundances of Stratospheric Ozone from Balloon-Borne High-Resolution Infrared Solar Spectra," *J. Geophys. Res.*, 94, 8467-8473, 1989.

8. A. Goldman, F.J. Murcray, R.D. Blatherwick, J.J. Kusters, F.H. Murcray, D.G. Murcray, and C.P. Rinsland, "New Spectral Features of Stratospheric Trace Gases Identified from High Resolution Infrared Balloon-Borne and Laboratory Spectra," *J. Geophys. Res.*, 94, 14,945-14,955, 1989.

9. A. Goldman, R.D. Blatherwick, J.J. Kusters, F.J. Murcray, F.H. Murcray, and D.G. Murcray, "Atlas of Very High Resolution Stratospheric IR Absorption Spectra, Volume I, Line Positions and Identifications, Volume II, The Spectra," *Department of Physics, University of Denver*, Dec., 1990.

10. J.-M. Flaud, C. Camy-Peyret, C.P. Rinsland, V. Malathy Devi, M.A.H. Smith, and A. Goldman, "Improved Line Parameters for the Ozone Bands in the  $10\text{-}\mu\text{m}$  Spectral Region," *Appl. Opt.*, 29, 3667-3671, 1990.

11. M. Dang-Nhu, R. Zander, A. Goldman, and C.P. Rinsland, "Identification of Magnetic Dipole Infrared Transitions of the Fundamental Band of Oxygen," *J. Molec. Spectrosc.*, 144, 366-373, 1990.

12. C.P. Rinsland, R. Zander, Ph. Demoulin, A. Goldman, M.R. Gunson, and C.B. Farmer, "The Fundamental Quadrupole Band of  $^{14}\text{N}_2$ : Line Positions from High Resolution Solar Absorption Spectra," To be submitted, 1991.

13. C.P. Rinsland, A. Goldman, F.J. Murcray, R.D. Blatherwick, J.J. Kusters, D.G. Murcray, N.D. Sze, and S.T. Massie, "Long-Term Trends in the Concentration of  $\text{SF}_6$ ,  $\text{CHClF}_2$ , and  $\text{COF}_2$  in the Lower Stratosphere from Analysis of High-Resolution Infrared Solar Occultation Spectra," *J. Geophys. Res.*, 95, D10, 16,477-16,490, 1990.

14. F.J. Murcray, F.H. Murcray, A. Goldman, D.G. Murcray, and C.P. Rinsland, "Infrared Measurements of Several Nitrogen Species above the South Pole in December 1980 and November-December 1986," *J. Geophys. Res.*, 92, 13,373-13,376, 1987.

15. A. Goldman, C.P. Rinsland, F.J. Murcray, F.H. Murcray, and D.G. Murcray, "Measurements of Atmospheric Gases above the South Pole in December 1986 from High-Resolution 3 to  $4\text{ }\mu\text{m}$  Solar Spectra," *J. Geophys. Res.*, 93, D6, 7069-7074, 1988.

16. C.P. Rinsland, A. Goldman, F.J. Murcray, F.H. Murcray, R.D. Blatherwick, and D.G. Murcray, "Infrared Measurements of Atmospheric Gases Above Mauna Loa, Hawaii, in February 1987," *J. Geophys. Res.*, 93, D10, 12,607-12,626, 1988.

17. C.P. Rinsland, A. Goldman, F.J. Murcray, F.H. Murcray, "Increased  $\text{CF}_2\text{Cl}_2$  (CFC-12) Absorption above the South Pole," *Appl. Opt.*, 27, 627-630, 1988.

18. F.J. Murcray, A. Matthews, A. Goldman, P. Johnston, and C.P. Rinsland, " $\text{NH}_3$  Column Abundances over Lauder, New Zealand," *J. Geophys. Res.*, 94, 2235-2238, 1988.

19. F.J. Murcray, A. Goldman, R.D. Blatherwick, A. Matthews and N. Jones, " $\text{HNO}_3$  and  $\text{HCl}$  Amounts over McMurdo during the Spring of 1987," *J. Geophys. Res.*, 94, D14, 16,615-16,618, 1989.

20. C.P. Rinsland, J.S. Levine, R. Zander, A. Goldman, N.D. Sze, M.K.W. Ko, and D.W. Johnson, "Infrared Measurements of HF and HCl Total Column Abundance above Kitt Peak, 1977-1990: Seasonal Cycles, Increases in Total Columns Ratio, and Comparisons with Two-Dimensional Model Calculations," submitted to *J. Geophys. Res.*, Nov. 1990.

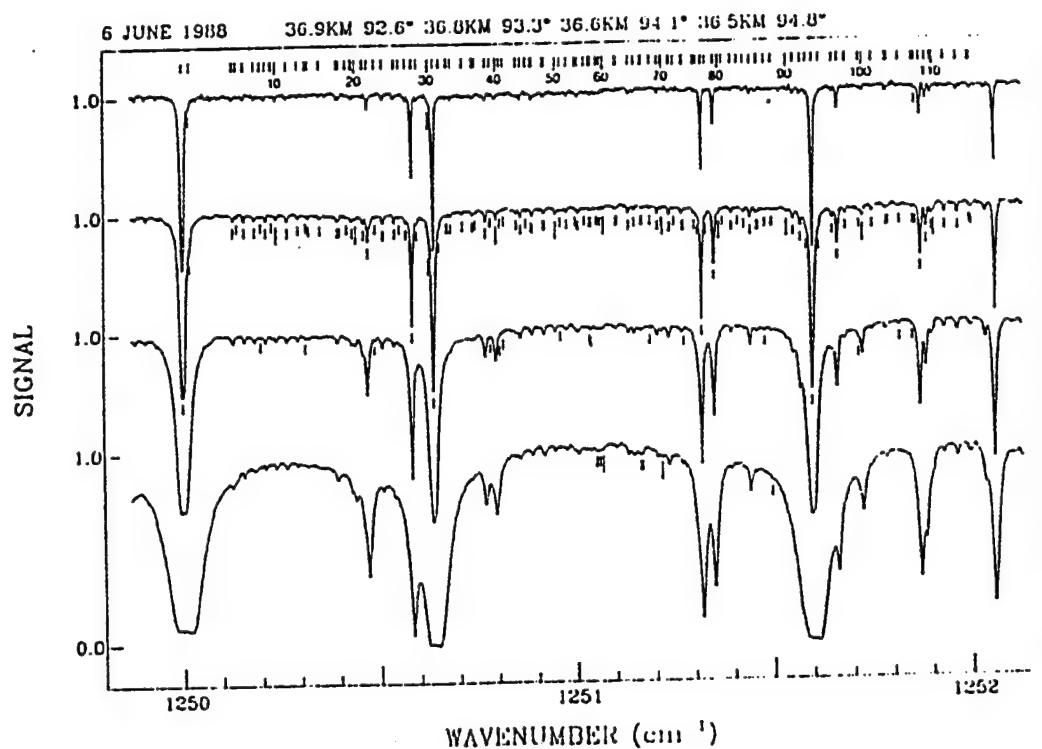


Fig.1. Sample spectra from the new atlas of high resolution ( $0.002 \text{ cm}^{-1}$ ) stratospheric IR absorption spectra in the  $1250\text{--}1252 \text{ cm}^{-1}$ . The spectral region contains several manifolds of the  $\text{COF}_2 \nu_4$  band.

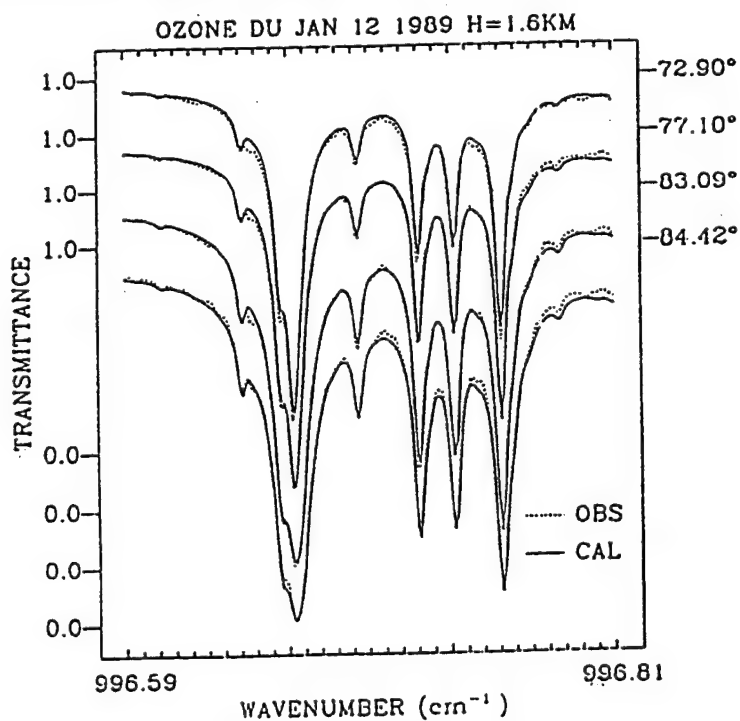


Fig.2. Nonlinear least-squares multi-scan fit of  $\text{O}_3$  with improved line parameters in the  $996 \text{ cm}^{-1}$  region, to solar spectra obtained from Denver, Colorado, during sunset on January 12, 1989, with a modified BOMEM model DA3.002 interferometer used for DU balloon flights. The total column of the fitted profile is  $7.46 \times 10^{18} \text{ molec/cm}^2$ .

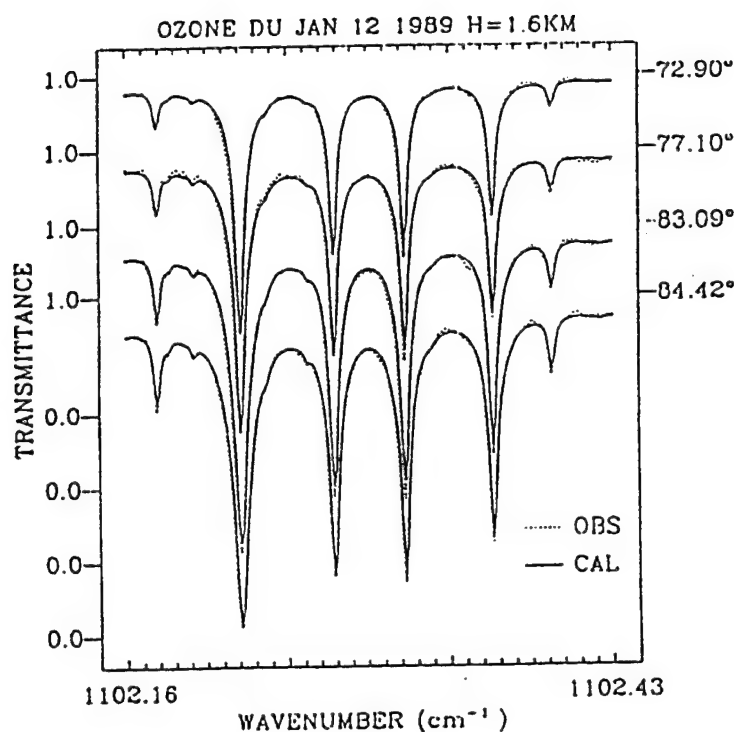


Fig.3. Nonlinear least-squares multi-scan fit of  $O_3$  with improved line parameters in the  $1102\text{ cm}^{-1}$  region, to solar spectra obtained from Denver, Colorado, during sunset on January 12, 1989, with a modified BOMEM model DA3.002 interferometer used for DU balloon flights. The total column of the fitted profile is  $7.33 \times 10^{18}$  molec/cm<sup>2</sup>.

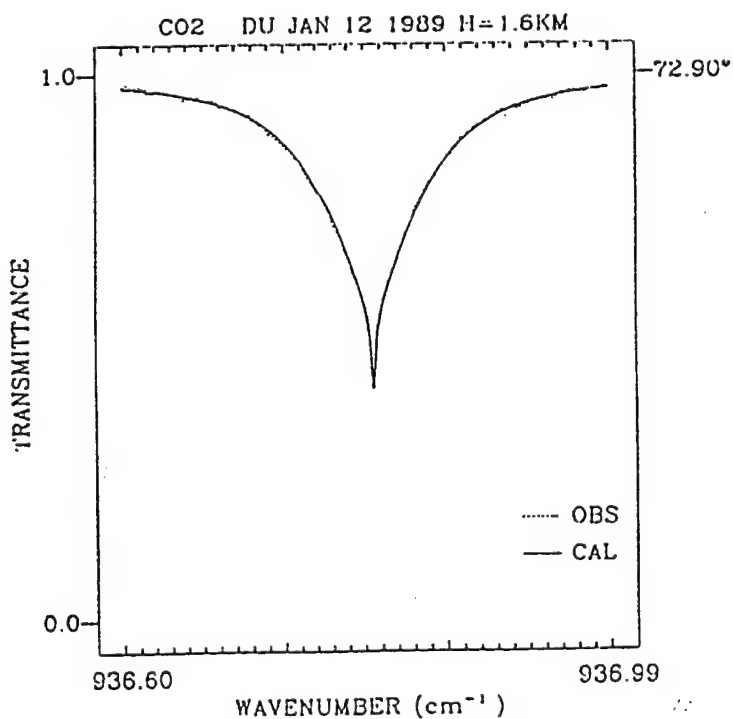


Fig.4. Nonlinear least-squares single scan fit of  $CO_2$  in the  $936\text{ cm}^{-1}$  region from solar spectra obtained from Denver, Colorado during sunset on January 12, 1989, with a modified BOMEM model DA3.002 interferometer used for DU balloon flights.



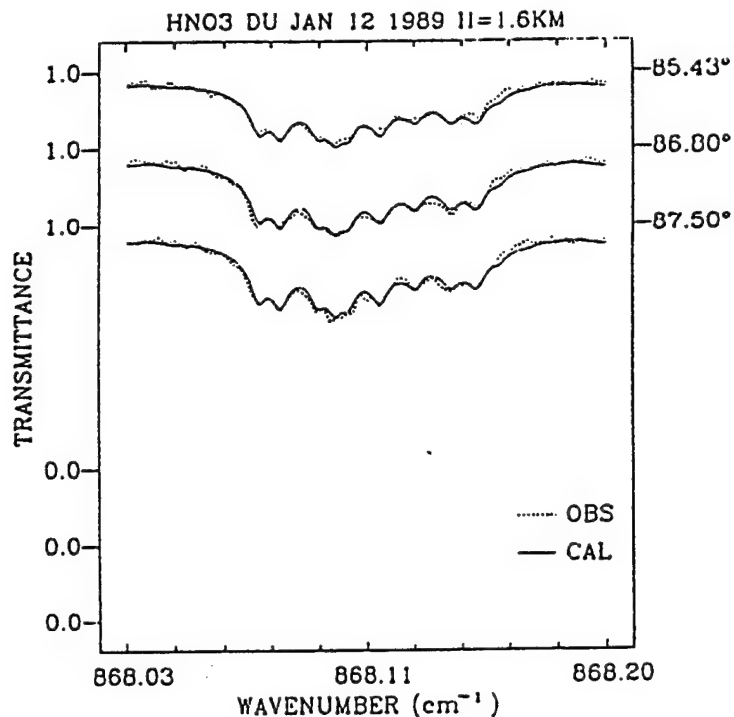


Fig.5. Nonlinear least-squares multi-scan fit of  $\text{HNO}_3$ , with improved line parameters in the  $868 \text{ cm}^{-1}$  region, to solar spectra obtained from Denver, Colorado, during sunset on January 12, 1989, with a modified BOMEM model DA3.002 interferometer used for DU balloon flights. The total column of the fitted profile is  $1.35 \times 10^{16} \text{ molec/cm}^2$ .

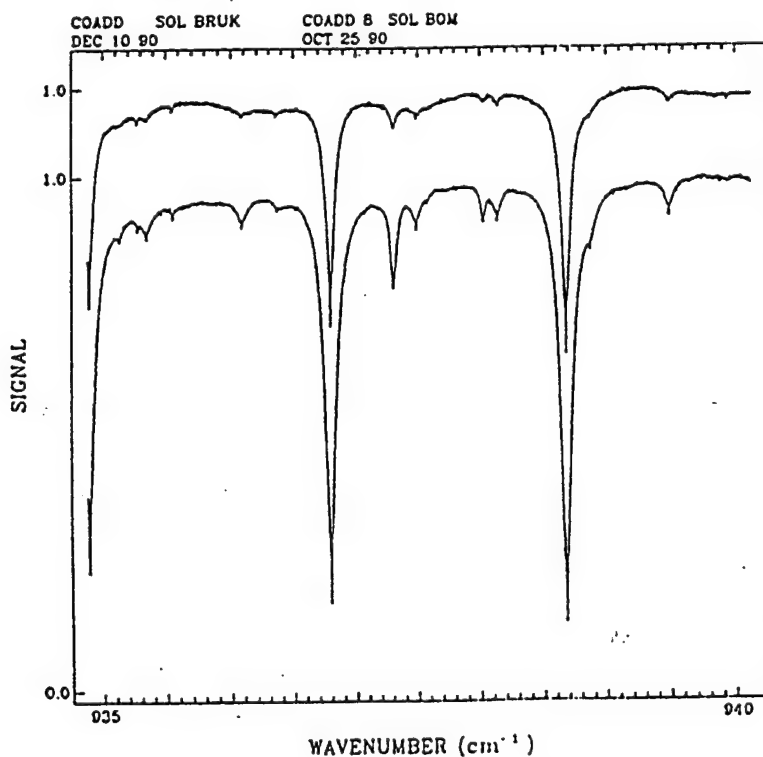


Fig.6. Solar spectra obtained from Denver, Colorado, during preliminary testing of the two interferometer systems BOMEM DA8.002 and BRUKER IFS 120 HR in the  $\text{CO}_2$   $935\text{-}940 \text{ cm}^{-1}$  region.

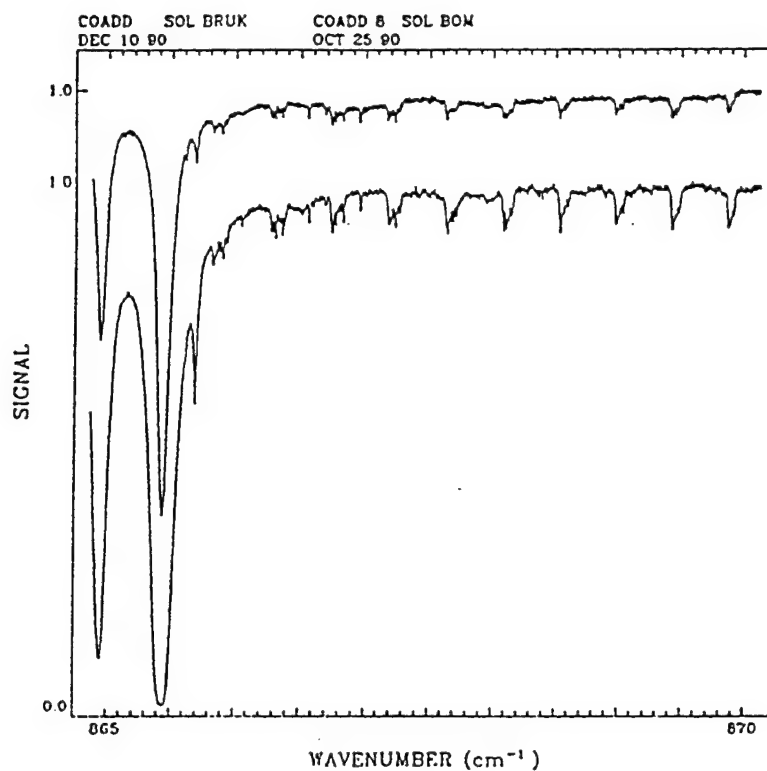


Fig.7.Solar spectra obtained from Denver, Colorado, during preliminary testing of the two interferometer systems BOMEM DA8.002 and BRUKER IFS 120 HR in the  $\text{HNO}_3$  865-870  $\text{cm}^{-1}$  region.

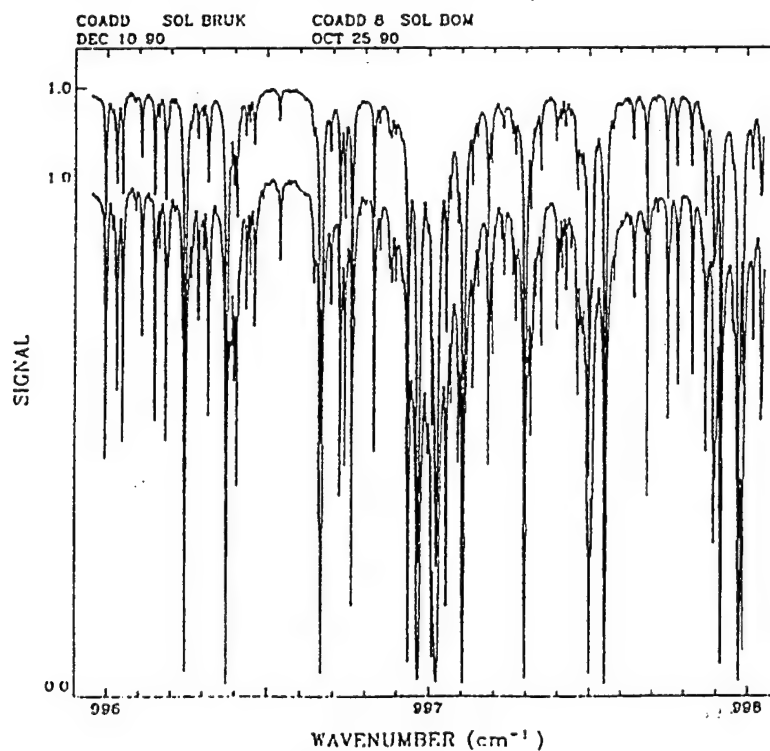


Fig.8.Solar spectra obtained from Denver, Colorado, during preliminary testing of the two interferometer systems BOMEM DA8.002 and BRUKER IFS 120 HR in the  $\text{O}_3$  996-998  $\text{cm}^{-1}$  region.

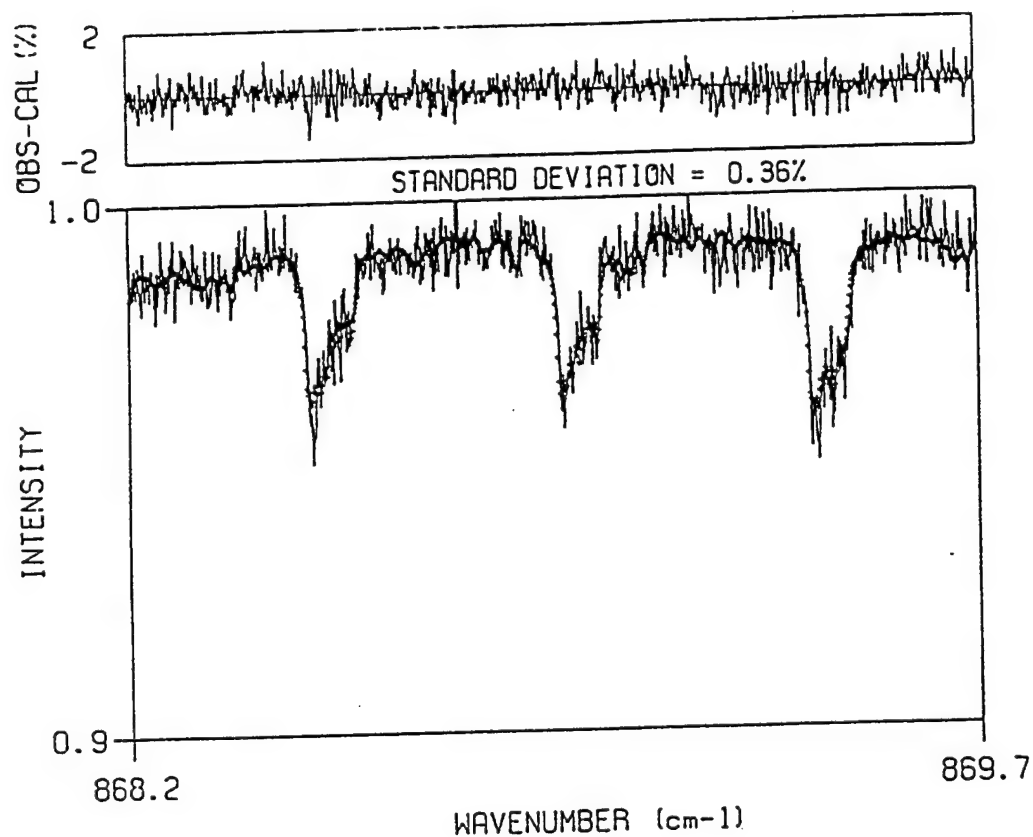


Fig.9. Nonlinear least-squares single scan fit of HNO<sub>3</sub> with improved line parameters in the 868 cm<sup>-1</sup> regions to solar spectra obtained from Denver, Colorado on December 10, 1990, with BRUKER model IFS 120 HR interferometer.

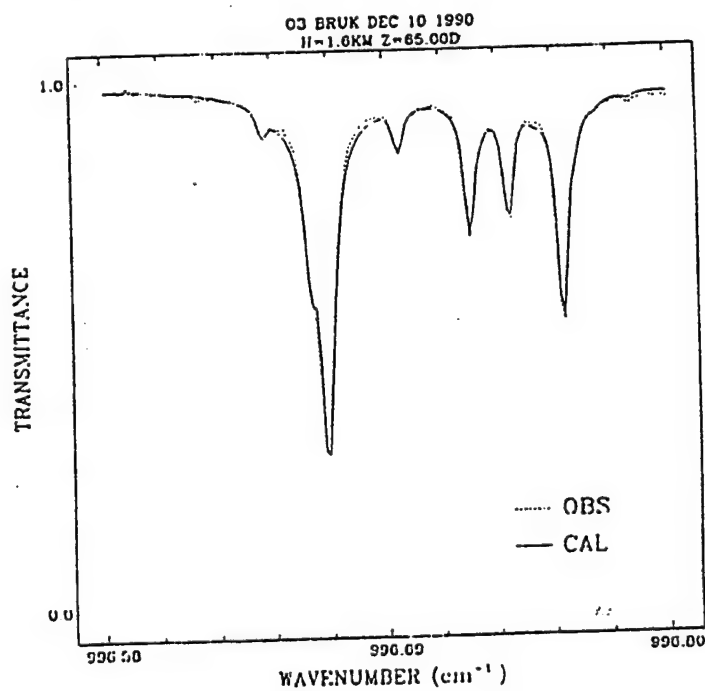


Fig.10. Nonlinear least-squares single scan fit of O<sub>3</sub> with improved line parameters in the 996 cm<sup>-1</sup> regions to solar spectra obtained from Denver, Colorado on December 10, 1990, with BRUKER model IFS 120 HR interferometer.

# Improved line parameters for ozone bands in the 10- $\mu$ m spectral region

Jean-Marie Flaud, Claude Camy-Peyret, Curtis P. Rinsland, V. Malathy Devi, Mary Ann H. Smith, and Aaron Goldman

A complete update of spectroscopic line parameters for the 10- $\mu$ m bands of ozone is reported. The listing contains calculated positions, intensities, lower state energies, and air- and self-broadened halfwidths of more than 53,000 lines. The results have been generated using improved spectroscopic parameters obtained in a number of recent high resolution laboratory studies. A total of eighteen bands of  $^{16}\text{O}_3$  (sixteen hot bands plus the  $\nu_1$  and  $\nu_3$  fundamentals) are included along with the  $\nu_1$  and  $\nu_3$  fundamentals of both  $^{16}\text{O}^{16}\text{O}^{18}\text{O}$  and  $^{16}\text{O}^{18}\text{O}^{16}\text{O}$ . As shown by comparisons of line-by-line simulations with 0.003-cm $^{-1}$  resolution balloon-borne stratospheric solar spectra, the new parameters greatly improve the accuracy of atmospheric calculations in the 10- $\mu$ m region, especially for the isotopic  $^{16}\text{O}^{16}\text{O}^{18}\text{O}$  and  $^{16}\text{O}^{18}\text{O}^{16}\text{O}$  lines.

The need for improvements in the accuracy of remote sounding measurements of ozone in the earth's atmosphere has motivated a number of recent studies devoted to the measurement and calculation of the spectrum of this molecule. In the IR, the strongest bands are at 10  $\mu$ m, where absorption is produced primarily by the  $\nu_3$  and  $\nu_1$  fundamentals of  $^{16}\text{O}_3$ . Hot bands of  $^{16}\text{O}_3$  and the  $\nu_3$  and  $\nu_1$  bands of  $^{16}\text{O}^{16}\text{O}^{18}\text{O}$  and  $^{16}\text{O}^{18}\text{O}^{16}\text{O}$  also contribute significantly to the total absorption by ozone.<sup>1</sup> The 10- $\mu$ m region has been used in a number of atmospheric studies of ozone, for example, the measurement of stratospheric  $\text{O}_3$  profiles by the Limb Infrared Monitor of the Stratosphere (LIMS) instrument on the Nimbus 7 satellite,<sup>2,3</sup> measurements of ozone total columns inside the Antarctic ozone hole using high resolution ground based solar spectroscopy,<sup>4</sup> and the measurement of ozone isotope ratios from ground based and balloon-borne high resolution solar spectra.<sup>5,6</sup> Accurate knowledge of the absorption properties of the 10- $\mu$ m ozone bands is also needed for climate models to estimate future changes in atmospheric and surface temperatures produced by the greenhouse effect.<sup>7-9</sup>

In the present paper, we report the calculation of improved line parameters for the ozone bands in the

10- $\mu$ m region. In addition to revising the eight bands on the 1986 HITRAN<sup>10</sup> and 1984 GEISA<sup>11</sup> line parameter compilations, the calculations have been extended to include fourteen additional bands. For example, only four hot bands of  $^{16}\text{O}_3$ , the  $\nu_1 + \nu_2 - \nu_2$ ,  $\nu_2 + \nu_3 - \nu_2$ ,  $\nu_1 + \nu_3 - \nu_1$ , and  $2\nu_3 - \nu_3$ , were included previously,<sup>10-12</sup> with upper state energy levels derived from spectra recorded at 0.02-cm $^{-1}$  resolution.<sup>13,14</sup> The new parameters listing includes a total of sixteen hot bands of  $^{16}\text{O}_3$  based on extensive analysis of positions and intensities from 0.005- to 0.01-cm $^{-1}$  resolution laboratory spectra. Also, for the first time, accurate parameters for the  $\nu_1$  and  $\nu_3$  bands of  $^{16}\text{O}^{16}\text{O}^{18}\text{O}$  and  $^{16}\text{O}^{18}\text{O}^{16}\text{O}$  are included. The  $\nu_3$  bands of both isotopic species appeared in the 1986 HITRAN and 1984 GEISA compilations,<sup>10,11</sup> but the crude approximations used to generate the line list make the data unreliable for high resolution studies. All the new results have been derived from laboratory absorption spectra of ozone recorded with the McMath Fourier transform spectrometer operated on Kitt Peak by the National Solar Observatory.<sup>15-24</sup>

A summary of the new parameters is given in Table I. The integrated band intensities  $S_{\text{band}}$  have been evaluated without a minimum intensity cutoff applied in the computer code. This procedure gives the most accurate estimate for the integrated band intensity but includes many very weak lines not readily observable in long path atmospheric or laboratory spectra. For this reason, the line listing was generated with minimum line intensity cutoffs of  $1.0 \times 10^{-25}$  cm $^{-1}$ /molecule cm $^{-2}$  at 296 K for the  $^{16}\text{O}_3$  bands and  $5.0 \times 10^{-23}$  cm $^{-1}$ /molecule cm $^{-2}$  at 296 K for the bands of the two  $^{18}\text{O}$ -monosubstituted ozone isotopes. The sum of intensities in this list, denoted  $S_{\text{list}}$ , is also reported in Table I. The calculations include a scaling of the

V. Malathy Devi is with College of William and Mary, Physics Department, Williamsburg, Virginia 23185; A. Goldman is with University of Denver, Physics Department, Denver, Colorado 80208; J. M. Flaud and C. Camy-Peyret are with Université Pierre et Marie Curie et CNRS, Molecular & Atmospheric Physics Laboratory, 4 place Jussieu, F-75252 Paris CEDEX 05, France; the other authors are with NASA Langley Research Center, Atmospheric Sciences Division, Hampton, Virginia 23665-5225.

Received 10 October 1989.

Table I. Summary of O<sub>3</sub> Bands Included in the Calculations

Vibrational States		Isotope <sup>a</sup>	Band Center (cm <sup>-1</sup> )	Calculated Intensities <sup>b</sup>		Number of Lines
Upper	Lower			S <sub>band</sub> <sup>c</sup>	S <sub>list</sub> <sup>d</sup>	
012	110	666	929.8447	4.16×10 <sup>-23</sup>	3.29×10 <sup>-23</sup>	164
002	100	666	954.7535	3.33×10 <sup>-21</sup>	3.27×10 <sup>-21</sup>	951
111	110	666	988.9772	2.12×10 <sup>-21</sup>	2.10×10 <sup>-21</sup>	1342
012	011	666	999.5841	6.01×10 <sup>-21</sup>	6.00×10 <sup>-21</sup>	1603
101	100	666	1007.6470	6.25×10 <sup>-20</sup>	6.25×10 <sup>-20</sup>	2646
001	000	686	1008.4528	2.65×10 <sup>-20</sup>	2.65×10 <sup>-20</sup>	2095
021	020	666	1008.6618	1.50×10 <sup>-20</sup>	1.50×10 <sup>-20</sup>	1511
002	001	666	1015.8068	1.68×10 <sup>-19</sup>	1.68×10 <sup>-19</sup>	3137
011	010	666	1025.5914	4.64×10 <sup>-19</sup>	4.64×10 <sup>-19</sup>	3883
001	000	668	1028.1120	5.12×10 <sup>-20</sup>	5.12×10 <sup>-20</sup>	3827
001	000	666	1042.0840	1.41×10 <sup>-17</sup>	1.41×10 <sup>-17</sup>	7224
111	011	666	1058.7166	1.22×10 <sup>-22</sup>	6.38×10 <sup>-23</sup>	252
101	001	666	1068.7003	5.31×10 <sup>-21</sup>	5.24×10 <sup>-21</sup>	2558
100	000	686	1074.3076	4.54×10 <sup>-22</sup>	4.54×10 <sup>-22</sup>	888
120	020	666	1087.3041	2.72×10 <sup>-22</sup>	2.21×10 <sup>-22</sup>	820
210	110	666	1089.9162	8.85×10 <sup>-23</sup>	3.33×10 <sup>-23</sup>	177
100	000	668	1090.3541	4.07×10 <sup>-21</sup>	4.07×10 <sup>-21</sup>	4425
110	010	666	1095.3308	1.27×10 <sup>-20</sup>	1.27×10 <sup>-20</sup>	3885
200	100	666	1098.0179	3.37×10 <sup>-21</sup>	3.30×10 <sup>-21</sup>	2931
100	000	666	1103.1373	5.40×10 <sup>-19</sup>	5.40×10 <sup>-19</sup>	6766
200	001	666	1159.0712	8.42×10 <sup>-21</sup>	8.34×10 <sup>-21</sup>	2057
210	011	666	1159.6556	1.95×10 <sup>-22</sup>	1.65×10 <sup>-22</sup>	593

Notes: a. 666 = <sup>16</sup>O<sub>3</sub>, 686 = <sup>16</sup>O<sup>18</sup>O<sup>16</sup>O, 668 = <sup>16</sup>O<sup>16</sup>O<sup>18</sup>O.  
b. Intensities are in cm<sup>2</sup>/molecule cm<sup>-2</sup> at 296 K units. Values are scaled to include the assumed natural molecular isotopic abundance of each species. See text.  
c. Integrated band intensity calculated by summing the individual line intensities without a minimum intensity cutoff.  
d. Sum of the intensities of all lines in list. The list was calculated with minimum intensity cutoffs. See text.

intensities by a multiplicative factor to convert the intensities from values for a pure isotopic species to values for a sample in natural isotopic molecular abundance. For this purpose, we adopted the isotopic ratios on the HITRAN compilation<sup>10</sup> (<sup>16</sup>O<sub>3</sub> = 0.9928, <sup>16</sup>O<sup>16</sup>O<sup>18</sup>O = 0.0040, and <sup>16</sup>O<sup>18</sup>O<sup>16</sup>O = 0.0020). The differences between S<sub>band</sub> and S<sub>list</sub> are significant only for the very weak bands.

It should be noted that recent studies (see Ref. 6 and references cited therein) have indicated that the isotopic abundances of the two <sup>18</sup>O-monosubstituted ozone isotopes are enhanced in the stratosphere compared to the expected normal isotopic values. Therefore, atmospheric simulations generated with the new line parameters, which incorporate the natural abundance factors used in the HITRAN compilation,<sup>10</sup> may underestimate the absorption produced by the <sup>16</sup>O<sup>16</sup>O<sup>18</sup>O and <sup>16</sup>O<sup>18</sup>O<sup>16</sup>O lines. The enrichment effect can be simulated by scaling the <sup>16</sup>O<sup>16</sup>O<sup>18</sup>O and <sup>16</sup>O<sup>18</sup>O<sup>16</sup>O line intensities by the appropriate isotopic enhancement factors in each atmospheric layer.

The calculations of the positions and intensities of the  $\nu_3$  and  $\nu_1$  fundamentals of <sup>16</sup>O<sub>3</sub> and the two <sup>18</sup>O-monosubstituted ozone isotopes have been described previously.<sup>15-17</sup> Since only relative intensities could be determined from the laboratory spectra, it is important to recall the assumptions used in scaling the relative intensities to obtain absolute values. For <sup>16</sup>O<sub>3</sub>, a value of  $(\partial\mu_z/\partial q_3)_e = -0.2662$  D was assumed, and for <sup>16</sup>O<sup>18</sup>O<sup>16</sup>O the intensities were computed by transferring the dipole moment of <sup>16</sup>O<sub>3</sub> to <sup>16</sup>O<sup>18</sup>O<sup>16</sup>O. The <sup>16</sup>O<sup>16</sup>O<sup>18</sup>O intensities have been calculated from rela-

tive intensities of <sup>16</sup>O<sup>16</sup>O<sup>18</sup>O and <sup>16</sup>O<sup>18</sup>O<sup>16</sup>O lines measured in the experimental spectra.<sup>15</sup> The amount of <sup>16</sup>O<sup>18</sup>O<sup>16</sup>O in the cell was first determined by comparing the measured relative intensities of the <sup>16</sup>O<sup>18</sup>O<sup>16</sup>O lines with the computed absolute values.<sup>17</sup> This amount was then multiplied by a factor of 2 to account for the difference in the relative concentrations of <sup>16</sup>O<sup>16</sup>O<sup>18</sup>O and <sup>16</sup>O<sup>18</sup>O<sup>16</sup>O.

The line positions for the hot bands  $\nu_2 + \nu_3 - \nu_2$  and  $\nu_1 + \nu_2 - \nu_2$  of <sup>16</sup>O<sub>3</sub> were computed from improved energy levels for the upper and lower states of both bands. The (011) and (110) energy levels were derived from analysis of the  $\nu_1 + \nu_2$  and  $\nu_2 + \nu_3$  bands in the 5.7- $\mu$ m region.<sup>18</sup> The energy levels for the (010) state were calculated<sup>20</sup> from a refit to line positions measured in the  $\nu_2$  and  $2\nu_2 - \nu_2$  bands.<sup>19</sup> The intensities of these hot bands were computed assuming transition moments derived from those of the  $\nu_1$  and  $\nu_3$  bands.

The line positions for the {(002),(101),(200)}-{(100),(001)} hot band system of <sup>16</sup>O<sub>3</sub> were computed from improved energy levels derived for the  $2\nu_3$ ,  $\nu_1 + \nu_3$ , and  $2\nu_1$  bands in the 4.8- $\mu$ m region<sup>21</sup> and the fundamental bands at 10  $\mu$ m.<sup>15</sup> As mentioned previously,<sup>21</sup> the observed energies of the (101) [19 2 17] and (101) [45 3 42] rovibrational levels are displaced from their calculated values probably because of a resonance with an unidentified nearby level. The calculated energies of both levels were replaced with their observed values in generating the line list. The intensities were computed from transition moments derived from those for the  $\nu_3$  and  $\nu_1$  bands and assuming the higher-order dipole moment derivatives are equal to zero [except for the transition moment of (002)-(001) which was determined to be  $0.5141 \times 10^{-2}$  D from a least-squares fit of measured intensities].

Positions for the lines from the {(021),(120)}-(020) system have been calculated from energy levels of the  $2\nu_2 + \nu_3$  and  $2\nu_2 + \nu_1$  bands obtained from the recent first high resolution analysis of these bands<sup>22</sup> and the constants for the (020) state reported by Flaud *et al.*<sup>20</sup> The intensities were computed assuming transition moments derived from those of the  $\nu_1$  and  $\nu_3$  bands.

Although the transitions are rather weak at atmospheric temperatures because of the Boltzmann factor, the {(012),(111),(210)}-{(110),(011)} system has been included to complete the description of the 10- $\mu$ m region. The positions were calculated from upper state energy levels determined from analysis of the  $\nu_2 + 2\nu_3$ ,  $\nu_1 + \nu_2 + \nu_3$ , and  $2\nu_1 + \nu_2$  bands in the 3.6- $\mu$ m region<sup>23</sup> and lower state energy levels determined from analysis of the  $\nu_1 + \nu_2$  and  $\nu_2 + \nu_3$  bands in the 5.7- $\mu$ m region.<sup>18</sup> The intensity calculation has been performed assuming that the transition moments of (210)-(011) and (012)-(110) are equal to zero, and the other ones were derived from those of the  $\nu_1$  and  $\nu_3$  bands.

The accuracies of the calculated line positions and intensities of the  $\nu_3$  and  $\nu_1$  bands of <sup>16</sup>O<sub>3</sub>, <sup>16</sup>O<sup>16</sup>O<sup>18</sup>O, and <sup>16</sup>O<sup>18</sup>O<sup>16</sup>O were given in the previous papers.<sup>15-17</sup> Also, the accuracies of the calculated positions of the <sup>16</sup>O<sub>3</sub> hot band lines can be estimated by combining the

uncertainties of the calculated upper and lower energy levels as reported previously.<sup>15,18,20-23</sup> A precise error budget is difficult to estimate for the  $^{16}\text{O}_3$  hot band line intensities since they have been calculated from transition moment expansions derived from those of the corresponding cold bands; generally, we expect the intensity errors of  $\sim 10\%$  with the accuracy degrading with increasing quantum numbers.

As an interim calculation, we have included air-broadened and self-broadened halfwidths based on empirical fits to recent laboratory measurements of

ozone halfwidths.<sup>24,25</sup> The following expression has been adopted:

$$\alpha_L = a_0 + a_1 J'' + a_2 J''^2 + a_3 J''^3,$$

where  $\alpha_L$  is the Lorentz broadening coefficient at 296 K (in  $\text{cm}^{-1} \text{atm}^{-1}$  units) and  $J''$  is the lower state total angular momentum quantum number. For the air-broadened halfwidths, the coefficients  $a_0 = 0.08735$ ,  $a_1 = -0.0007447$ ,  $a_2 = 6.08 \times 10^{-6}$ , and  $a_3 = 0.0$  have been used. On average, the measured air-broadened halfwidths in the  $\nu_1$  band<sup>24</sup> are  $\sim 10\%$  larger than corresponding values on the 1986 HITRAN compilation.<sup>10,26</sup> The self-broadened halfwidths were calculated with the coefficients  $a_0 = 0.11083$ ,  $a_1 = -0.0016721$ ,  $a_2 = 5.0084 \times 10^{-5}$ , and  $a_3 = -4.6741 \times 10^{-7}$  for  $J'' \leq 25$ . For  $J'' > 25$ ,  $\alpha_L = 0.093$  has been adopted. Self-broadened halfwidths were not included on the 1986 HITRAN<sup>10</sup> and 1984 GEISA compilations.<sup>11</sup>

The new ozone line parameters yield considerable improvement in the accuracy of high resolution atmospheric transmission and emission calculations in the  $10\text{-}\mu\text{m}$  region, especially for the isotopic  $^{16}\text{O}^{16}\text{O}^{18}\text{O}$  and  $^{16}\text{O}^{18}\text{O}^{16}\text{O}$  bands and the hot bands of  $^{16}\text{O}_3$ . To illustrate the quality of the new line parameters, Figs. 1–3 show comparisons of synthetic spectra with  $0.003\text{-cm}^{-1}$  resolution stratospheric solar occultation spectra recorded with a balloon-borne Fourier transform spectrometer.<sup>6,27,28</sup> In all cases, the agreement between measurement and calculation is very good, even for the weakest lines. Figure 1 includes a comparison of the stratospheric spectra with a simulation of generated data with the 1986 HITRAN compilation ozone line parameters.<sup>10</sup> The limitations of the previous data for high resolution spectroscopic studies are obvious.

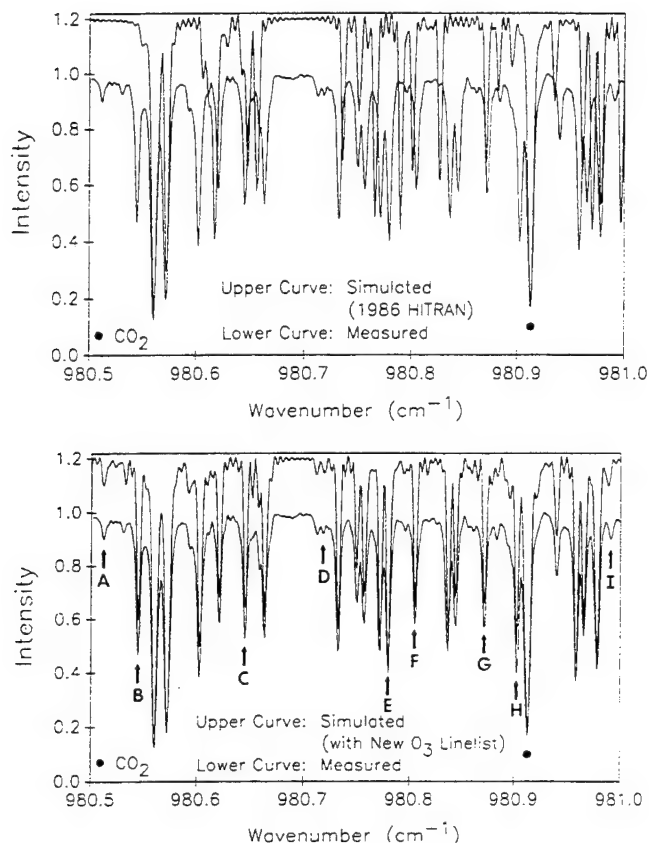


Fig. 1. Comparison of a  $0.003\text{-cm}^{-1}$  resolution solar occultation spectrum and a simulation of the data generated including the 1986 HITRAN ozone line parameters<sup>10</sup> (upper panel) and a simulation of the data generated with new ozone line parameters (lower panel). In each panel, the upper curve is the line-by-line simulation which has been displaced vertically by 0.2 for clarity. The lower curve shows a solar spectrum obtained at sunset 6 June 1988 during a balloon flight from Palestine, TX conducted by the University of Denver atmospheric spectroscopy group. The spectrum (normalized to the highest intensity in the interval) was recorded with a Michelson interferometer from a float altitude of 36.85 km and at a solar astronomical zenith angle of  $92.61^\circ$ . The corresponding refracted tangent height is 30.27 km. Arrows and capital letters in the lower panel indicate examples of ozone spectral features produced by different vibration-rotation bands. The ozone isotopic species and vibrational bands corresponding to the marked features are A =  $^{16}\text{O}_3(002)-(100)$ , B =  $^{16}\text{O}^{16}\text{O}^{18}\text{O}(001)-(000)$ , C =  $^{16}\text{O}_3(002)-(001)$ , D =  $^{16}\text{O}^{16}\text{O}^{18}\text{O}(001)-(000)$ , E =  $^{16}\text{O}_3(011)-(010)$ , F =  $^{16}\text{O}_3(101)-(100)$ , G =  $^{16}\text{O}_3(100)-(000)$ , H =  $^{16}\text{O}_3(001)-(000)$ , and I =  $^{16}\text{O}_3(021)-(020)$ . The R28 line of the 00011-10001 band of  $^{12}\text{C}^{16}\text{O}_2$  at  $980.9132\text{ cm}^{-1}$  (marked by a solid circle in both panels) is the only significant non- $\text{O}_3$  absorption feature in this spectral interval.

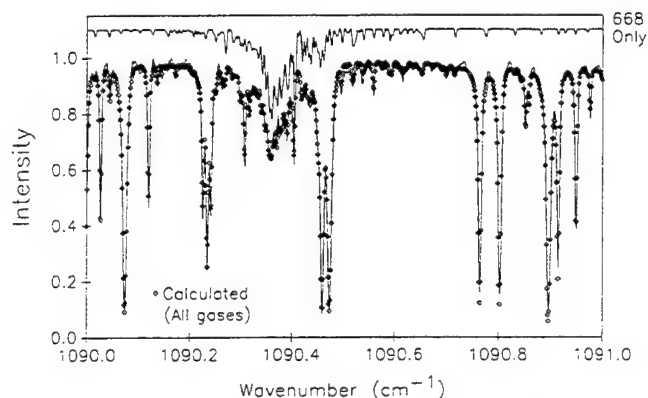


Fig. 2. Comparison of a  $0.003\text{-cm}^{-1}$  resolution stratospheric solar occultation spectrum (same scan as shown in Fig. 1) and line-by-line simulations with the new ozone line parameters. The upper spectrum, which has been displaced vertically by 0.1 for clarity, shows the absorption computed for the  $^{16}\text{O}^{16}\text{O}^{18}\text{O}$  isotopic species only. The feature near  $1090.36\text{ cm}^{-1}$  is the Q-branch of the  $\nu_1$  band. More than 300 lines are included in the calculations. The two lower spectra show a comparison of the measured solar spectrum (solid line) with a simulation of the absorption by all gases (open diamonds). The absorption in this region is due almost entirely to  $^{16}\text{O}_3$  lines and the lines of the  $^{16}\text{O}^{16}\text{O}^{18}\text{O}$   $\nu_1$ -band Q-branch.

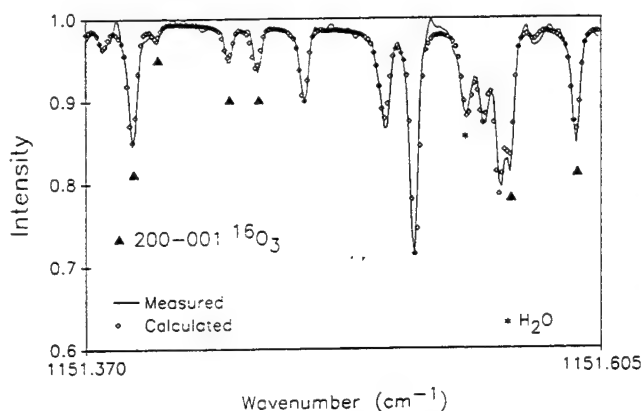


Fig. 3. Comparison of a  $0.003\text{-cm}^{-1}$  resolution stratospheric solar occultation spectrum (same scan as shown in Figs. 1 and 2) and a line-by-line simulation including the new ozone line parameters. A number of features of the (200)-(001) band of  $^{16}\text{O}_3$  are identified.

The total number of ozone lines in the new  $10\text{-}\mu\text{m}$  line list is 53,735 compared with 20,969 in the 1986 HITRAN compilation.<sup>10</sup> The substantial increase in the number of lines is likely to affect atmospheric retrievals over long atmospheric paths, particularly limb-viewing paths through the lower stratosphere where the ozone abundance is a maximum. The new line list also includes some significant changes in the distribution of the intensities within the stronger  $^{16}\text{O}_3$  bands. An important example is the  $\nu_1$  band of  $^{16}\text{O}_3$ . Although the integrated intensity of the band in the new line list is only slightly different ( $5.40 \times 10^{-19}$  compared with  $5.56 \times 10^{-19} \text{ cm}^{-1}/\text{molecule cm}^{-2}$  at 296 K in the 1986 HITRAN list<sup>10</sup>), the intensities of individual lines selected for ozone retrievals from high resolution atmospheric spectra are in most cases higher than on the 1986 HITRAN list,<sup>10</sup> resulting in correspondingly lower inferred ozone amounts.<sup>29,30</sup> The

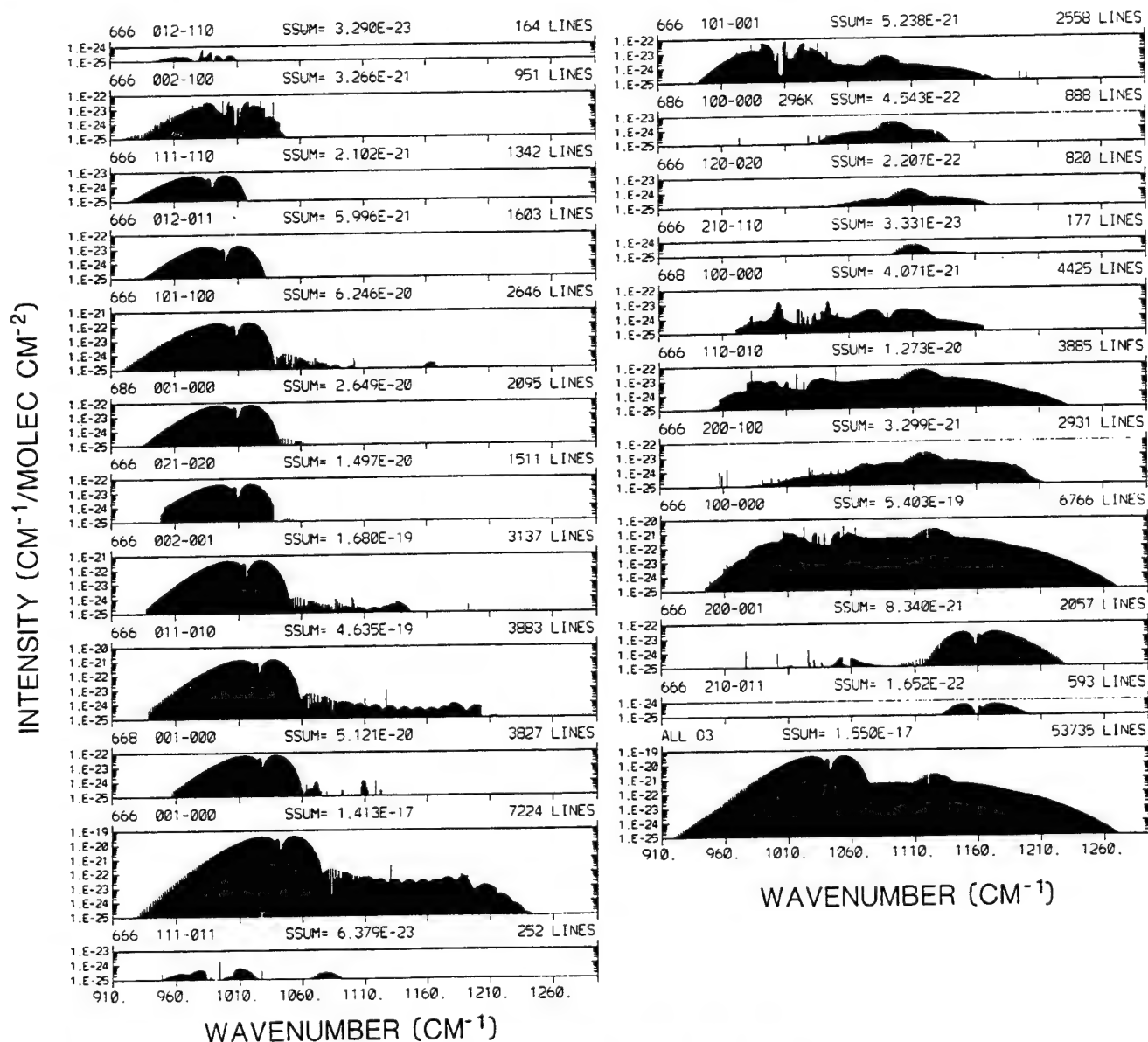


Fig. 4. Absorption line intensity ( $\text{cm}^{-1}/\text{molecule cm}^{-2}$  at 296 K units) on a base 10 logarithm vs wavenumber scale for each ozone band. A plot with all the lines is presented in the same format at the bottom of the right column.



retrievals with the new line parameters are in better agreement with correlative ozone measurements than those derived with the earlier line list.<sup>29,30</sup> Note that changes in the  $^{16}\text{O}_3$  line intensities have an important effect on the derivation of  $^{16}\text{O}^{16}\text{O}^{18}\text{O}/^{16}\text{O}_3$  and  $^{16}\text{O}^{18}\text{O}^{16}\text{O}/^{16}\text{O}_3$  isotopic enhancement ratios from high resolution IR spectra. The recent analysis of 0.003- $\text{cm}^{-1}$  resolution stratospheric solar absorption spectra by Goldman *et al.*<sup>6</sup> determined these ratios using the line parameters reported in this paper.

To provide an overview of the structures and the relative intensities of the bands in the new line list, Fig. 4 presents plots of absorption line intensity ( $\text{cm}^{-1}/\text{molecule cm}^{-2}$  at 296 K units) on a base 10 logarithm vs wavenumber scale for each ozone band. The bands are ordered by increasing band center, starting at the top of the left column and ending at the bottom of the right column. The final plot (lower right) contains all the lines displayed in the same format. The irregular distribution of intensity vs wavenumber within the bands results from the numerous resonances, both smooth and localized, occurring between the interacting states.

The National Solar Observatory is operated by the Association of Universities for Research in Astronomy under contract with the National Science Foundation. Research at the College of William and Mary and at the University of Denver is supported under cooperative agreements with the National Aeronautics and Space Administration.

## References

1. A. Goldman, T. G. Kyle, D. G. Murcray, F. H. Murcray, and W. J. Williams, "Long Path Atmospheric Ozone Absorption in the 9-10- $\mu\text{m}$  Region Observed from a Balloon-Borne Spectrometer," *Appl. Opt.* **9**, 565-580 (1970).
2. E. E. Remsberg *et al.*, "The Validation of NIMBUS 7 LIMS Measurements of Ozone," *J. Geophys. Res.* **89**, 5161-5178 (1984).
3. S. R. Drayson *et al.*, "Spectroscopy and Transmittances for the LIMS Experiment," *J. Geophys. Res.* **89**, 5141-5146 (1984).
4. C. B. Farmer, G. C. Toon, P. W. Schaper, J.-F. Blavier, and L. L. Lowes, "Stratospheric Trace Gases in the Spring 1986 Antarctic Atmosphere," *Nature London* **329**, 126-130 (1987).
5. C. P. Rinsland, V. Malathy Devi, J.-M. Flaud, C. Camy-Peyret, M. A. H. Smith, and G. M. Stokes, "Identification of  $^{18}\text{O}$ -Isotopic Lines of Ozone in Infrared Ground-Based Solar Absorption Spectra," *J. Geophys. Res.* **90**, 10,719-10,725 (1985).
6. A. Goldman *et al.*, "Isotopic Abundances of Stratospheric Ozone from Balloon-Borne High Resolution Infrared Solar Spectra," *J. Geophys. Res.* **94**, 8467-8473 (1989).
7. V. Ramanathan, R. J. Cicerone, H. B. Singh, and J. T. Kiehl, "Trace Gas Trends and Their Potential Role in Climate Change," *J. Geophys. Res.* **90**, 5547-5566 (1985).
8. R. E. Dickinson and R. J. Cicerone, "Future Global Warming from Atmospheric Trace Gases," *Nature London* **319**, 109-115 (1986).
9. D. P. Kratz and R. D. Cess, "Infrared Radiation Models for Atmospheric Ozone," *J. Geophys. Res.* **93**, 7047-7054 (1988).
10. L. S. Rothman *et al.*, "The HITRAN Database: 1986 Edition," *Appl. Opt.* **26**, 4058-4097 (1987).
11. N. Husson *et al.*, "The GEISA Spectroscopic Line Parameters Data Bank in 1984," *Ann. Geophys.* **4**, 185-190 (1986).
12. J.-M. Flaud, C. Camy-Peyret, and L. S. Rothman, "Improved Ozone Line Parameters in the 10- and 4.8- $\mu\text{m}$  Regions," *Appl. Opt.* **19**, 655 (1980).
13. A. Barbe, C. Secroun, P. Jouve, C. Camy-Peyret, and J.-M. Flaud, "High Resolution Infrared Spectrum of the  $\nu_2 + \nu_3$  and  $\nu_1 + \nu_2$  Bands of Ozone," *J. Mol. Spectrosc.* **75**, 103-110 (1979).
14. J.-M. Flaud, C. Camy-Peyret, A. Barbe, C. Secroun, and P. Jouve, "Line Positions and Intensities for the  $2\nu_3$ ,  $\nu_1 + \nu_3$ , and  $2\nu_1$  Bands of Ozone," *J. Mol. Spectrosc.* **80**, 185-199 (1988).
15. J.-M. Flaud, C. Camy-Peyret, V. Malathy Devi, C. P. Rinsland, and M. A. H. Smith, "The  $\nu_1$  and  $\nu_3$  Bands of  $^{16}\text{O}_3$ : Line Positions and Intensities," *J. Mol. Spectrosc.* **124**, 209-217 (1987).
16. J.-M. Flaud, C. Camy-Peyret, V. Malathy Devi, C. P. Rinsland, and M. A. H. Smith, "The  $\nu_1$  and  $\nu_3$  Bands of  $^{16}\text{O}^{18}\text{O}^{16}\text{O}$ : Line Positions and Intensities," *J. Mol. Spectrosc.* **118**, 334-344 (1986).
17. C. Camy-Peyret, J.-M. Flaud, A. Perrin, V. Malathy Devi, C. P. Rinsland, and M. A. H. Smith, "The Hybrid-Type Bands  $\nu_1$  and  $\nu_3$  of  $^{16}\text{O}^{16}\text{O}^{18}\text{O}$ : Line Positions and Intensities," *J. Mol. Spectrosc.* **118**, 345-354 (1986).
18. V. Malathy Devi, J.-M. Flaud, C. Camy-Peyret, C. P. Rinsland, and M. A. H. Smith, "Line Positions and Intensities for the  $\nu_1 + \nu_2$  and  $\nu_2 + \nu_3$  Bands of  $^{16}\text{O}_3$ ," *J. Mol. Spectrosc.* **125**, 174-183 (1987).
19. H. M. Pickett *et al.*, "The Vibrational and Rotational Spectra of Ozone for the (0,1,0) and (0,2,0) States," *J. Mol. Spectrosc.* **128**, 151-171 (1988).
20. J.-M. Flaud, C. Camy-Peyret, C. P. Rinsland, M. A. H. Smith, and V. Malathy Devi, "Line Parameters for  $^{16}\text{O}_3$  Bands in the 7- $\mu\text{m}$  Region," *J. Mol. Spectrosc.* **134**, 106-112 (1989).
21. C. P. Rinsland, M. A. H. Smith, J.-M. Flaud, C. Camy-Peyret, and V. Malathy Devi, "Line Positions and Intensities of the  $2\nu_3$ ,  $\nu_1 + \nu_3$ , and  $2\nu_1$  Bands of  $^{16}\text{O}_3$ ," *J. Mol. Spectrosc.* **130**, 204-212 (1988).
22. C. P. Rinsland, M. A. H. Smith, V. Malathy Devi, J.-M. Flaud, and C. Camy-Peyret, "The  $2\nu_2 + \nu_3$  and  $2\nu_2 + \nu_1$  Bands of  $^{16}\text{O}_3$  at 4.1  $\mu\text{m}$ : Line Positions and Intensities," *J. Mol. Spectrosc.* **139**, 343-352 (1990).
23. M. A. H. Smith, C. P. Rinsland, V. Malathy Devi, J.-M. Flaud, and C. Camy-Peyret, "The 3.6  $\mu\text{m}$  Region of Ozone: Line Positions and Intensities," *J. Mol. Spectrosc.* **139**, 171-181 (1989).
24. M. A. H. Smith, C. P. Rinsland, V. Malathy Devi, D. C. Benner, and K. B. Thakur, "Measurements of Air-Broadened and Nitrogen-Broadened Half-Widths and Shifts of Ozone Lines near 9  $\mu\text{m}$ ," *J. Opt. Soc. Am. B* **5**, 585-592 (1988).
25. M. A. H. Smith, C. P. Rinsland, and V. Malathy Devi, "Measurements of Self-Broadening of Ozone," in *Technical Digest, Forty-Fourth Symposium on Molecular Spectroscopy*, Ohio State U., Columbus (1989), paper TE11.
26. R. R. Gamache and L. S. Rothman, "Theoretical  $\text{N}_2$ -Broadened Halfwidths of  $^{16}\text{O}_3$ ," *Appl. Opt.* **24**, 1651-1656 (1985).
27. A. Goldman *et al.*, "New Spectral Features of Stratospheric Trace Gases Identified from High-Resolution Infrared Balloon-Borne and Laboratory Spectra," *J. Geophys. Res.* **94**, 14,945-14,955 (1989).
28. F. J. Murcray, J. J. Kusters, R. D. Blatherwick, J. Olson, and D. G. Murcray, "High Resolution Solar Spectrometer System for Measuring Atmospheric Constituents," *Appl. Opt.* **29**, 1520-1525 (1990).
29. C. P. Rinsland, A. Goldman, F. J. Murcray, F. H. Murcray, and D. G. Murcray, "Infrared Measurements of Atmospheric Gases Above Mauna Loa, Hawaii, in February 1987," *J. Geophys. Res.* **93**, 12,607-12,626 (1988).
30. M. R. Gunson *et al.*, "Measurements of  $\text{CH}_4$ ,  $\text{N}_2\text{O}$ ,  $\text{CO}$ ,  $\text{H}_2\text{O}$  and  $\text{O}_3$  in the Middle Atmosphere by the ATMOS Experiment on Spacelab 3," *J. Geophys. Res.*, in press.



## APPENDIX 10

Infrared Emission Measurements of Morning Stratospheric  $\text{N}_2\text{O}_5$ 

R. D. BLATHERWICK, D. G. MURCRAY, F. H. MURCRAY,  
F. J. MURCRAY, AND A. GOLDMAN

*Department of Physics, University of Denver, Denver, Colorado*

G. A. VANASSE

*Air Force Geophysics Laboratory, Bedford, Massachusetts*

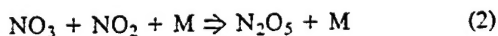
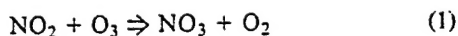
S. T. MASSIE AND R. J. CICERONE

*National Center for Atmospheric Research, Boulder, Colorado*

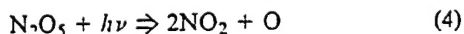
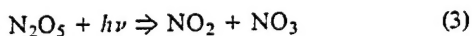
Infrared emission spectra obtained during a balloon flight of the Air Force Geophysics Laboratory SCRIBE system by the University of Denver are used to measure stratospheric  $\text{N}_2\text{O}_5$  after sunrise over New Mexico (latitude  $33^\circ\text{N}$ ). This is the first daytime measurement of  $\text{N}_2\text{O}_5$ . Comparisons with photochemical modeling show consistency between the observed and predicted decline of  $\text{N}_2\text{O}_5$  during the morning hours.

## INTRODUCTION

$\text{N}_2\text{O}_5$  is an important stratospheric reservoir species for  $\text{NO}_x$ , produced during the night by the reactions



After sunrise,  $\text{N}_2\text{O}_5$  gradually photolyzes back into  $\text{NO}_2$ :



The diurnal variation of stratospheric  $\text{N}_2\text{O}_5$ , as computed in photochemical models [Brasseur and Solomon, 1984], is a periodic function; it decays due to photolysis after sunrise and increases through reaction (2) at night.

Nighttime  $\text{N}_2\text{O}_5$  was tentatively observed by Roscoe [1982] and Evans [1986]. A definitive observation of  $\text{N}_2\text{O}_5$  was made by Toon *et al.* [1986] and Toon [1987], who observed the  $\nu_{12}$  band ( $\sim 1230$ – $1260 \text{ cm}^{-1}$ ) and the  $\nu_1$  and  $\nu_{11}$  bands ( $\sim 1680$ – $1770 \text{ cm}^{-1}$ ) in transmission spectra obtained with the ATMOS instrument at sunrise. Recently, Kunde *et al.* [1988] have measured nighttime  $\text{N}_2\text{O}_5$  from infrared emission spectra in the  $\nu_{12}$  region.

In the present work, infrared emission data are analyzed to demonstrate the first measurement of daytime  $\text{N}_2\text{O}_5$ , and the results are compared with the predictions of a one-dimensional photochemical model.

## OBSERVATIONS

The data were obtained during a balloon flight of the Air Force Geophysics Laboratory (AFGL) SCRIBE system (Stratospheric Cryogenic Interferometer Balloon Experiment) by the University of Denver from Roswell, New

Mexico, on July 5, 1984. The instrumentation consisted of a  $\text{LN}_2$ -cooled Michelson interferometer system employing cat's eye optics and having a maximum path difference of  $\sim 9 \text{ cm}$ . The time for a single scan was  $\sim 30 \text{ s}$ , including a 5-s fly-back. The field of view was  $\sim 0.8^\circ$ . Data for the radiometric calibration of the emission spectra were recorded during the flight by occasionally moving an on-board black body into the instrument field of view. For a detailed discussion of the SCRIBE instrumentation, see Murcray *et al.* [1984].

The balloon was launched at 0610 MDT (Mountain Daylight Time), and reached a float altitude of 30.6 km at 0740 MDT. Data were recorded at a number of zenith angles. Of these, the scans at  $90.6^\circ$  and  $91.1^\circ$  were selected as most suitable for the detection and measurement of daytime  $\text{N}_2\text{O}_5$ . The  $90.6^\circ$  data displayed here are actually the average of 14 individual scans selected from those recorded between 0751 and 0759 MDT, while the  $91.1^\circ$  data are the average of 12 scans recorded during the interval 0916–0923.5 MDT. Sunrise occurred at the balloon float altitude at approximately 0530 MDT, and at ground level at the local time of 0456 MST (Mountain Standard Time).

## ANALYSIS AND RESULTS

The data were analyzed by comparison with synthetic spectra generated using a line-by-line computer program developed at the University of Denver. The program, which takes refractive effects into account through a ray-tracing routine, calculates transmittance or emission over a user-selected number of atmospheric layers at a net interval of  $0.001 \text{ cm}^{-1}$ . The 1986 edition of the HITRAN data base [Rothman *et al.*, 1987] is used as input to the program. Line parameters for  $\text{N}_2\text{O}_5$  do not exist, but the absorption coefficients needed to compute the  $\text{N}_2\text{O}_5$  contribution to the atmospheric emission are generated by the program using the absorption cross sections for  $\text{N}_2\text{O}_5$  which are also included in the HITRAN data base. Finally, the computed radiances are degraded in resolution by convolution with an appropriate instrument line shape function.

Copyright 1989 by the American Geophysical Union.

Paper number 89JD02893.  
10148-0227/89/89JD-02893\$05.00

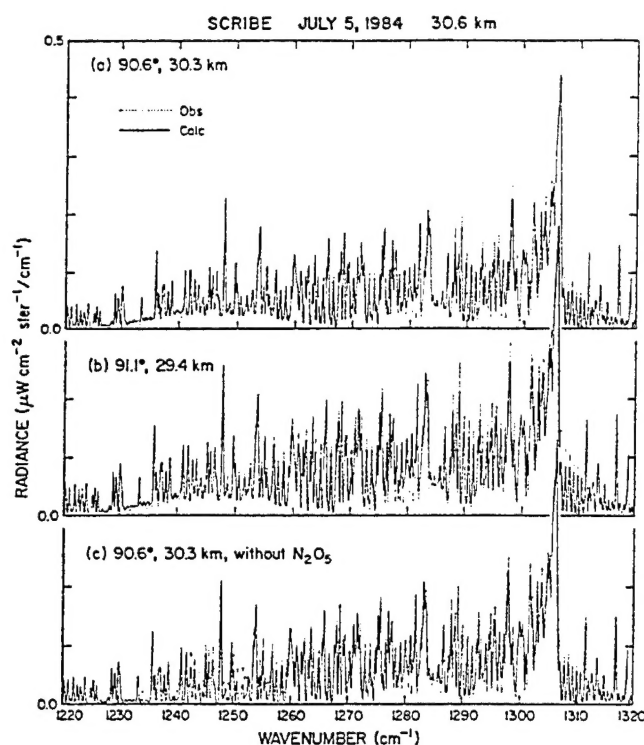


Fig. 1. Comparisons of observed (dotted curves) and calculated (solid curves) atmospheric emission spectra in the 1220–1320  $\text{cm}^{-1}$  region. The spectra were obtained during a balloon flight made on July 5, 1984, by the University of Denver with the AFGL SCRIBE system from balloon float altitude of 30.6 km. Zenith angles and tangent altitudes are indicated in the figure. The top two frames include N<sub>2</sub>O<sub>5</sub> in the spectral calculations while for the bottom frame N<sub>2</sub>O<sub>5</sub> was excluded from the calculation.

Residual background radiance was present at both observation angles (0.06 and 0.08  $\mu\text{W cm}^{-2} \text{sr}^{-1}/\text{cm}^{-1}$  at 90.6° and 91.1°, respectively). For the present analysis the data were adjusted by applying a wavelength dependent correction, described by a linear function such that theory and observation agreed in the “mini windows” centered at 1227.0 and 1267.07  $\text{cm}^{-1}$  and at the N<sub>2</sub>O-CH<sub>4</sub> blend at 1268.31  $\text{cm}^{-1}$ . These three positions are away from significant N<sub>2</sub>O<sub>5</sub> absorption. The peak N<sub>2</sub>O<sub>5</sub> cross section is  $1.90 \times 10^{-18} \text{ cm}^2$  at 1246  $\text{cm}^{-1}$  (with no temperature correction), whereas the cross sections for the three calibration points are  $\leq 1.5 \times 10^{-19} \text{ cm}^2$ . Validity of the adjustment is apparent in the reasonable agreement to the CH<sub>4</sub> spectrum longward of 1268  $\text{cm}^{-1}$  and insensitivity of the N<sub>2</sub>O<sub>5</sub> quantification to the background radiance. Subsequently, a least squares fitting for N<sub>2</sub>O<sub>5</sub> amounts over the 1240–1247  $\text{cm}^{-1}$  interval (with N<sub>2</sub>O and CH<sub>4</sub> fixed) was made. Recent measurements of N<sub>2</sub>O<sub>5</sub> cross sections [Cantrell *et al.*, 1988b] show  $1.79 \times 10^{-18}$  and  $1.82 \times 10^{-18} \text{ cm}^2$  at 1246  $\text{cm}^{-1}$  for 298 and 233K, respectively. Due to the small differences in comparison to the (room temperature) HITRAN value and the small temperature dependence, we did not adjust the HITRAN values.

The pressure-temperature profile used in these simulations was taken from a radiosonde ascent from White Sands Missile Range at 0800 MDT on the same day as the balloon flight. Mixing ratio profiles for the various constituents (except N<sub>2</sub>O<sub>5</sub>) are from Smith [1982].

Figures 1a and 1b show a comparison between the calculated (solid curve) and observed (dotted curve) emission for

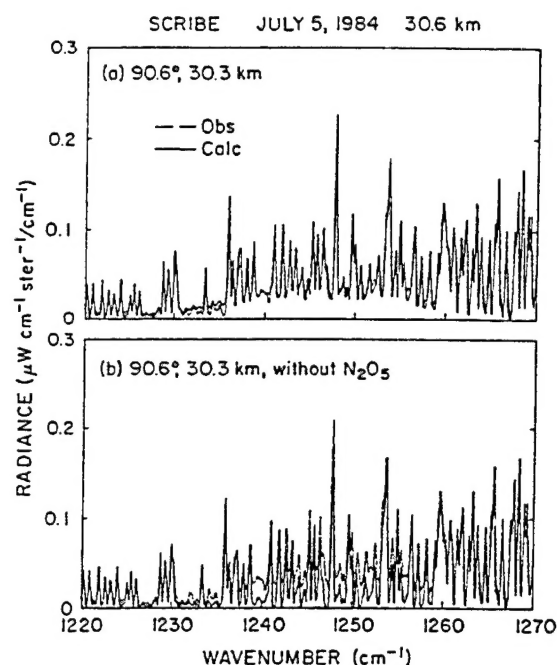


Fig. 2. Comparison of observed (dotted curves) and calculated (solid curves) atmospheric emission spectra in the N<sub>2</sub>O<sub>5</sub> 1220–1270  $\text{cm}^{-1}$  region. Figures 2a and 2b are expanded versions of Figures 1a and 1c.

zenith angles of 90.6° and 91.1°, respectively. (Tangent heights are 30.3 km and 29.4 km.) The data have been smoothed by a triangular filter to 0.25  $\text{cm}^{-1}$  resolution. The region is dominated by sharp emission lines of CH<sub>4</sub>, N<sub>2</sub>O, H<sub>2</sub>O, and, to a considerably lesser extent, CO<sub>2</sub>. At lower zenith angles there are also contributions from HNO<sub>3</sub> above ~1280  $\text{cm}^{-1}$ , as well as from CF<sub>4</sub> (~1283  $\text{cm}^{-1}$ ) and ClONO<sub>2</sub> (~1292  $\text{cm}^{-1}$ ), but these molecules do not contribute appreciably at the zenith angles shown here. The broad, smooth emission feature in Figure 1a and 1b from 1230 to 1260  $\text{cm}^{-1}$  is due to stratospheric N<sub>2</sub>O<sub>5</sub>. This can be seen from Figure 1c, which is the same as Figure 1a, except that no N<sub>2</sub>O<sub>5</sub> has been included in the calculation. Figure 2 shows an expanded plot of the N<sub>2</sub>O<sub>5</sub> 1220–1270  $\text{cm}^{-1}$  region from Figures 1a and 1c. Figure 3 presents the observed

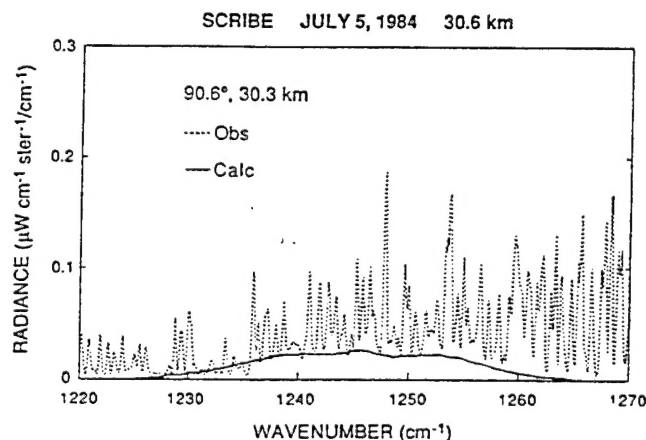


Fig. 3. Observed emission spectra (dotted curves) and theoretical calculation (solid curve) only including the N<sub>2</sub>O<sub>5</sub> contribution.

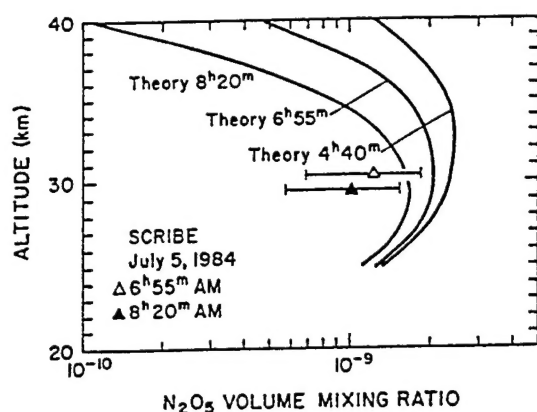


Fig. 4. One-dimensional photochemical-transport model (see text) mixing ratio profiles (solid curves) of N<sub>2</sub>O<sub>5</sub> for predawn (0440 MST) and morning conditions used for comparison with the experiment. The triangles show the measured N<sub>2</sub>O<sub>5</sub> mixing ratios 1.26 and 1.04 ppb, at the tangent altitudes 30.3 and 29.4 km.

radiance at 90.6° and a theoretical calculation which only includes the contribution due to N<sub>2</sub>O<sub>5</sub>.

The synthetic spectra of Figures 1a and 1b were computed using N<sub>2</sub>O<sub>5</sub> profiles of the same general shape as the solid curves of Figure 4, which are generated as described below, multiplied by a scaling factor. The triangles in Figure 4 show the resulting N<sub>2</sub>O<sub>5</sub> mixing ratios, 1.26 and 1.04 ppb, at the tangent altitudes of the two scans, 30.3 and 29.4 km, respectively. Theoretical N<sub>2</sub>O<sub>5</sub> mixing ratios are 2.10 and 1.65 ppb for the corresponding times of 0655 and 0820 MST. The observed relative decrease in N<sub>2</sub>O<sub>5</sub> is therefore 0.83, whereas the theoretical value is 0.79. The estimated accuracy of the absolute N<sub>2</sub>O<sub>5</sub> measurements is  $\pm 45\%$ . This is based on uncertainties in radiance calibration and pointing (10%), vertical slope of the theoretical N<sub>2</sub>O<sub>5</sub> mixing ratios (10%), spectral line parameters (15%), and the N<sub>2</sub>O, CH<sub>4</sub> profiles (10%). Error in the observed relative change is estimated as  $\pm 15\%$  (due to partial cancellation of systematic errors).

The theoretical N<sub>2</sub>O<sub>5</sub> mixing ratios curves were calculated by a one-dimensional photochemical transport model [Cicerone *et al.*, 1983]. The time dependent calculation extended between 10 and 80 km altitude. The pressure-temperature profile was that mentioned above, and the solar declination of +23° and the latitude of +33° matched that for the balloon flight.

Reaction rates for 81 two- and three-body gas-phase processes and 25 photolysis processes for 38 gaseous species follow that of the Jet Propulsion Laboratory (JPL 1987) [DeMore *et al.*, 1987], but with the Cantrell *et al.* [1988b] equilibrium constant for reaction (2). At 30 km at a temperature of 231K, the Cantrell and JPL 1987 equilibrium constants differ by 27%. However, for the geometry of the July 5 observation, the rate of thermal decomposition of N<sub>2</sub>O<sub>5</sub> is slower than the diurnal average of N<sub>2</sub>O<sub>5</sub> photolysis by a factor of 78, so the influence of the revised equilibrium constant upon the N<sub>2</sub>O<sub>5</sub> mixing ratio is small. The total odd-chlorine (Cl + ClO + HOCl + ClONO<sub>2</sub> + HCl + ClO<sub>2</sub>) mixing ratios are 2.17 and 2.61 ppb at 30 and 60 km, respectively. The  $J$  values at 30 km are  $3.42 \times 10^{-5} \text{ s}^{-1}$  and  $5.78 \times 10^{-5} \text{ s}^{-1}$  for N<sub>2</sub>O<sub>5</sub> photolysis (reactions (3) and (4)) for 0655 and 0820 MST, respectively. The albedo value was

0.35, and  $J$  is insensitive to changes in the albedo (e.g.,  $J$  equals  $5.62 \times 10^{-5} \text{ s}^{-1}$  for an albedo of 0.25 at 0820 MST).

Since N<sub>2</sub>O<sub>5</sub> is but one member of the NO<sub>y</sub> family (N + NO + NO<sub>2</sub> + NO<sub>3</sub> + HNO<sub>3</sub> + HNO<sub>4</sub> + 2\*N<sub>2</sub>O<sub>5</sub> + ClONO<sub>2</sub>), the theoretical value of N<sub>2</sub>O<sub>5</sub> is related to the total NO<sub>y</sub> mixing ratio. For the theoretical curves of Figure 2, NO<sub>y</sub> is equal to 15.0 and 14.3 ppb at 40 and 30 km, respectively. Observations of Russell *et al.* [1988] for May 1985, sunset, 30°N latitude indicate NO<sub>y</sub> near 16.7 and 15.2 ppb at 40 and 30 km, roughly 11% higher than our one-dimensional theoretical predictions.

The model N<sub>2</sub>O<sub>5</sub> and NO<sub>y</sub> profiles are reasonable, though they may not accurately represent the mixing ratio profiles of July 5, 1984, due to seasonal variations and model limitations. Differences between one- and two-dimensional models are illustrated, for example, in Figure 10-58 of *World Meteorological Organization (WMO)/NASA* [1986], in which the two modeling techniques at 30 km estimate different amounts of NO<sub>y</sub> and, presumably, different amounts of N<sub>2</sub>O<sub>5</sub>. Despite such differences, the present measurement of the relative change of N<sub>2</sub>O<sub>5</sub> during the morning hours is consistent with the temporal change of the one-dimensional calculation. Our observed early morning decline in N<sub>2</sub>O<sub>5</sub> concentration is also consistent qualitatively (see equations (1)–(4)) with measured early morning increases in both NO and NO<sub>2</sub> [e.g., Ridley *et al.*, 1977; Flaud *et al.*, 1988; Rinsland *et al.*, 1988].

The present morning N<sub>2</sub>O<sub>5</sub> results and the sunrise and nighttime N<sub>2</sub>O<sub>5</sub> observations by Toon *et al.* [1986] and Kunde *et al.* [1988], all report N<sub>2</sub>O<sub>5</sub> mixing ratios in the 1- to 2-ppb range near 30 km altitude. One sees that our observed mixing ratios at 0755 MDT and 0920 MDT are ~60% smaller than the values predicted by our model. Kunde *et al.* [1988] showed that their observed nighttime N<sub>2</sub>O<sub>5</sub> is 20–30% smaller in comparison to a (different) photochemical model. However, the relative decrease of 0.83 over the 1.5 hours between the observations is consistent with that of 0.79 predicted by the model. The relative decrease in N<sub>2</sub>O<sub>5</sub> concentration during the morning can be approximated by  $D = \exp(-J \Delta t)$ , where  $J$  is the average N<sub>2</sub>O<sub>5</sub> photolysis rate over the time interval  $\Delta t$ . With  $J = 4 \times 10^{-5} \text{ s}^{-1}$  and  $\Delta t = 1 \text{ hour } 25 \text{ min}$ ,  $D = 0.81$ , in good agreement with the detailed model results of 0.79.  $D$  is not sensitive to the actual N<sub>2</sub>O<sub>5</sub> amount, and thus the absolute difference between models and measurements of N<sub>2</sub>O<sub>5</sub> is less important than the temporal variations.

**Acknowledgments.** Research at the University of Denver was supported in part by the Air Force Office of Scientific Research (AFOSR) as part of AFGL task 2310G1, by NASA under grant NAG2-351, and by NSF under grant ATM 87-11572. Acknowledgment is made to the National Center for Atmospheric Research, which is supported by the National Science Foundation, for computer time used in this research. Research at NCAR was supported in part by the NASA UARS program under contract S-10782-C.

## REFERENCES

- Brasseur, G., and S. Solomon, *Aeronomy of the Middle Atmosphere*, D. Reidel, Hingham, Mass., 1984.
- Cantrell, C. A., J. A. Davidson, A. H. McDaniel, R. E. Shetter, and J. G. Calvert, Infrared absorption cross sections for N<sub>2</sub>O<sub>5</sub>, *Chem. Phys. Lett.*, 148, 358–363, 1988a.
- Cantrell, C. A., J. A. Davidson, A. H. McDaniel, R. E. Shetter, and J. G. Calvert, The equilibrium constant for N<sub>2</sub>O<sub>5</sub>  $\rightleftharpoons$  NO<sub>2</sub> +

- $\text{NO}_3$ ; absolute determination by direct measurement from 243 to 397K, *J. Chem. Phys.*, **88**, 4997-5006, 1988b.
- Cicerone, R. J., S. Walters, and S. C. Liu, Nonlinear response of stratospheric ozone column to chlorine injections, *J. Geophys. Res.*, **88**, 3647-3661, 1983.
- DeMore, W. B., M. J. Molina, S. P. Sander, D. M. Golden, R. F. Hampson, M. J. Kurylo, C. J. Howard, and A. R. Ravishankara, Chemical kinetics and photochemical data for use in stratospheric modeling, Evaluation Number 8, *JPL Publ. 87-41*, 196 pp., 1987.
- Evans, W. F. J., Observations of the  $8\text{ }\mu\text{m}$   $\text{N}_2\text{O}_5$  thermal emission feature in the stratosphere, *Appl. Opt.*, **25**, 1866-1868, 1986.
- Flaud, J.-M., C. Camy-Peyret, J. W. Brault, C. P. Rinsland, and D. Cariolle, Nighttime and daytime variation of atmospheric  $\text{NO}_2$  from ground-based infrared measurements, *Geophys. Res. Lett.*, **15**, 261-264, 1988.
- Kunde, V. G., J. C. Brasunas, W. C. Maguire, J. R. Herman, S. T. Massie, M. M. Abbas, L. W. Herath, and W. A. Shaffer, Measurement of nighttime stratospheric  $\text{N}_2\text{O}_5$  from infrared emission spectra, *Geophys. Res. Lett.*, **15**, 1177-1180, 1988.
- Murcray, F. H., F. J. Murcray, D. G. Murcray, J. Pritchard, G. Vanasse, and H. Sakai, Liquid nitrogen-cooled Fourier transform spectrometer system for measuring atmospheric emission at high altitudes, *J. Atmos. Oceanogr. Technol.*, **1**, 351-357, 1984.
- Ridley, B. A., M. McFarland, J. T. Bruin, H. I. Schiff, and J. C. McConnell, Sunrise measurements of stratospheric nitric oxide, *Can. J. Phys.*, **55**, 212-221, 1977.
- Rinsland, C. P., A. Goldman, F. J. Murcray, F. H. Murcray, R. D. Blatherwick, and D. G. Murcray, Infrared measurements of atmospheric gases above Mauna Loa, Hawaii, in February 1987, *J. Geophys. Res.*, **93**, 12,607-12,626, 1988.
- Roscoe, H. K., Tentative observation of stratospheric  $\text{N}_2\text{O}_5$ , *Geophys. Res. Lett.*, **9**, 901-902, 1982.
- Rothman, L. S., et al., The HITRAN database: 1986 edition, *Appl. Opt.*, **26**, 4058-4097, 1987.
- Russell, J. M., III, C. B. Farmer, C. P. Rinsland, R. Zander, L. Froidevaux, G. C. Toon, B. Gao, J. Shaw, and M. Gunson, Measurements of odd nitrogen compounds in the stratosphere by the ATMOS experiment on Spacelab 3, *J. Geophys. Res.*, **93**, 1718-1736, 1988.
- Smith, M. A. H., Compilation of atmospheric gas concentration profiles from 0 to 50 km, *NASA Tech. Memo.*, 83289, 1982.
- Toon, G., Reply: Detection of stratospheric nitrogen species, *Nature*, **330**, 427, 1987.
- Toon, G. C., C. B. Farmer, and R. H. Norton, Detection of stratospheric  $\text{N}_2\text{O}_5$  by infrared remote sounding, *Nature*, **319**, 570-571, 1986.
- World Meteorological Organization/NASA, Atmospheric Ozone 1985: Assessment of our understanding of the processes controlling its present distribution and change, report, World Meteorol. Organ., Geneva, 1986.
- R. D. Blatherwick, A. Goldman, D. G. Murcray, F. H. Murcray, and F. J. Murcray, Department of Physics, University of Denver, Denver, CO 80208.
- R. J. Cicerone and S. T. Massie, Atmospheric Chemistry Division, National Center for Atmospheric Research, P.O.B. 3000, Boulder, CO 80307.
- G. A. Vanasse, Air Force Geophysics Laboratory, Hanscom Air Force Base, Bedford, MA 01731.

(Received June 21, 1989;  
revised September 1, 1989;  
accepted September 8, 1989.)